UNIVERSITÀ DEGLI STUDI DI SALERNO

DIPARTIMENTO DI CHIMICA E BIOLOGIA

TESI DI DOTTORATO

IN

CHIMICA (XXX CICLO)

Development of new in vitro models based on the use of electrospun scaffolds and their imaging by multiphoton microscopy coupled with fluorescence lifetime imaging microscopy

Relatore:
Ch.ma Prof.
Brigida BOCHICCHIO

Correlatore:
Ch.ma Prof.
Antonietta PEPE

Candidato:
Germano Pasquale PICCIRILLO

Matr.: 8800100001

ANNO ACCADEMICO 2016-2017

INDEX

LIST OF ABBREVIATIONS 1

GENERAL INTRODUCTION 4

OUTLINE AND OBJECTIVES 8

CHAPTER 1. MATERIALS AND METHODS 10

1.1. Synthesis of Diclofenac-Glycine (DCF-Gly) 10
1.2. Nuclear magnetic resonance (NMR) analysis 11
1.3. Electrospinning 12
1.4. Reverse phase high performance liquid chromatography (RP-HPLC) 13
1.5. Cross-linking procedure 14
1.6. Hyaluronic acid (HA) coating 14
1.7. Swelling test analysis 15
1.8. Liquid displacement method 15
1.9. Scanning electron microscopy (SEM). 16
1.10. Drug release experiments 16
1.11. Contact angle measurements 17
1.12. Uniaxial tensile testing 18
1.13. Cell culture and seeding 18
1.14. Multiphoton microscopy (MPM) 19
1.15. In vitro cytotoxicity assay 20
1.16. Fluorescence lifetime imaging microscopy (FLIM) 21
1.17. ImageStream® analysis 22
1.18. Raman microspectroscopy. 23
1.19. Data analysis 23

CHAPTER 2. IMAGING OF DICLOFENAC INDUCED CELL DEATH IN HUMAN DERMAL FIBROBLASTS USING MULTIPHOTON MICROSCOPY COUPLED WITH FLUORESCENCE LIFETIME IMAGING MICROSCOPY 24

2.1. Introduction 24
2.2. Results 26

2.2.1. Production and characterization of the scaffolds 26
2.2.1.1. Electrospinning 26
2.2.1.2. SEM and fiber diameter analysis 26
2.2.1.3. Drug release experiments 27
2.2.1.3.1. UV-monitoring and fitting using Peppas equation 28
2.2.1.3.2. RP-HPLC 28
2.2.1.3.3. Electron X-ray dispersive spectroscopy (EDX) 30
2.2.1.3.4. Nuclear magnetic resonance (NMR) analysis 32
2.2.1.4. Tensile tests 33
2.2.1.5. Contact angle measurement 34
2.2.1.6. In vitro cytotoxicity 35
2.2.2. MPM and FLIM analysis 35
2.2.3. ImageStream® analysis 38
2.2.4. MPM and FLIM real time analysis 39
2.3. Discussion 41
2.4. Conclusions 46

CHAPTER 3. PRODUCTION AND CHARACTERIZATION OF AN ELECTROSPUN PLA SCAFFOLD LOADED WITH A SYNTHETIC DICLOFENAC PRODRUG FOR THE LOCAL TREATMENT OF ACTINIC KERATOSIS. 47

3.1. Introduction 47
3.2. Results 50
3.2.1. Synthesis of a Diclofenac prodrug via SPPS 50
3.2.2. Production of the scaffolds by electrospinning 50
3.2.3. SEM and fiber diameter analysis 50
3.2.4. Contact angle measurements 52
3.2.5. Tensile tests 52
3.2.6. MPM analysis 53
3.2.7. Drug release experiments 54
3.2.8. In vitro cytotoxicity 55
3.2.9. FLIM analysis 55
3.3. Discussion 57
3.4. Conclusions 62

CHAPTER 4. HYBRID GELATIN/POLY-L-LACTIDE ELECTROSPUN SCAFFOLDS WITH CONTROLLED HYDROPHOBICITY AND WETTABILITY .. 63

4.1. Introduction 63
4.2. Results 69
4.2.1. HYBRID GELATIN/POLY-L-LACTIDE SCAFFOLDS WITH CONTROLLED POROSITY AND WETTABILITY 69
4.2.1.1. Production of the scaffolds by electrospinning and cross-linking 69
4.2.1.2. SEM and fiber diameter analysis 70
4.2.1.3. Porosity, swelling properties and contact angle measurements 74
4.2.1.4. Tensile tests 76
4.2.1.5. Raman spectra and principal component analysis (PCA) 78
4.2.1.6. Scaffolds biocompatibility 81
4.2.2. HYBRID GELATIN/POLY-L-LACTIDE *IN 1:1 RATIO SCAFFOLDS WITH CONTROLLED HYDROPHOBICITY* 81
4.2.2.1. Functionalization of the scaffolds with hyaluronic acid 81
4.2.2.2. SEM and fiber diameter analysis. 82
4.2.2.3. Porosity, swelling properties and contact angle measurements 84
4.2.2.4. Tensile tests 85
4.2.2.5. Raman spectra and principal component analysis (PCA) 87
4.2.2.6. Scaffolds biocompatibility. 90
4.2.3. MPM AND FLIM ANALYSIS OF HUMAN DERMAL FIBROBLASTS ON HYBRID GELATIN/POLY-L-LACTIDE SCAFFOLDS 91
4.2.3.1 *MPM imaging* 91
4.2.3.2 *FLIM analysis* 92
4.3. Discussion 95
4.4. Conclusions 99

SUMMARY AND CONCLUDING REMARKS 100

SUPPLEMENTARY MATERIALS 101

REFERENCES 110

ACKNOWLEDGEMENTS 151

Siqua meis fuerint, ut erunt, vitiosa libellis,
excusata suo tempore, lector, habe.
exul eram, requiesque mihi, non fama petita est,
mens intenta suis ne foret usque malis.

Ovidio, Tristia, Liber IV, I, 1-4.

LIST OF ABBREVIATIONS

[3-(4,5-dimethylthiazol-2-yl -5-(3-carboxymethoxyphenyl -2-(4-sulfophenyl -2H-tetrazolium] = MTS

1,1,1,3,3,3-Hexafluoro-2-propanol = HFIP

1-Hydroxybenzotriazole hydrate = HOBT

2,2,2-Trifluoroethanol = TFE

2-Chloro Trityl Chloride = 2-CTRL-Cl

4, 4-dimethyl-4-silapentane-1-sulfonic acid = DSS

7-aminoactinomycin D = 7-AAD

Acetic acid = AcOH

Acetonitrile = CH_3CN

Actinic keratosis = AK

After release = a.r.

Arbitrary unit = a.u.

Aspartic acid = L-Asp

Basal cell carcinoma = BCC

Benzotriazol-1-yloxy-tripyrrolidino-phosphoniumhexafluorophosphate = PyBOP

Cross-linked = X-linked

CTRL = control

Deuterated dimethyl sulfoxide = DMSO-d_6

Deuterium oxide = D_2O

Dichloromethane = DCM

Diclofenac sodium salt = DCF

Diclofenac-Glycine = DCF-Gly

Dimethyl sulfoxide = DMSO

Dimethylformamide = DMF

Double distilled water = ddH_2O

Dulbecco's modified eagle medium = DMEM

Electron X-ray dispersive spectroscopy = EDX

Ethanol = EtOH

Extracellular matrix = ECM

Fetal calf serum = FCS

Fluorescence lifetime imaging microscopy = FLIM

Food and Drug Administration = FDA

Fourier-transformed infrared spectroscopy = FTIR

Gelatin = GE

Glass-transition temperature = T_g

Glutamic acid = L-Glu

Glycosaminoglycan = GAG

Gray value intensity = GVI

Human dermal fibroblasts = HDFs

Hyaluronic acid = HA

Isoelectric point = IEP

Matrix-assisted laser desorption ionization mass spectrometry = MALDI-MS

Melting temperature = T_m

Methanol = MeOH

Multiphoton microscopy = MPM

N-(3-Dimethylaminopropyl)-N'-ethylcarbodiimide hydrochloride = EDC·HCl

N,N-Diisopropylethylamine = DIPEA

Negative control = NC

N-Hydroxysuccinimide = NHS

Non-steroidal anti-inflammatory drugs = NSAIDs

Nuclear magnetic resonance = NMR

Phosphate buffer saline (1X) = PBS

(DMSO containing) Poly-L-lactide scaffold = PLA (w DMSO)

(DMSO containing) Diclofenac sodium salt loaded poly-L-lactide scaffold = PLA + DCF (w DMSO)

Diclofenac sodium salt loaded poly-L-lactide scaffold = PLA + DCF

Diclofenac-Glycine loaded poly-L-lactide scaffold = PLA + DCF-Gly

Poly-DL-lactic acid = PDLLA

Poly(lactic-co-glycolic) acid = PLGA

Poly-L-lactide = PLA; PLLA

Positive control = PC

Principal component analysis = PCA

Reduced (phosphorylated) nicotinamide adenine dinucleotide = NAD(P)H

Reverse phase high performance liquid chromatography = RP-HPLC

Room temperature = r.t.

Scanning electron microscopy = SEM

Second harmonic generation = SHG

Sodium dodecyl sulfate = SDS

Solid phase peptide synthesis = SPPS

Squamous cell carcinoma = SCC

Stratum corneum = SC

TFA = 2,2,2-Trifluoroacetic acid

Time correlated single photon counting = TCSPC

Two-photon-excitated fluorescence = TPEF

Volume = v

Weigth = w

GENERAL INTRODUCTION

One of the greatest challenges in the biomaterials field is to obtain versatile *in vitro* systems that can be easily controlled and adapted in order to reproduce properties that still belong only to *in vivo* models [1]. To reach this purpose the information and the technologies available nowadays must be combined together taking into account all the possible variables [2]. In the last 30 years, electrospinning has gained growing interest as a polymer processing technique for applications in tissue engineering and drug delivery [3]. Electrospinning is regarded as a simple approach for creating nanofibrous networks that can mimic the structure of the extracellular matrix (ECM). Interactions between cells and ECM are crucial to cellular differentiation and in regulating cell function [4–8]. Actually, the cells typically lose some of their normal *in vivo* behavior when they are removed from their microenvironment and cultured *in vitro*. A principal objective of tissue engineering, therefore, is to recreate in an *in vitro* culture system some of the essential factors of the cellular microenvironment, which control and regulate cell function *in vivo*. In this way, the high surface to volume ratio of nanofibrous electrospun scaffolds combined with their microporous structure can favor cell adhesion, proliferation, migration, and differentiation, all of which are highly desired properties for tissue engineering applications [9]. Electrospinning is a process that utilizes a high voltage source to inject charge of a certain polarity into a polymer solution or melt, which is then accelerated toward a collector of opposite polarity [3]. A typical electrospinning setup is shown in Fig.1.

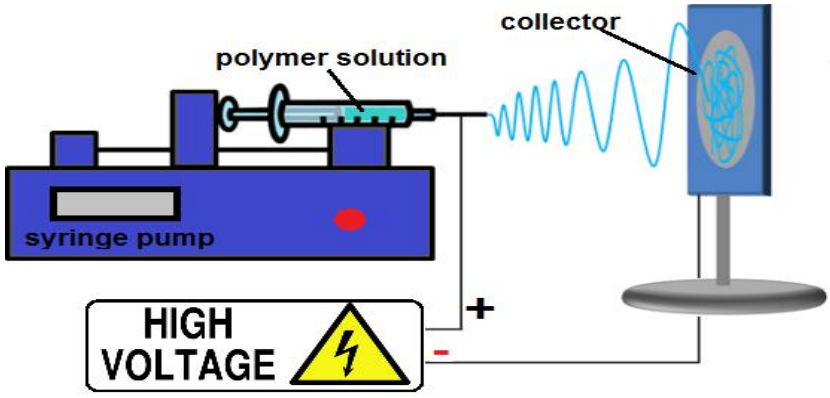

Fig. 1. Schematic diagram of an electrospinning setup.

The high surface to volume ratio of electrospun scaffolds can be also used for the efficient release of drugs after their incorporation in the scaffolds. After tissue engineering, drug delivery represents nowadays the second most exploited application field of electrospun scaffolds [3, 10-14]. Besides being a system that ensures a controlled and targeted drug-delivery, nanofibrous electrospun scaffolds have also the benefit of being matrices that can favor the healing process [15]. In the last 20 years a variety of electrospun fibrous scaffolds for biomedical applications have been developed [9-23]. Biodegradable and natural materials can be electrospun, and a wide range of molecules as drugs and proteins can be incorporated in the scaffolds too [9-23]. To date, electrospinning has been applied for the fabrication of nanofibrous scaffolds from numerous biodegradable synthetic polymers, such as polylactic acid [16], polyglycolic acid [17], polyurethane [18] and the copolymer poly(lactic-co-glycolic) acid [19]. Furthermore, incorporation of collagen and other biological components such as alginate [20], hyaluronic acid [21] and starch [22] into synthetic polymers was used to improve the scaffold biocompatibility or to introduce essential components of the ECM. In addition, the direct electrospinning of various biological substances, such as collagen, silk, fibrinogen, gelatin and chitosan, alone or together with synthetic polymers, has been investigated [23]. Since the scientific community has paid attention to electrospinning this technique has been regarded with constantly rising interest, and nowadays we have a great number of information about materials that can be electrospun and about their possible

applications [9-23]. Only some of them have been presented in this introduction and many new ones are daily investigated and published. However, the production of structures that can mimic biological tissues and samples is not the one and only goal when aiming to establish *in vitro* models that should be as close as possible to what happens *in vivo*. The development of methodologies that allow the dynamic imaging and analysis of living organisms in a neither invasive nor destructive way represents another great challenge [24]. Multiphoton microscopy (MPM) has grown extremely in this field since its first use for bioimaging [25]. MPM is a technique based on nonlinear optical processes such as two-photon-excited fluorescence (TPEF) or second harmonic generation (SHG). The simultaneous absorption of two photons is very unlikely to occur and short-pulsed femtosecond lasers operating in the near infrared (near-IR) are necessary [26, 27]. Nevertheless, the usage of this kind of lasers offers many advantages when aiming to image biological samples. For example, relative low average powers (in the milliwatts range) are needed for the analysis since the excitation is limited to the focal point. At the same time, no absorption and fluorescence occur above and below the plane of focus and so photobleaching and phototoxicity are generally avoided [27]. Not least, the use of excitation wavelength in the near-IR (700 nm or even greater) makes this technique less biologically harmful, and allows a deeper penetration in tissues or scattering samples when compared for example to confocal microscopy [27]. Moreover, many endogenous biomolecules (elastin, reduced nicotinamide adenine dinucleotide, flavin adenine dinucleotide) exhibit autofluorescence or are able to generate second harmonic signals (collagen) after excitation at specific wavelengths, and so they do not need to be stained [26-29]. All these aspects make MPM a technique that allows high-resolution imaging of untreated samples without damaging them. To date, MPM has already been employed for the *in vivo* evaluation of basal cell carcinoma [29]. Besides the imaging, other information can be obtained from each single pixel of a MPM acquisition if the system is specifically modified. Fluorescence lifetime imaging microscopy (FLIM) represents one of the techniques that can

be coupled with MPM. FLIM allows, for example, the discrimination between fluorophores exhibiting different decay times [26, 27], or helps to gain information about cellular metabolism and biological microenviroment when having specific endogenous fluorophores as target molecules [28, 29]. The demand for versatile, reliable *in vitro* models will increase in the years ahead. One of the biggest limits of many *in vitro* models already available is that they can be highly specific and sensitive for particular applications, but they cannot be extended to other fields [30]. Thus, the challenge of creating new systems, easily adaptable depending on the final desired application, and that can be analyzed unmodified with non-invasive methodologies, could help to obtain closer to *in vivo*, innovative *in vitro* models.

OUTLINE AND OBJECTIVES

In this PhD innovative *in vitro* applications for electrospun scaffolds are presented. Besides, multiphoton microscopy (MPM) coupled with fluorescence lifetime imaging microscopy (FLIM) has been employed for the imaging and the analysis of the samples, representing a neither invasive nor destructive methodology. These techniques have been combined together with the final aim of developing new versatile *in vitro* models. The work has been structured in three different parts. In the first part of the thesis (chapter 2) we aimed to develop a new model to assess drugs cytotoxicity *in vitro*. For this purpose the cytotoxic unmodified Diclofenac sodium salt (DCF) has been encapsulated in a pure poly-L-lactide (PLA) scaffold in order to obtain a system for its controlled release over time. A system ensuring a sustained drug release helps to better mimic a real therapeutic condition. The drug loaded scaffold has been then incubated together with human dermal fibroblasts (HDFs), before analyzing the cells exposed to the cytotoxic drug with MPM coupled with FLIM. These microscopies allow the imaging of unmodified biological samples without damaging them. In this thesis they have been chosen in order to develop a model to image morphological changes in the treated cells with MPM and evaluate their metabolic activity with FLIM. At the end, the use of an electrospun scaffold as a system for a specific and prolonged drug release together with the non-invasive analysis of the drug-exposed cells with MPM coupled with FLIM would offer a novel approach to investigate drugs cytotoxicity. In the second part of the thesis (chapter 3) we instead aimed to synthesize a non cytotoxic prodrug of DCF. Solid phase synthesis has been chosen representing a clean, versatile synthetic method. Moreover, we also aimed to encapsulate the synthesized DCF prodrug in a PLA scaffold and investigate *in vitro* its effects on HDFs comparing the prodrug to the cytotoxic DCF. To reach this purpose, a marker-free analysis of the unmodified cells based on the use of MPM coupled with FLIM is proposed. In the last part of the thesis (chapter 4), we aimed to obtain extracellular matrix (ECM)

mimicking scaffolds with tunable properties such as porosity and hydrophilicity and to investigate cell-material interactions *in vitro* with a non-invasive approach. To reach this purpose hybrid gelatin/PLA scaffolds have been produced by electrospinning, further modified and characterized. By blending naturally derived polymers with synthetic ones it is possible to obtain final structures with unique properties. Electrospinning allows the production of nanofibrous, high porous tridimensional scaffolds. Thus, this technique helps to obtain ECM-like final structures. According to our idea, by electrospinning gelatin, a biopolymer, together with PLA, a synthetic one, it may be possible to achieve final hybrid structures with unique properties that can be even further modified. Besides, we aimed to image cellular growth of HDFs on the hybrid scaffolds, and analyze their metabolic activity with MPM and FLIM, respectively. By working with hybrid electrospun scaffolds and analyzing them with a non-invasive methodology it would be possible to final obtain innovative versatile tridimensional *in vitro* models. On resuming, in this PhD thesis different applications of electrospun scaffolds are presented, while MPM and FLIM are proposed as imaging tools to analyze unmodified samples in a non-invasive, non-destructive and marker-free way. At the end, we aim to demonstrate how the versatility of the electrospinning process and the use of MPM coupled with FLIM offer together a broad spectrum of possibilities for the development of versatile *in vitro* models that can be analyzed unmodified in a non-invasive way. Particurarly, in this PhD these techniques have been combined together to finally develop *in vitro* models to investigate drugs cytotoxicity and cell-material interactions.

CHAPTER 1. MATERIALS AND METHODS

1.1. Synthesis of Diclofenac-Glycine (DCF-Gly)

Diclofenac-Glycine (DCF-Gly). ***2-{2-[(2,6-dichlorophenyl)-(N-glycine)-amino]phenyl} acetic acid*** **($C_{16}H_{14}Cl_2N_2O_3$).** All coupling reagents were purchased from Novabiochem (EMD Millipore by Merck KGaA, Darmstadt, Germany). 2-chlorotrityl chloride resin preloaded with glycine (H-Gly-2ClTrt Resin), the solvents and DCF sodium salt (DCF) were purchased by Sigma-Aldrich (Steinheim, Germany). Diclofenac free acid was obtained by the dissolution of DCF in water followed by acidification and extraction [31]. For the synthesis, H-Gly-2ClTrt resin (227 mg, 0.250 mmol, substitution 1.1 mmol/g, mesh 75-150) was suspended in a solvent mixture (Dimethylformamide (DMF):Dichloromethane (DCM) = 1:1) to a final volume of 10 mL, using a glass frittered disk sealed in glass column equipped with a faucet. The suspension was stirred (250 rpm) for 2 hours using an orbital shaker. The solvent was then removed by filtration and 8 mL of a DCM:DMF = 1:1 solution containing 148 mg (0.5 mmol) of Diclofenac free acid, 520 mg (1mmol) of Benzotriazol-1-yloxy-tripyrrolidino-phosphoniumhexafluorophosphate (PyBOP) and 150 mg (1mmol) of 1-Hydroxybenzotriazole hydrate (HOBT) were added to the resin. After shaking the mixture manually for a few minutes, 175 µL (1 mmol) of N,N-Diisopropylethylamine (DIPEA) was added and the mixture was shaken (280 rpm) using an orbital shaker for 20 hours. Thereafter, the solvent was removed by filtration, the resin was washed (2x10 mL DMF, 3x10 mL methanol (MeOH), 2x10 mL DMF, 3x10 mL DCM), and the functionalized amino acid was cleaved by adding 10 mL of a mixture of acetic acid (AcOH):2,2,2-Trifluoroethanol (TFE):DCM = 1:1:8. The solution was shaken (250 rpm) employing an orbital shaker for 30 minutes. The cleavage mixture was then filtered, and the resin was washed with DCM (3 x 5mL). The filtrates were combined and evaporated under reduced pressure to 5% of the initial volume, and 10 mL of double distilled water (ddH_2O) was then added to precipitate the desired product. The final

product was lyophilized twice to remove any solvent residual, and recovered as a white fluffy powder in a final yield of 98% (86.5 mg, 0.245 mmol). The final product was characterized by nuclear magnetic resonance (NMR) and matrix-assisted laser desorption ionization mass spectrometry (MALDI-MS, analysis by Dr. Emiliano Bedini, University Federico II of Naples). ***^{1}H-NMR*** *(500MHz, DMSO-d_6): δ= 3.61 (s, 2H); 3.75 (d, J=5.6 Hz, 2H); 6.25 (d, J= 8.0 Hz, 1H); 6.81 (t, J= 7.5 Hz, 1H); 7.00 (t, J= 7.9 Hz,1H); 7.12 (t, J =8.1 Hz, 1H); 7.18(d, J= 7.6 Hz, 1H) 7.47 (d, J= 8.2 Hz, 2H); 8.14(s, 1H); 8.63 (t, J= 5.6 Hz, 1H) ppm;* ***^{13}C-NMR*** *(500MHz, DMSO-d_6): δ= 39.12, 41.35, 116.44, 121.14, 125.52, 125.72, 127.68, 129.61, 129.90, 130.90, 137.61, 143.38, 171.43, 172.31.* ***MS (MALDI)*** calcd for $C_{16}H_{14}Cl_2N_2O_3^+$ $[(M+H)^+]$: 353.1997, found: 353.2356; calcd for $C_{16}H_{14}Cl_2N_2NaO_3^+$ $[(M+Na)^+]$: 376.1895, found: 376.9826.

1.2. Nuclear magnetic resonance (NMR) analysis

The crude DCF-Gly was characterized by ^{1}H- and ^{13}C- nuclear magnetic resonance (NMR) analysis. The ^{1}H- and ^{13}C- NMR spectra were acquired at room temperature on a Inova 500 NMR spectrometer (Varian, Agilent technologies, Inc., Palo Alto, CA, USA), equipped with a 5 mm triple resonance probe and z-axial gradients operating at 500 MHz for ^{1}H nuclei and 125 MHz for ^{13}C nuclei. Reference peaks for ^{1}H and ^{13}C spectra were respectively set to chemical shift (δ) 2.49 and δ 39.5 for deuterated dimethyl sulfoxide (DMSO-d_6). The pure DCF spectra were instead acquired in deuterium oxide (D_2O, Sigma-Aldrich), adding 2µl of 4, 4-dimethyl-4-silapentane-1-sulfonic acid (DSS) 10mM/D_2O. Reference peak for ^{1}H was in this case set to δ of 0.00 for DSS. The residual water signal signal was removed by double pulsed field gradient spin echo (DPFGSE) pulse sequence [32], in order to increase sensitivity of the receiver and thus reveal the signals of the highly diluted DCF solution extracted from the scaffold. All the acquired spectra were processed with ACD®/ NMR Processor Academic Edition (Advanced Chemistry Development, Inc., Toronto, Canada).

1.3. Electrospinning

Poly-L-lactide (PLA, viscosity ~1.0 dL/g, 0.1% weight/volume (w/v) in chloroform (25°C), M_n 59000, M_w 101 kDa, ester terminated) and gelatin (GE, gelatin from bovine skin, type B, cell culture tested, M_w 50-100 kDa, Bloom strength ~225 Bloom) were purchased by Sigma-Aldrich. The electrospun scaffolds were obtained starting from polymer solutions either containing or not the drug of interest too. When we aimed to obtain drug-loaded scaffolds the drug of interest was firstly allowed to complete dissolve before polymer addition. DCF-Gly was added to a final w/v% of 1%, while DCF to a final w/v% of 2% in chapter2 (when aiming to assess DCF cytotoxicity) and of 1% in chapter 3 (when aiming to compare it with DCF-Gly), respectively. After polymer(-s) addition the solutions were let stay at 37°C under magnetic stirring between 2 and 24 hours until they appeared completely clear. 1,1,1,3,3,3-Hexafluoro-2-propanol (HFIP, Sigma-Aldrich) was used as solvent for all the experiments. When using dimethyl sulfoxide (DMSO, ≥99.9%, for molecular biology, Bioreagent, Sigma-Aldrich) a 19:1 mixture represented the final HFIP:DMSO volume:volume ratio. All electrospinning experiments were performed with a customized device (Fig. 2).

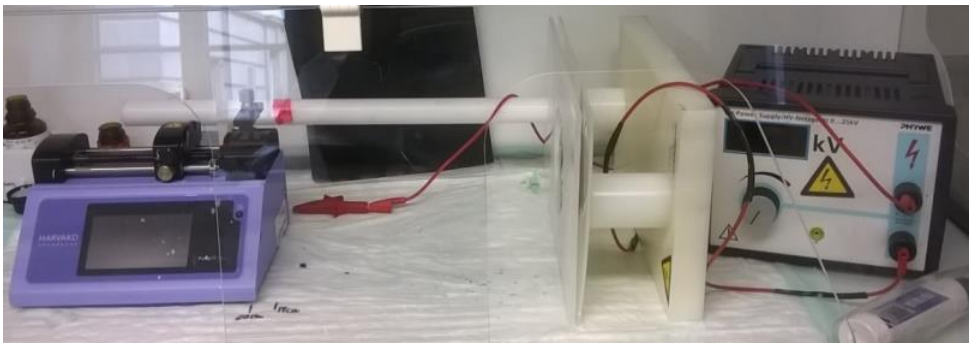

Fig.2. Electrospinning customized device.

The parameters used for the electrospinning experiments are reported in Table 1. For the drug-loaded electrospun scaffolds the parameters were the same used for pure PLA. In all cases an 18G stainless steel needle was employed.

POLYMER(S)	FINAL w/v POLYMER(S) CONTENT (%)	FINAL VOLUME (mL)	APPLIED VOLTAGE (kV)	DISTANCE NEEDLE COLLECTOR(cm)	FLOW-RATE (mL/h)
PLA	15	1	18	18	4
GE	10	3	19.5	19	1.2
GE:PLA=4:1	12.5	3	19.5	19	1.6
GE:PLA=5:2	14	3	19.5	19	1.6
GE:PLA=1:1	15	3	19.5	19	2.1

Table 1. Parameters used in the electrospinning experiments.

1.4. Reverse phase high performance liquid chromatography (RP-HPLC)

All RP-HPLC analyses were performed on a Shimadzu (Shimadzu Europa GmbH, Duisburg, Germany) automated HPLC system supplied with a Jupiter C5 column (Phenomenex, 250 x 4.6 mm, 5µ, 300 Å) with a flow rate of 1 mL/min, and UV detection. A binary gradient was used and the solvents were ddH_2O with 0.1% TFA (2,2,2-Trifluoroacetic acid, Romil Super purity Solvent (SpS™), Romil Ltd, Waterbeach, Cambridge, UK) and HPLC purity grade acetonitrile (CH_3CN, Romil Ltd). Products were eluted with a gradient of acetonitrile from 5 to 70% over 30 min (5→40% over the first 10 min followed by 40→50% over the next 15 min and 50→70% over the last 5 min). Reference chromatograms were obtained by injecting 20 µL of a 1 mg/mL solution of the compound of interest in phosphate buffer saline 1X (PBS, Gibco™ by Life Technologies GmbH, Darmstadt, Germany). The reported chromatograms were recorded at 270 nm as wavelength for UV detection.

1.5. Cross-linking procedure

All solvents and reagents were purchased by Sigma-Aldrich unless stated otherwise. Sodium hyaluronate (molecular weight blend: 240kDa, 480kDa and 800kDa) was obtained by Simply Essential™ (Palmerston, New Zealand). For the cross-linking a solution in EtOH 95%/ ddH_2O of N-(3-Dimethylaminopropyl)-N′-ethylcarbodiimide hydrochloride (EDC·HCl, Novabiochem®, EMD Merck Millipore) and N-Hydroxysuccinimide (NHS, Sigma-Aldrich) in equimolar ratio, both at the concentration of 50mM, was used. The electrospun scaffolds were immersed with a rate of 9mg/mL in a final mixture composed of the cross-linking and a sodium hyaluronate/ ddH_2O (or pure ddH_2O) solutions in a 9:1 volume:volume ratio, as described by Yang et al. [33]. Sodium hyaluronate/ ddH_2O solutions with four different final w/v% (0.015%, 0.02%, 0.025%, 0.03%) were tested. After immersion, the scaffolds were shaken at room temperature (r.t.) for 24 hours using an orbital shaker (60 rpm). After the 24 hours, the scaffolds were gently dried on filter paper and washed with ddH_2O (3x used volume of the cross-linking mixture for each side). Thereafter, they were allowed to stay 24 hours at 37°C in ddH_2O (same volume used for the cross-linking mixture) and finally washed again with ddH_2O (1x used volume of the cross-linking mixture for each side). After the washing procedure, the excess of water was removed using filter paper. The scaffolds were finally immersed in 70% EtOH/ddH_2O (half the volume of the cross-linking mixture) for 30 minutes, then dried on filter paper and allowed to stay overnight at r.t. to complete evaporate any solvent residual.

1.6. Hyaluronic acid (HA) coating

Cross-linked GE:PLA in a 1:1 weight:weight (w:w) ratio scaffolds were fully immersed at a rate of 9mg/mL in a 0.025% w/v HA solution in EtOH 85%/ ddH_2O and gently mixed at r.t for 24 hours using an orbital shaker (60 rpm). Thereafter, the scaffolds were let dry overnight

at r.t., and used for further characterization either before or after being washed. The washing procedure was the same used for the cross-linked scaffolds, and described in the section 1.5.

1.7. Swelling test analysis

For each sample 16 different pieces obtained from four different scaffolds (4 pieces for each scaffolds) were employed. Each scaffold piece was immersed in 10 mL of ddH_2O and allowed to mix at r.t. for 1 hour using an orbital shaker (60 rpm). After that time each side of the scaffold piece was let drip for 10 seconds. The excess of water was gently removed using filter paper, in case water drops on the scaffold surface were clearly visible. The rate of water absorbed by each piece was calculated according to the next shown formula (Scheme 1):

$$Swelling\ (\%) = \frac{wet\ scaffold\ w\ (mg) - dry\ scaffold\ w\ (mg)}{dry\ scaffold\ w\ (mg)} x100$$

Scheme 1. Formula used for the swelling test.

1.8. Liquid displacement method

The porosity of the scaffolds was estimated using the liquid displacement method, as previously described [34-36]. Absolute ethanol was used as the displacement liquid. Scaffold samples were immersed in a cylinder containing a known volume of absolute ethanol (V_1) for 30 minutes. After that time, the scaffold was gently pressed to remove air bubbles and the final volume represented by ethanol and ethanol-impregnated scaffold was recorded as V_2. Finally the ethanol-impregnated scaffold was removed and the residual ethanol volume in the cylinder was recorded as V_3. The porosity was calculated as follows (Scheme 2):

$$p(\%) = \frac{(V_1 - V_3)}{(V_2 - V_3)} x100$$

Scheme 2. Formula used for the porosity measurement according to the liquid displacement method.

1.9. Scanning electron microscopy (SEM)

The morphology of the electrospun scaffolds was determined using a scanning electron microscope (1530 VP, Zeiss, Jena, Germany). After platinum sputter coating, images were acquired at a distance of 8 mm from the detector, a voltage of 15 kV and different magnifications. The ImageJ® software supplied with the DiameterJ plug-in was used for fiber diameter and pores size/number analyses. Electron X-ray dispersive spectroscopy (EDX) analyses were instead performed on a scanning electron microscope (E-SEM XL30, FEI, Eindhoven, The Netherlands) equipped with energy dispersive X-ray spectrometer (EDAX GEMINI 4000, Zeiss). A voltage between 4 and 10kV was used to focus on the unsputtered scaffolds, and then set to 30kV for the EDX analysis. The working distance was in this case set to 10 mm from the detector. The schematic diagram of the analysis is represented in Fig.3. EDX spectra were acquired and plotted by Mr. Alessandro Laurita (University of Basilicata, Potenza, Italy).

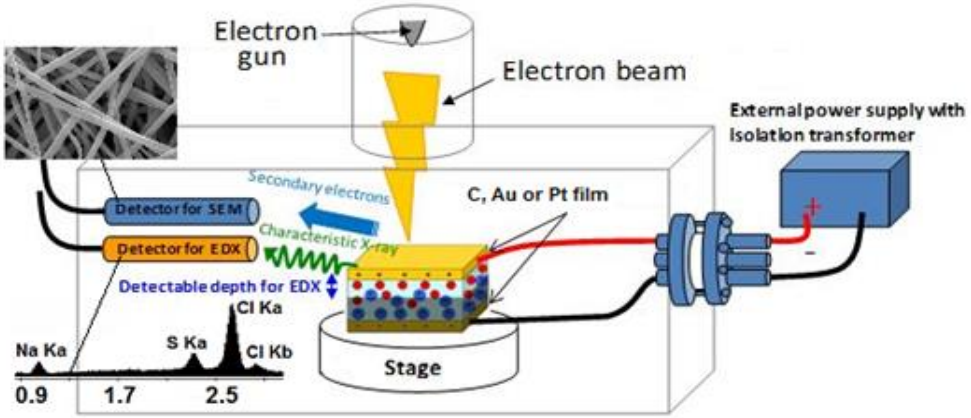

Fig.3. Schematic diagram of the SEM and EDX analysis.

1.10. Drug release experiments

For the drug release experiments, the scaffolds were incubated at 37°C in PBS (Gibco™ by Life Technologies GmbH). In particular, 9 mg of the drug-loaded scaffolds were fully immersed in 3 mL of PBS. At different time points, 800 µL of the supernatant was taken to

read the absorbance. Reading wavelength was set to 272 nm. After each measurement we returned the supernatant to the scaffold containing solution. The amount of the released drug was estimated according to previously calculated calibration curves. Micro UV-cuvettes (BrandTech™ 759210, Brand™ by Thermo Scientific, Darmstadt, Germany) and a TECAN® Infinite 200 Reader were used for all the UV measurements. The final drug release profiles were obtained from 4 release experiments by each different scaffold. In all cases, the absorbance value at 272 nm was constant after the first 24 hours. This time was therefore set as the end point measurement. The amount of released drug was plotted over time. The obtained points (M(t)) were also fitted using the equation developed by Peppas et al. (Scheme 3 [37,38]). The drug amount released after 24 hours was set as M(∞) in Peppas equation.

$$\frac{M(t)}{M(\infty)} = k \times t^n$$

Scheme 3. Peppas-Korsmeyer equation [37, 38]. k represents the release rate constant while n the release exponent.

1.11. Contact angle measurements

Hydrophilicity of the electrospun substrates was analyzed using contact angle measurements with an OCA 40 device (DataPhysics Instruments GmbH, Filderstadt, Germany). A water drop with the volume of 2 µl was placed onto the sample and the contact angle was measured 10 seconds after the water deposition using a video setup and the SCA20 software (DataPhysics Instruments) as previously described [39]. Final results were calculated from 16 measurements obtained from 4 different scaffold pieces for each sample.

1.12. Uniaxial tensile testing

Electrospun scaffolds were cut into 10 mm × 20 mm rectangular pieces and clamped into the uniaxial tensile testing device (Electroforce 5500, ElectroForce® Systems Group, Bose Corporation, Minnesota, USA). The exact sample dimensions were determined before each measurement and recorded with the software for further calculations of the Young's modulus (E-modulus) and the tensile strength. The scaffolds were pulled to failure by applying a stretch of 0.025mm/s. The Young's modulus was calculated from the initial linear slope of the stress *versus* strain curve for each measurement. Measured values are presented as average±standard deviation (each group n=4).

1.13. Cell culture and seeding

All research was carried out in compliance with the rules for investigation of human subjects, as defined in the Declaration of Helsinki. This study was carried out in accordance with the institutional guidelines and was approved by the local research Ethics Committee (F-2012-078). After informed written consent was given, skin biopsies were obtained and human dermal fibroblasts (HDFs) were isolated by enzymatic digestion as previously described [40]. Cells were cultured in Dulbecco's modified eagle medium (DMEM, with L-Glutamine, Gibco™, Life Technologies GmbH) supplemented with 10% fetal calf serum (FCS, PAA Laboratories, Pasching, Austria) and 1% penicillin / streptomycin (100 U/mL Penicilium and 100 µg/mL Streptomycin, Life Technologies GmbH). Cells were cultured in an incubator at 37 °C and in a 5% CO_2 atmosphere. Cell culture medium was changed every 3 days and cells were passaged or seeded using trypsin-EDTA (15090046, PAA Laboratories) at approximately 70% confluence. When seeding the cells directly on electrospun scaffolds, HDFs were seeded in number of $7x10^5$ in 12-well plates using inserts (CellCrown™, Scaffdex, Tampere, Finland). In this case, cells were analyzed 24 hours after seeding.

1.14. Multiphoton microscopy (MPM)

A titanium-sapphire femtosecond laser (MaiTai XF1, Spectra Physics, Santa Clara, USA) was used to generate 2-photon excitation. An excitation wavelength of 710 nm and a laser power of 3.2 mW were employed. The spectral emission filter ranged from 425 to 509 nm. For the imaging of the drug encapsulation, punches (Ø =12 mm) of the scaffolds were put on Ibidi® (Ibidi GmbH, Planegg/Martinsried, Germany) glass bottom dishes (35mm) and carefully pressed on the bottom with a cover glass before analysis. HDFs morphology was assessed on glass bottom dishes (Ibidi®, 35mm) with a density of 5 x 10^4 cells per dish. After 24 h, the medium was removed and 2 mL of fresh DMEM (+ 10% FCS) was added. When the cells were incubated with the (drug-loaded) scaffolds, punches (Ø=28 mm) of previously sterilized (254 nm, 2 hours) scaffolds were given as well. When analyzing HDFs, the laser power was adjusted to 18 mW. The experimental setup is schematized in Fig. 4.

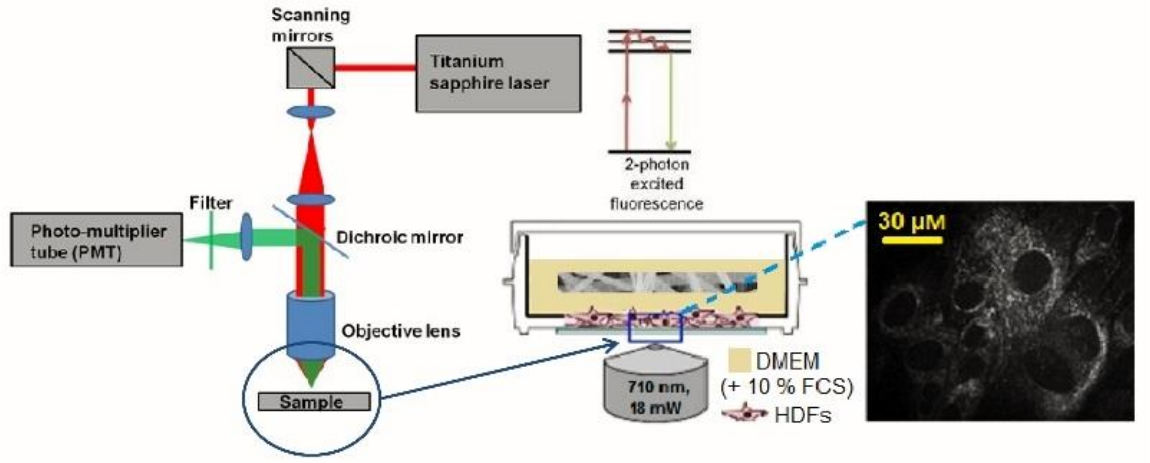

Fig. 4. Experimental setup for the MPM experiments.

When imaging cells directly on scaffolds, the electrospun scaffolds were instead removed from the inserts, flipped and carefully pressed on the bottom with a cover glass before analysis. For the mean gray value intensity (GVI) analysis of the drug-loaded scaffolds, ImageJ® was used as software to process and analyze the images.

1.15. In vitro cytotoxicity assay

According to an ISO 10993 accredited protocol, HDFs were exposed to an extract of the samples. The test was carried out as previously described [41]. In particular, the electrospun scaffolds were sterilized by UV irradiation (254nm) for 2h. 6cm^2 of each sample was then incubated in 1 mL FCS- and antibiotic-free DMEM medium. Each extract was prepared in triplicate. After 24 hours (72 hours in the case of the hybrid GE/PLA scaffolds, chapter 4), seeded HDFs were exposed for further 24 hours to the extracts supplied with 10% FCS. The extraction medium was removed and a tetrazolium salt ([3-(4,5-dimethylthiazol-2-yl)-5-(3-carboxymethoxyphenyl)-2-(4-sulfophenyl)-2H-tetrazolium], MTS, Fig. 5) assay (CellTiter 96Aqueous One Solution Cell Proliferation Assay, Promega, Mannheim, Germany) was performed as per the manufacturer's protocol.

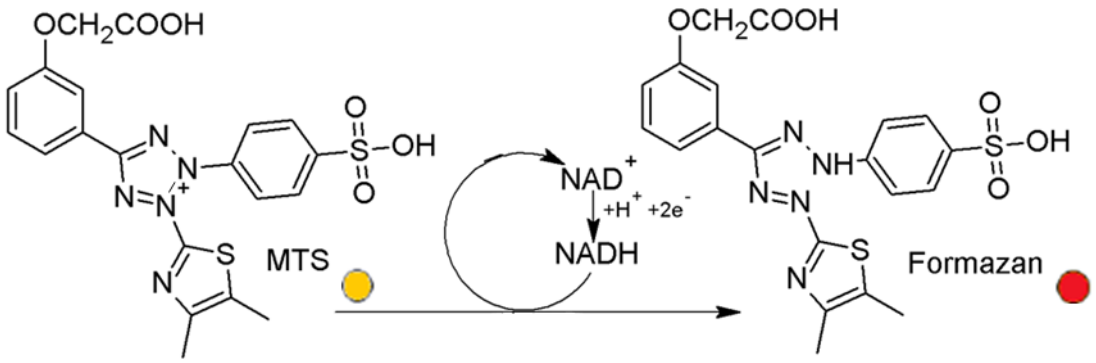

Fig. 5. Mechanism of the reduction reaction of MTS to Formazan.

Briefly, 20 µL of MTS solution was added to 100 µL of culture media. After incubation for 35 minutes at 37°C, the absorbance of each well was measured at 492 nm using a TECAN® Infinite 200 Reader. The test was performed for a blind, a negative control (NC; DMEM + 10% v FCS) and a sodium dodecyl sulfate (SDS, Life Technologies GmbH, 1% w/v in DMEM) treated positive control (PC). The procedure used to perform the MTS assay is schematized in Fig. 6. For analysis, the NC was set to 100%.

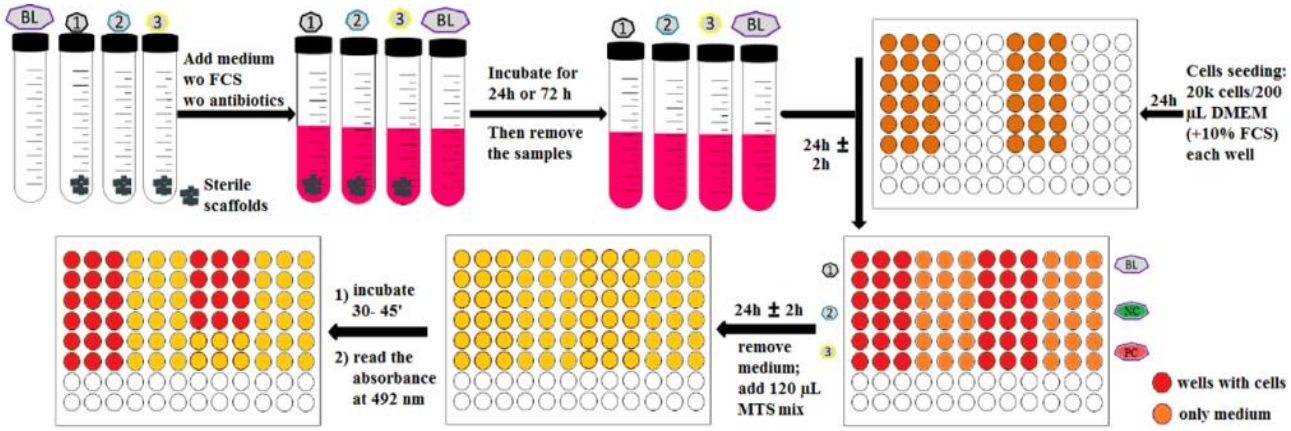

Fig.6. Schematic diagram of the protocol employed to perform the MTS assay.

1.16. Fluorescence lifetime imaging microscopy (FLIM)

FLIM was performed to assess reduced (phosphorylated) nicotinamide adenine dinucleotide (NAD(P)H) using time correlated single photon counting (TCSPC) at an excitation wavelength of 710 nm and a laser power of 18 mW. Analyzed samples were handled as described for MPM in section 1.14. FLIM data were recorded at an acquisition time of 180s for 512x512 pixels with 64 time channels. The instrument response function was recorded using urea crystals (Sigma-Aldrich) at an excitation wavelength of 920 nm and a laser power of 4.5 mW for 120s. The FLIM images were analyzed using the SPCImage software (Becker &Hickl GmbH, Berlin, Germany). A biexponential decay fitting model (Scheme 4) was employed at each pixel since NAD(P)H has two different lifetimes represented by τ_1 and τ_2 [42]. A χ^2<1.1 was accepted for a good fitting.

$$I(t) = \alpha_1 e^{-\tau_1} + \alpha_2 e^{-\tau_2} + C$$

Scheme 4. Biexponential decay fitting used for the FLIM analysis. τ_1 represents the free NAD(P)H lifetime time, while τ_2 the protein bound NAD(P)H one.

A binning factor of 6 was used in the analysis. Final data arise from 4 different donors. For each donor 3 different dishes were seeded with cells (50000 cells/dish) and 5 images were acquired per dish at each different time point. Between the different time point measurements

the dishes with the seeded cells were returned to 37°C/5%CO_2. By the real time and ImageStream® analyses (sections 3.2.2 and 3.2.3.), and when imaging HDFs on scaffolds (section 4.3.3.), only one donor was considered. Mean values arise in these cases from 12 images for each experimental point obtained from 3 different dishes (4 images/dish).

1.17. ImageStream® analysis

Annexin V (Annexin V Apoptosis Detection Kit eFluor™ 450) and 7-aminoactinomycin D (7-AAD, 7-AAD Viability Staining Solution) were purchased from eBioscience™ (part of Thermo Fischer Scientific, Darmstadt, Germany). By the analysis, for each group cells were obtained from three different dishes that were previously analyzed with FLIM as described in the 1.16 section. After FLIM analysis, cells were treated with trypsin-EDTA (PAA Laboratories), recovered per centrifugation, counted and washed (PBS, Gibco^{TM}). Thereafter, cells were harvested and stained with Annexin V eFluor™ 450 and 7-AAD as per the manufacturer's protocol. In particular, the cells were re-suspended at a rate of 10^6 cells/mL in Annexin V binding buffer (1X binding buffer diluted with ddH_2O from the starting 10X buffer). Samples were then stained with Annexin V-FITC (ApopNexin™ FITC, APT750a, Merck Millipore) and 7-AAD in Annexin V binding buffer (5 µL of fluorochrome-conjugated to 100 µL of the cell suspension) and left for 10 min at r.t. protecting from light. After that time, they were immediately placed on ice before analysis on an ImageStreamX Mark II (Amnis® part of Merck Millipore, Darmstadt, Germany) supplied with the INSPIRE (Amnis®) instrument controller software. The resultant data, obtained from at least 10000 cells/sample were then analyzed with the IDEAS (Amnis®) software. All samples were gated on single cells in focus (40X magnification) and then analyzed for Annexin V and 7-AAD. All ImageStream® analyses were carried out by Simone Pöschel (M.Sc., Women's hospital, University of Tübingen, Germany).

1.18. Raman microspectroscopy

The Raman system and acquisition parameters used in this study were previously described [43]. Briefly, a 784 nm diode laser with an output laser power of 85 mW was focused through a water-immersion objective (60X, NA 1.2, Olympus, Tokyo, Japan). The total acquisition time per spectrum was 100 s (10x10s acquisitions). All Raman spectra were analyzed in the range from 700 to 1800 cm^{-1}. Spectra were background-subtracted, baseline-corrected and vector-normalized using OPUS (Bruker Optics, Ettlingen, Germany) and Unscrambler X 10.3 (Camo, Oslo, Norway) as previously described [43]. Principal component analysis (PCA) was performed using Unscrambler X 10.3 (Camo) to reduce spectral variables and identify spectral differences among the compared samples. Seven PCs were calculated for each PCA. PC loadings were considered in detail to identify the molecular components that were relevant for the comparison of the spectra.

1.19. Data analysis

All the reported graphs were plotted using Microsoft™ Excel. All data are presented as mean±standard deviation (n=4, unless stated otherwise in the materials and methods). Statistical significance was determined by a Student's two-tailed unpaired t-test. Either $p \leq 0.01$ (**) or $p \leq 0.05$ (*) were defined as statistically significant.

CHAPTER 2. IMAGING OF DICLOFENAC INDUCED CELL DEATH IN HUMAN DERMAL FIBROBLASTS USING MULTIPHOTON MICROSCOPY COUPLED WITH FLUORESCENCE LIFETIME IMAGING MICROSCOPY

2.1. Introduction

Diclofenac (as a sodium salt, DCF) is one of the most sold and used non-steroidal anti-inflammatory drugs (NSAIDs) prescribed to millions of people worldwide [44, 45]. DCF is successfully used to treat osteoarthritis, rheumatoid arthritis [46, 47] and muscle pain [48], among others [49]. Besides, Diclofenac exhibits also anticancer effects, like other anti-inflammatory drugs [50-53] and is, for example, efficiently employed for the treatment of actinic keratosis (AK) in combination with hyaluronic acid (HA) [54]. DCF pharmaceutical properties are mainly releated to its activity as a potent non-selective cyclooxygenase inhibitor [45, 55]. However, scientists have been widely researching on other possible explanations for its complex mechanism of action [56]. Many progresses have been made thus far also to explain the toxic side-effects related to (prolonged) DCF therapies [57-64]. Diclofenac toxicity is proved in both animals [58] and humans [59]. Tomic et al. [60] and a few other studies [61-64] have shown the hepato- and nephro-toxicity of DCF. Detailed analysis of single patients has revealed clinical features that could be compatible with a direct toxic effect of DCF or any of its metabolites [65], rather than a drug-allergy mechanism [66-69]. Since the liver toxicity represents the most reported complication related to a prolonged or high-dosage use of DCF, *in vitro* studies have been mainly carried out using hepatocytes as target cells. To date, many different studies with cultured hepatocytes from various species have proved that high DCF concentrations (400 μM to 500 μM) are able to induce acute cell injury [70-77]. Recently, *in vitro* toxicity of DCF has been demonstrated also in other cell lines [78-82]. However, the mechanism behind DCF acute cellular toxicity has not been clearly determined, and the use of such high concentrations has been questioned, as it doesn't mimic a clinical

therapeutic situation. While DCF hepato- [61-68, 83-85] and nephro-toxicity [58-60] has been widely investigated, not that much is known about its activity as an anti-cancer drug [49-54]. For example, the mode of action of DCF in combination with HA in the local treatment of cutaneous AK is largely elusive, but its chemotherapeutic activity could be associated with drug induced apoptosis [86, 87]. In this thesis we proved DCF induced cell death in human dermal fibroblasts (HDFs) using a new effective, non-destructive *in vitro* model. Herein, HDFs were incubated together with a DCF-loaded electrospun poly-L-lactide (PLA) scaffold, which ensured to obtain a controlled drug release over 24 hours. The DCF exposed cells were imaged using multiphoton microscopy (MPM) and their metabolic activity was investigated using fluorescence lifetime imaging microscopy (FLIM). For the FLIM and MPM analysis reduced (phosphorylated) nicotinamide adenine dinucleotide (NAD(P)H), an endogenous fluorophore, was chosen as target [88]. NAD(P)H is mainly present in the mitochondria and directly involved in the ATP synthesis [89] which are both damaged in the cells after DCF exposure [90, 91]. Induced apoptotic and necrotic events were observed and then confirmed with ImageStream® analysis [92]. Besides, we investigated how the use of dimethyl sulfoxide (DMSO) as a co-solvent system in the electrospinning affected the scaffold morphology and its properties. Herein, we demonstrated that DMSO, a high boiling solvent, was not completely evaporated under our experimental conditions, thus being retained in the electrospun fibers. However, after water immersion DMSO diffused from the scaffold which regained the morphology typical of electrospun structures. Moreover, when the drug-loaded scaffolds were characterized we found that while diffusing DMSO enhanced DCF initial burst release. This aspect could be of great interest when producing nanofibrous scaffolds for drug delivery by electrospinning, also considering that DMSO is efficiently employed as a skin penetration enhancer in many pharmaceutical formulations [93, 94]. The effects of the presence of DMSO on the scaffold morphology were investigated using scanning electron microscopy (SEM). Besides, the effective release of DCF and DMSO from the electrospun

scaffolds was proved with energy-dispersive X-ray spectroscopy (EDX), reverse-phase high performance liquid chromatography (RP-HPLC) and nuclear magnetic resonance (NMR). The obtained results suggest that the here described model could represent an interesting way to control the diffusion of encapsulated bio-active molecules and test them using a marker-free, non-invasive approach.

2.2. Results

2.2.1. Production and characterization of the scaffolds

2.2.1.1. Electrospinning

PLA was dissolved in HFIP (+DMSO) either alone or in presence of DCF. Various electrospinning parameters were tested and those leading to stable Taylor's cone and jet as well as to smooth and uniform fibers (Fig.7 A-C, G-I and Fig.8 A-C, G-I) were then used throughout the study. The conditions were first defined for pure PLA and then adapted for the other (drug-loaded) scaffolds.

2.2.1.2. SEM and fiber diameter analysis

The morphology and fiber sizes of the scaffolds, before and after PBS immersion (after release, a.r.) was investigated using SEM (Fig.7 A-C, G-I and Fig.8 A-C, G-I). It was possible to generate scaffolds with a random fiber orientation. In all conditions, we obtained uniform scaffolds (Fig.7 A-C and Fig.8 A-C) but when using DMSO the fibrous morphology of the electrosun scaffolds appeared altered (Fig.7 A, C and Fig.8 A, C). After drug release (Fig.7 G-I and Fig.8 G-I), morphological changes were clearly visible in the samples electrospun using DMSO (Fig.7 G, I and Fig.8 G, I). In all cases, after the release experiment, the fibers were still uniform and randomly oriented (Fig.7 G-I and Fig.8 G-I). When using no DMSO the

fiber size was not affected after the drug release (PLA + DCF: 143±6 nm *versus* PLA + DCF a. r.: 146±9 nm; p=0.74). In all other cases there was a significant decrease in fiber size after 24 hours PBS immersion (PLA (w DMSO): 317±6 nm *versus* PLA (w DMSO) a.r.: 179±7 nm; p=0.004; PLA + DCF (w DMSO): 187±10 nm *versus* PLA + DCF (w DMSO) a.r.: 134±6 nm; p=0.008). Besides, when encapsulating DCF the fiber size significantly decreased (PLA + DCF (w DMSO) *versus* PLA (w DMSO), p=0.005). This happens probably because of the use of DCF as sodium salt, which enhances the conductivity of the solution used for the electrospinning experiment. A similar behavior was found by Kim et al. when working with the antibiotic cefoxitin sodium [95]. All the significant differences observed in the fiber size are shown in Fig.7M (**: $p \leq 0.01$).

2.2.1.3. Drug release experiments

2.2.1.3.1. UV-monitoring and fitting using Peppas equation

The ability of the scaffold to release the drug was firstly investigated by UV detection. The absorbance at 272 nm of the PBS solution, in which the drug-loaded scaffold was immersed, was constantly monitored for the first 6 hours and then was measured again after 24, 48 and 72 hours. In order to be sure that the absorbance was not affected by the release of solvent residuals, absorbance values were corrected against a blank represented by a PBS solution containing a pure PLA or a PLA (w DMSO) scaffold for the PLA + DCF scaffold and the PLA + DCF (w DMSO) scaffold, respectively. In all cases by the release experiments, the absorbance value at 272 nm was constant after the first 24 hours. This time was therefore set as the end point measurement. The amount of released drug was plotted over time (Fig.7N). The obtained points were also fitted using the equation developed by Peppas et al. (Fig.7O). The drug amount released after 24 hours was set as $M(\infty)$ in Peppas equation. Peppas equation offers a simple model to study the release mechanism of incorporated molecules from

polymers [37, 38, 96, 97]. No significant differences (p=0.82) in the release exponent (n) could be found between the sample containing DCF alone and the one containing DCF and DMSO, since the obtained values were 0.10±0.02 and 0.10±0.03 (p=0.87), respectively. In both cases the exponent values suggest that the release undergoes a controlled diffusion [97]. According to our results, the use of DMSO affects the initial burst release of the drug since the obtained values for the release rate constant (k) were 0.67±0.4 $h^{-0.1}$ and 0.42±0.3 $h^{-0.1}$ (p=0.003), when having DMSO or not, respectively.

2.2.1.3.2. RP-HPLC

The effectiveness of the DCF release from the scaffolds was verified using RP-HPLC. A binary gradient of CH_3CN/ddH_2O from 5 to 70% over 30 minutes (5→40% over the first 10 min followed by 40→50% over the next 15 min and 50→70% over the last 5 min) was used allowing a good separation for pure DCF in PBS (retention time: 19.7 min by 46.7% CH_3CN/ ddH_2O, Fig.S1A). The same conditions were then used also for the elution of the supernatant of the scaffold extracts. In all cases, DCF with a high purity could be eluted indicating that the encapsulated drug doesn't undergo any side-reaction during the electrospinning process. Chromatograms are reported in the supplementary materials section (Fig.S1B and Fig.S1C for DCF, released from pure PLA and PLA with DMSO, respectively).

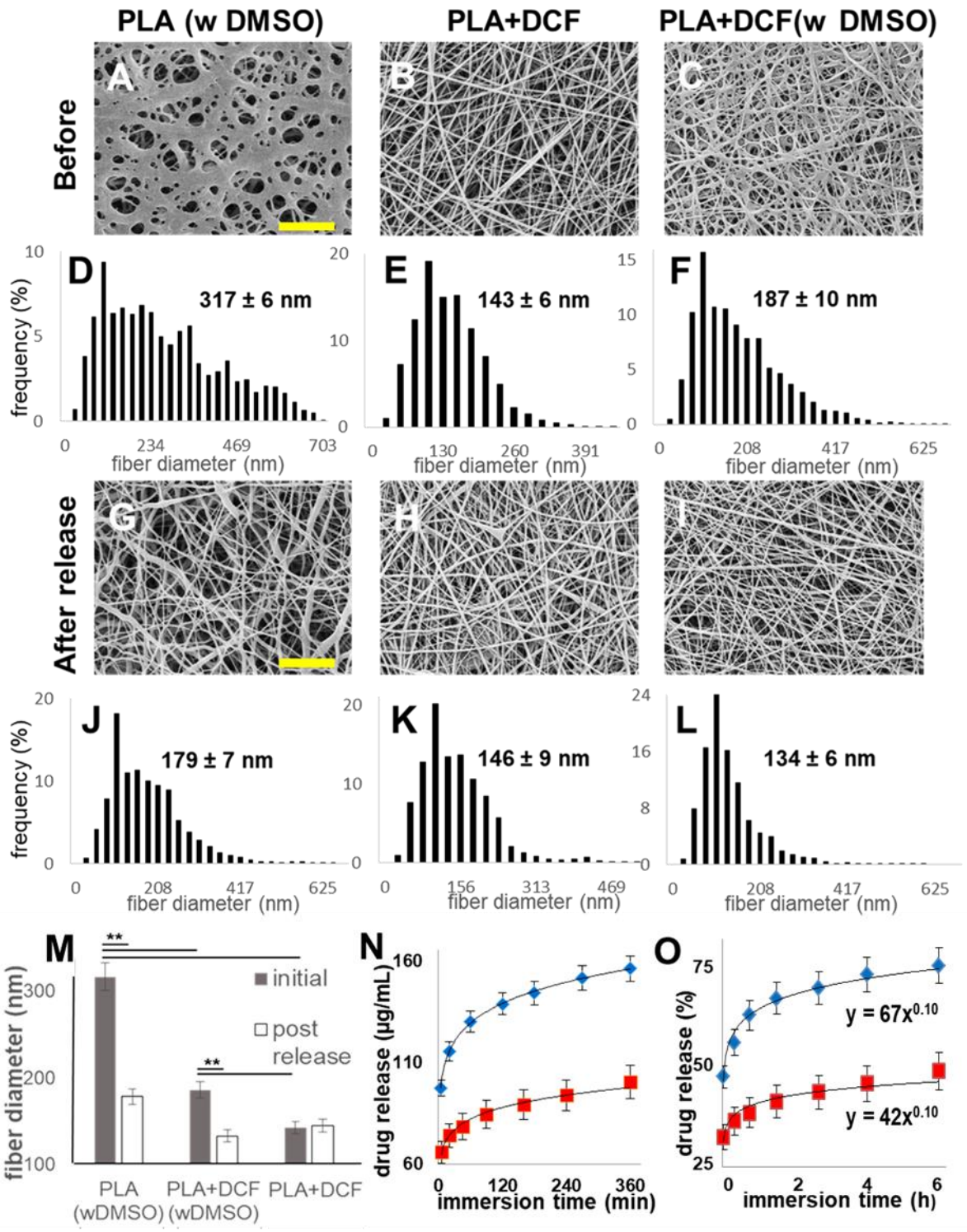

Fig.7. A-C and G-I. SEM images of the electrospun scaffolds at 2kX magnification before (A-C) and after (G-I) 24h PBS immersion (after release, a.r.). Scale bars equal 50 µm. A. Pure PLA (w DMSO); B. PLA + DCF; C. PLA + DCF (w DMSO). G. Pure PLA (w DMSO) a.r.; H. PLA + DCF a.r.; I. PLA + DCF (w DMSO) a.r. D-F and J-L. Histograms for the fiber distribution of the electrospun scaffolds before (D-F) and after (J-L) 24h PBS immersion

(a.r.). D. Pure PLA (w DMSO); E. PLA + DCF; F. PLA + DCF (w DMSO). J. Pure PLA (w DMSO) a.r.; K. PLA + DCF a.r.; L. PLA + DCF (w DMSO) a.r. M. Fiber mean diameter comparison after ImageJ® segmentation and DiameterJ® analysis. N-O. Drug-release profile (N) and fitting according to Peppas-Korsmeyer model (O) for the PLA + DCF scaffold (red squares) and the PLA + DCF (w DMSO) scaffold (blue rhombi).

2.2.1.3.3. Electron X-ray dispersive spectroscopy (EDX)

The effective DCF encapsulation and its release from the PLA scaffolds were verified with EDX analysis as well (Fig.8 D-F and Fig.8 J-L). Carbon (C) and Oxygen (O) signals arose mainly from PLA and did not allow us to assign them to the other molecules. Sulfur (S) signal was attributed to the presence of DMSO. Chlorine (Cl) and Sodium (Na) revealed instead the presence of DCF (Fig.8 D-F). After 24 hours PBS immersion (after release, a.r.), neither S nor Cl and Na signals could be detected (Fig.8 J-L), suggesting the diffusion of DMSO and DCF, respectively. Entire EDX spectra are reported in the supplementary materials (Fig.S2A-S6F) together with two example SEM images of the unsputtered scaffolds acquired to focus on the samples (Fig.S3).

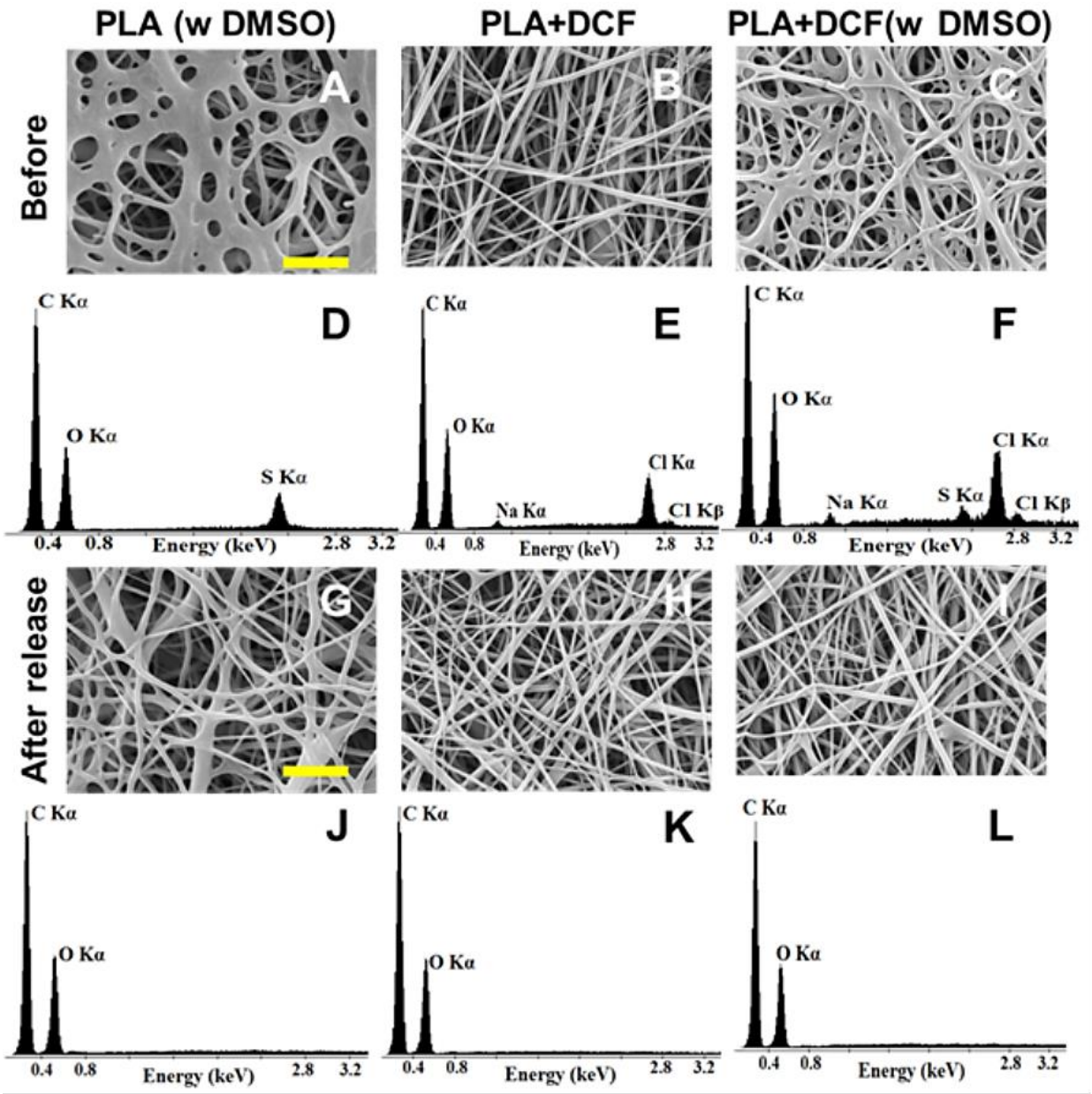

Fig.8. A-C and G-I. SEM images of the electrospun scaffolds at 10kX magnification before (A-C) and after (G-I) 24h PBS immersion (after release, a.r.). Scale bars equal 10 μm. A. Pure PLA (w DMSO); B. PLA + DCF; C. PLA + DCF (w DMSO). G. Pure PLA (w DMSO) a.r.; H. PLA + DCF a.r.; I. PLA + DCF (w DMSO) a.r. D-F and J-L. EDX spectra of the electrospun scaffolds before (D-F) and after (J-L) 24h PBS immersion (after release, a.r.) between 0 and 3.3 keV. D. Pure PLA (w DMSO); E. PLA + DCF; F. PLA + DCF (w DMSO). J. Pure PLA (w DMSO) a.r.; K. PLA + DCF a.r.; L. PLA + DCF (w DMSO) a.r.

2.2.1.3.4. Nuclear magnetic resonance (NMR) analysis

NMR analysis of the supernatant was done, after water removal by freeze-drying. PBS salts cannot be revealed by ^{1}H-NMR, and so did not affect the analysis. DCF 1mg/mL in D_2O was used as reference for signal comparison (Fig.9A). According to the NMR results, DCF diffused from both pure PLA (Fig.9B) and PLA with DMSO (Fig.9C). DMSO could be detected as well (singlet, δ = 2.71 ppm [98]) after its diffusion from PLA with DMSO (Fig.9C). The water signal (singlet, δ = 4.79 ppm [99]) could not be completely removed when using samples from the release experiments because the samples were too diluted (Fig.9B and 15C).

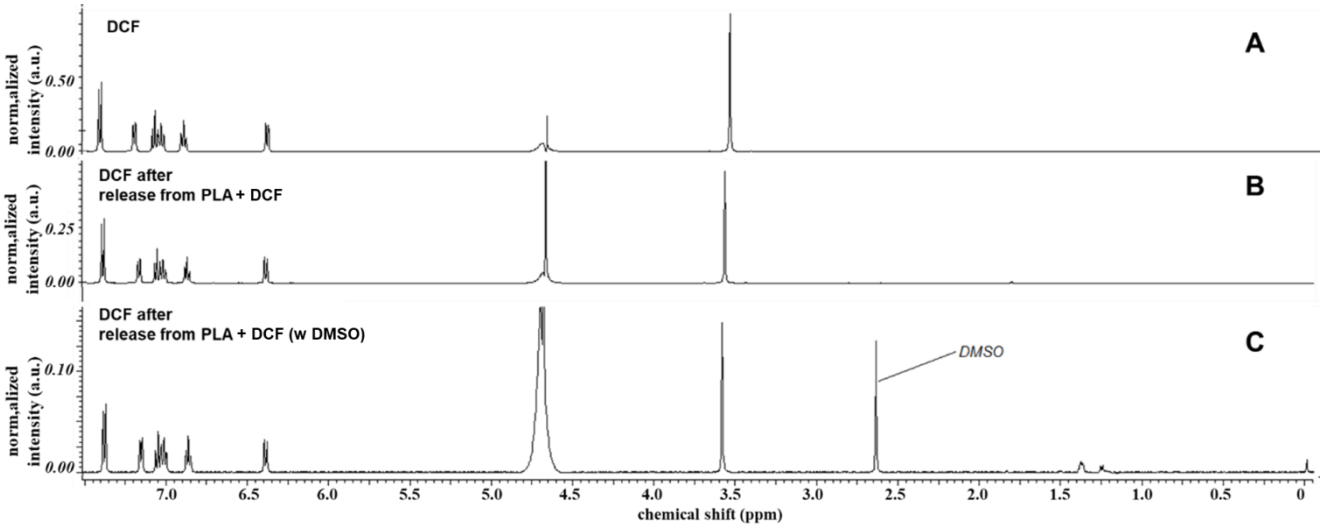

Fig.9. A. ^{1}H-NMR spectra in D_2O of pure DCF. B, C. ^{1}H-NMR spectra of the extracts in PBS of DCF-loaded PLA (B) and DCF-loaded PLA (w DMSO) (C) scaffolds after water removal by freeze-drying.

2.2.1.4. Tensile tests

PLA is an elastic and electrospinnable polymer. Pure electrospun PLA was previously characterized [88]. Representative stress-strain experimental curves are shown in Fig.10A-C. Generally, the mechanical properties of PLA were affected by the addition of DCF and DMSO (Fig.10A-E). The DCF encapsulation lowered the scaffold elasticity (Fig.10D, E-modulus, PLA + DCF: 133.8±13.6 MPa *versus* PLA: 24.4±9.7 MPa [88], p=0.0002; PLA + DCF (w DMSO): 74.8±9.7 MPa *versus* PLA (w DMSO): 14.0±1.2 MPa, p=0.004). Opposite, DMSO retain improved scaffolds elasticity, lowering the E-modulus (Fig.10D, PLA (w DMSO) *versus* PLA, p=0.0012; PLA + DCF (w DMSO) *versus* PLA + DCF, p=0.006). Generally, the E-modulus decreased with the increasing fiber diameter as previously described [100, 101]. However, the DCF encapsulation strongly increased the E-modulus, making the scaffold structure less elastic (Fig.10D). Not so big differences could be found in regards to tensile strength (Fig.10E). Nevertheless, pure PLA showed the highest tensile strength (1.84±0.19 MPa [88]). Actually, the addition of either DCF or DMSO as well as both of them led to significantly lower tensile strength values (Fig.10E, PLA (w DMSO): 0.83±0.18 MPa; PLA + DCF: 1.02±0.19MPa; PLA + DCF (w DMSO): 1.37±0.17 MPa) when compared with pure PLA ($p \leq 0.01$ in all cases). Moreover, the scaffold containing both DCF and DMSO showed a tensile strength significantly higher when compared to the other PLA scaffolds containing only one of the two encapsulated molecules (Fig.10E, PLA + DCF (w DMSO) *versus* PLA (w DMSO), p=0.0034; PLA + DCF (w DMSO) *versus* PLA + DCF, p=0.0073). According to these results we suggest that the DCF encapsulation alters the PLA mechanical properties, but no direct correlations between the fiber morphology and the scaffold properties can be determined. On the other hand, DMSO encapsulation lowers E-modulus and tensile strength values. That finding can be correlated with the increase in the fiber size (Fig.7M) according to literature data [100, 101].

2.2.1.5. Contact angle measurements

Wettability of the scaffolds was determined using contact angle measurements. The analysis showed that the hydrophobicity of the scaffolds was not significantly affected by the presence of DCF and/or DMSO (Fig.10F). No significant changes were observed in the contact angle values for all the scaffolds characterized in this work (Fig.10F, PLA w DMSO: 132±2°; PLA + DCF: 129±3°; PLA + DCF w DMSO: 131±3°) when compared to pure PLA (131±7°, [88]). The measurements suggest that all the scaffolds remained hydrophobic (Fig.10E).

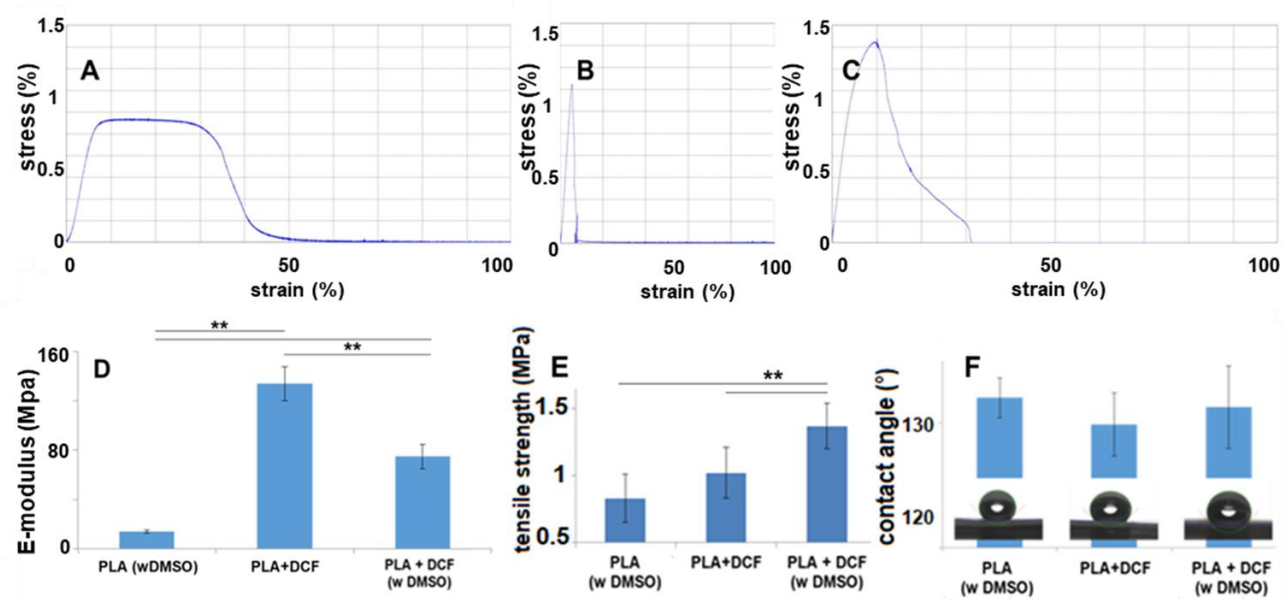

Fig.10. Analysis of the mechanical/physical properties of the electrospun scaffolds. A-C. Representative stress-strain curves of: a DMSO-containing PLA (PLA (w DMSO)) scaffold (A), a DCF-loaded PLA (PLA + DCF) scaffold (B) and a DMSO-containing DCF-loaded PLA (PLA + DCF (w DMSO)) scaffold (C). D.Comparison of the elastic modulus (E-modulus) among the PLA (w DMSO), PLA + DCF and PLA + DCF (w DMSO) scaffolds. E. Comparison of the ultimate tensile strength among the PLA (w DMSO), PLA + DCF and PLA + DCF (w DMSO) scaffolds. F. Contact angle values, after water drop deposition, of the PLA (w DMSO), PLA + DCF and PLA + DCF (w DMSO) scaffolds.

2.2.1.6. In vitro cytotoxicity

The biocompatibility of the modified scaffolds was assessed with a MTS assay [102] using a standardized protocol and HDFs as cells, as previously described [88]. Accordingly, we determined that the use of DMSO did not affect PLA scaffold biocompatibility (cell proliferation: PLA (w DMSO) = 102±7%). On the other hand, the DCF containing scaffolds showed a severe cytotoxicity towards HDFs (cell proliferation: PLA + DCF = 12±1%; PLA + DCF (w DMSO) = 13±2%, $p \leq 0.01$ in both cases when compared to the NC). Thus, we assessed the scaffolds cytotoxic effects as a result of the DCF release, while the DMSO concentration in the extracts was probably too low to determine cytotoxic effects [103-105]. The results of the MTS assay are reported in the supplementary materials (Fig.S4).

2.2.2. MPM and FLIM analysis

MPM and FLIM analyses were performed to analyze endogenous NAD(P)H in HDFs and to detect metabolic changes and cytotoxic effects in the target cells due to the incubation together with the drug-loaded scaffolds. In order to demonstrate that the observed cytotoxicity would be due to DCF and not to the presence of the scaffold itself limiting, for example, the oxygen exchange, the measurements were carried out either in presence or in absence of a pure PLA scaffold by using as control HDFs on glass. Besides, the treated cells were analyzed also after the removal of the scaffold. In all cases, no significant differences after 24 hours incubation time in the α_1(%) and τs values could be found between the compared samples (Fig.S5). Once assessed that the presence of the scaffold did not affect the FLIM measurements, we decided to investigate the supposed DCF cytotoxicity towards HDFs after its release from PLA scaffolds. The DCF-loaded scaffolds used by the FLIM analysis were all electrospun without DMSO, in order to limit the variables and to ascribe the potential cytotoxicity only to DCF. The *in vitro* system described in this thesis ensured us to have a

controlled drug release over 24 hours. Two different time points, 6 and 24 hours, were chosen. The first one represented the reaching of a maximum in the drug release profile (Fig.7N), while the second one represents the incubation time used for the MTS assay. The control (CTRL) was also measured after 6 and 24 hours (times refer to the incubation time after having changed the culture medium, 24 hours after cell seeding). However, since no significant differences in the α_1 and τs values could be found in the CTRL for the two different time points, only the values obtained after 6 hours incubation were analyzed. Besides the FLIM analysis, MPM images were acquired to monitor cell morphology. Cell morphology appeared altered in the treated cells already after 6 hours (Fig.11B) when compared to the control (Fig.11A). However, cell showing the normal elongated fibroblasts shape could still be imaged after the first 6 hours DCF exposure (Fig.11B). After 24 hours cell morphology appeared completely different from the one of the control. In particular, cells that showed a nuclear and cytoplasmic condensation were assessed as apoptotic (Fig.11C), while cells showing both swelling and vacuolation of the cytoplasm were considered to undergo necrosis (Fig.11D), as previously described by Seidenari et al. [28]. According to the FLIM analysis already after 6 hours a significant increase in the τ_1 values (Fig.11E, τ_1 CTRL: 0.63±0.02 ns *versus* τ_1 DCF/6h: 0.72±0.02 ns, p=0.003) as well as a significant decrease in the α_1% values could be detected for the DCF-exposed cells, when compared with the control (Fig.11F, α_1% CTRL: 73.3±0.9% *versus* α_1% DCF/6h: 63.9±1.1%, p=0.002). After 24 hours incubation a significant increase in the τ_1 values could still be found for the treated sample when compared with the control (Fig.11E, τ_1 CTRL: 0.63±0.02 ns *versus* τ_1 DCF/24h: 0.74±0.02 ns, p=0.0025). On the other side, the difference in the τ_1 values after 24 hours was not significant when compared to the ones obtained after 6 hours (Fig.11E, τ_1 DCF/6h: 0.72±0.02 ns *versus* τ_1 DCF/24h: 0.74±0.02 ns, p=0.47). The α_1% values of the samples after 24 hours incubation instead significant decreased when compared to both control (Fig.11F, α_1% CTRL:

73.3±0.9% *versus* α_1% DCF/24h: 62.1±1.2%, p=0.0016) and 6 hours exposed cells (Fig.11F, α_1% DCF/6h: 63.9±1.1% *versus* α_1% DCF/24h: 62.1±1.2%, p=0.0084).

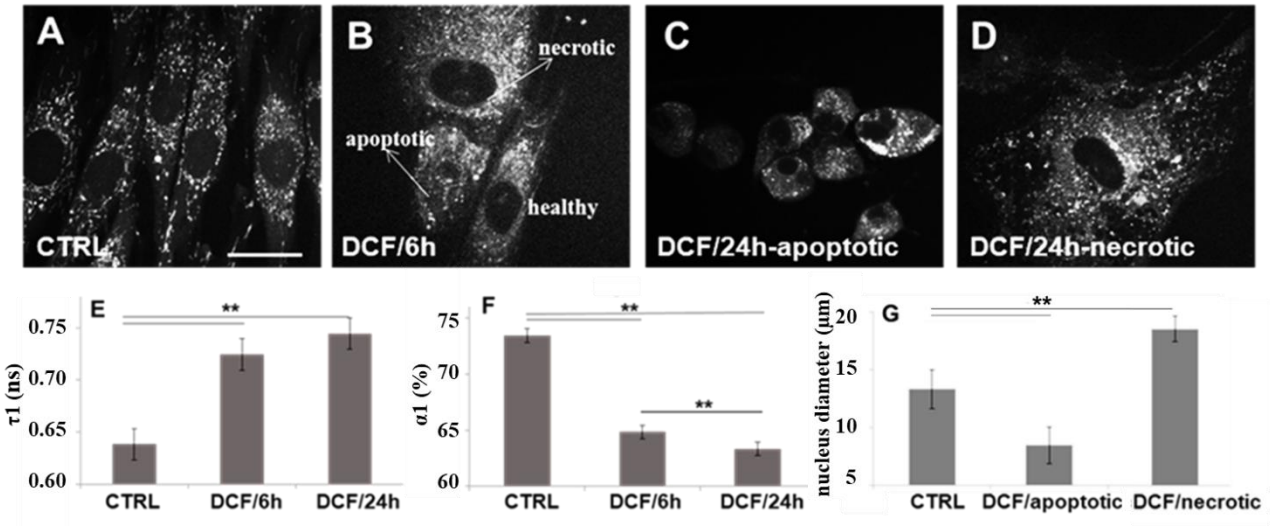

Fig.11. MPM imaging (A-D) and FLIM analysis (E, F) of HDFs exposed to a DCF-loaded PLA scaffold. A-D Untreated HDFs (A); DCF-treated HDFs after 6h incubation time (B); DCF-treated HDFs assessed as apoptotic (C) and necrotic (D) after 24h incubation time. Scale bar equals 20 μm. E. Comparison of the τ_1 values among control (CTRL) and DCF-treated samples after 6 and 24h. F. Comparison of the α_1 (%) values among CTRL and DCF-treated samples after 6 and 24h. G. Comparison of the nucleus diameter values among normal untreated fibroblasts (CTRL) and DCF-treated cells assessed either as apoptotic or necrotic.

According to these morphological changes, we were also able to determine changes in the nucleus diameter [28] of the fibroblasts after the 24 hours DCF exposure (Fig.11G). In particular, cells assessed as apoptotic showed a significant decrease in the nucleus diameter when compared to the untreated samples (Fig.11G, DCF/apoptotic: 7.8±1.7 μm *versus* CTRL: 13.1±2.2 μm, p=0.007). On the other hand, necrotic cells had an increase in the nucleus diameter (Fig.11G, DCF/necrotic: 18.7±1.4 μm *versus* CTRL, p=0.008) due to a significant cytoplasmatic swelling.

2.2.3. ImageStream® analysis

DCF induced cell death was proved with ImageStream® since it is considered a reliable method [92]. In particular, Annexin V was used as a marker for apoptosis (blue staining) and 7-AAD for necrosis (red staining, Fig.12A). It was also possible to distinguish between early and late apoptotic cells, since the first ones could be only stained with Annexin V (Fig.12A) while the second with both Annexin V and 7-AAD (Fig.12A). According to the ImageStream® analysis both apoptotic and necrotic events occurred, but while about 40% (39.4±4.7%, Fig.12B) of the cells did undergo necrosis already after 6 hours DCF exposure, only obout 10% of them were either early (4.6±0.7%, Fig. 18C) or late apoptotic (6.8±0.4%, Fig.12D), after 6 hours DCF exposure. After 24 hours about 50% of the cells were instead either early (21.1±3.8%, Fig. 18C) or late apoptotic (28.2±2.3%, Fig.12D). This observation agrees with previous works that show how necrotic events generally occur earlier than apoptotic ones after cell exposure to toxic hazards [106, 107]. However, we believe that the real percentage of dead cells in the DCF treated samples would be greater, since we only took into account the cells that were still adherent, which are the same analyzed by FLIM. Finally, about 20% of dead cells could be found already in the control (20.8±2.2% and 25.1 ±2.3% after 6 and 24 hours, respectively, Fig.12B) mainly because of being out of the incubator during the FLIM measurements as well as by preparing the samples for the ImageStream® analysis. Besides, also the chosen cell harvesting method could affect the results of the analysis leading to an overestimation of the necrotic cells [108]. Nevertheless, the percentage of the apoptotic (either early or late) and of the total dead cells was significant higher in the treated samples when compared to the control, both after 6 (Fig.12B, DCF treated: 50.8±5.3% *versus* CTRL: 20.8±2.2%, p=0.008) and 24 hours (Fig.12B, DCF treated: 56.7±5.6% *versus* CTRL: 25.1 ±2.3%, p=0.007).

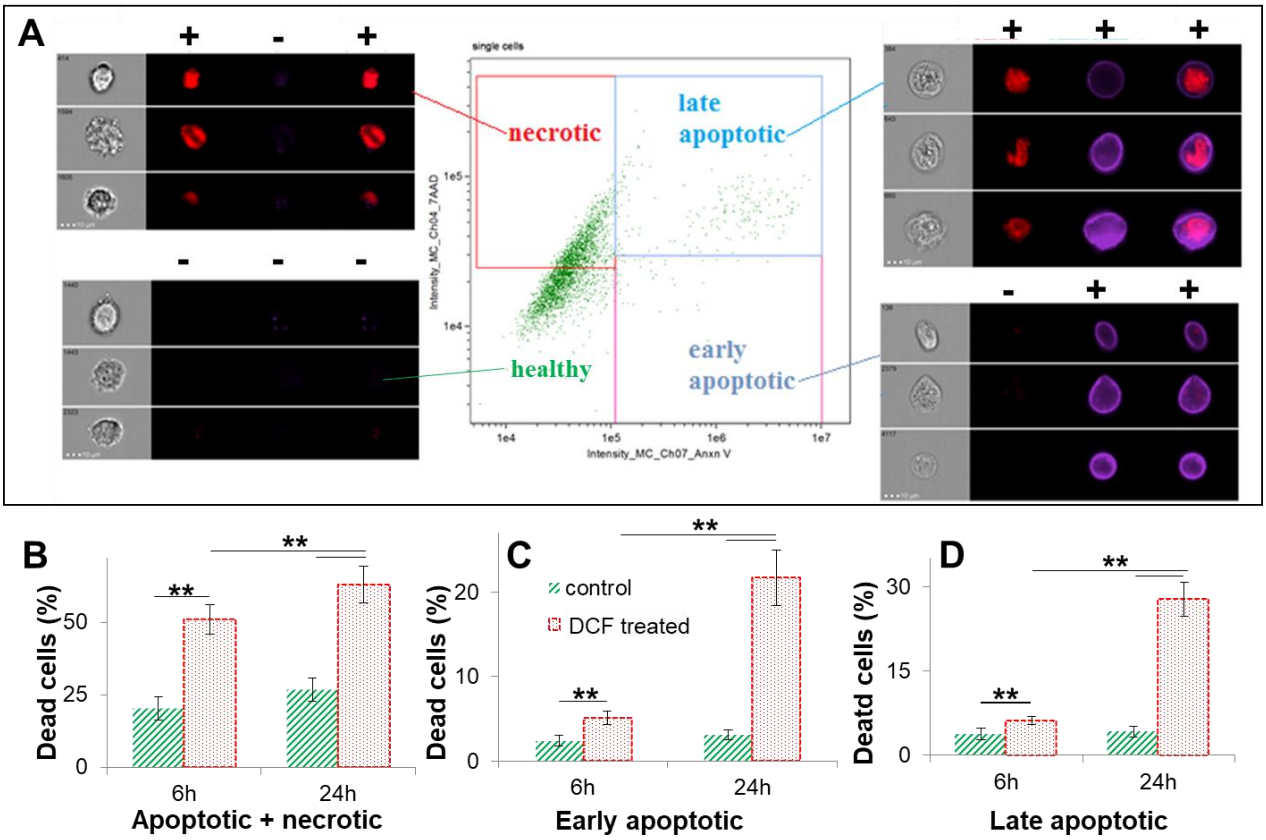

Fig.12. ImageStream® analysis of HDFs exposed to a DCF-loaded PLA scaffold. A. Staining with Annexin V (blue) and 7-AAD (red) allowed us to distinguish among healthy (blue-; red-), necrotic (blue-; red+), early (blue+; red-) and late (blue+; red+) apoptotic cells. B-D. Data analysis of the cells after staining and counting (CTRL: green stripes; DCF treated: red dots): total percentage of dead cells (B); early (C) and late (D) apoptotic cells percentage.

2.2.4. MPM and FLIM real time analysis

Since we could find a strong significant change in both α_1 (%) and τ_1 values, as well as in the cell morphology of HDFs, already after 6 hours incubation together with a DCF-loaded scaffold, we decided to analyze the treated cells over the first 6 hours exposure too. Using a IBIDI® heating system we analyzed always the same cells with MPM and we could image the morphological change due to the induced cell death (Fig.13 A-L).

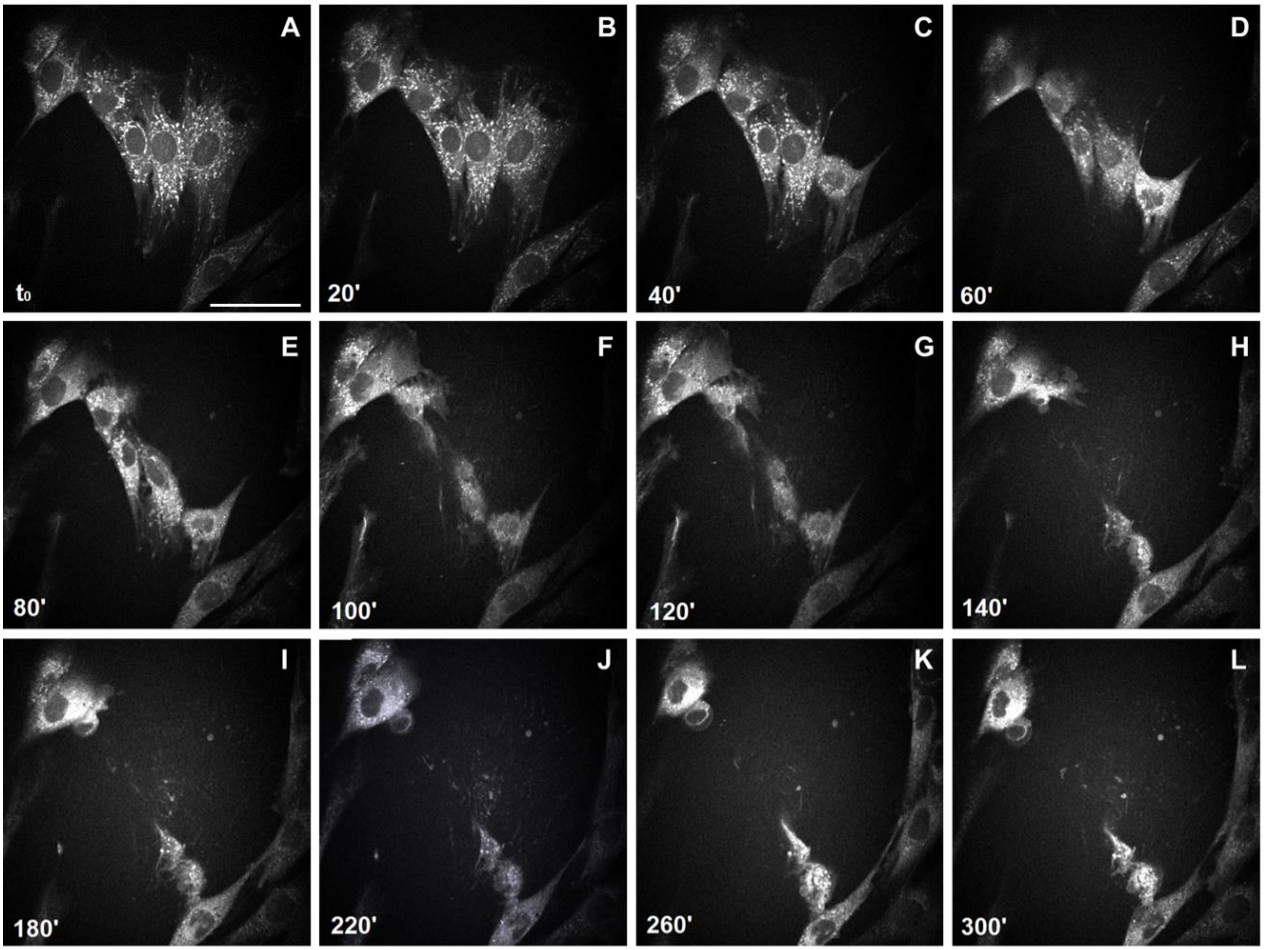

Fig.13. MPM imaging of HDFs exposed to a DCF-loaded PLA scaffold for 5 hours. Dish was kept by 37°C using a IBIDI® heating system that suited the microscope and the same cells were imaged every 20 minutes for the first 140 minutes (A-H) and then every 40 minutes (I-L). Scale bar equals 50µM.

Cells were imaged every 20 minutes (after 140 minutes images are shown every 40 minutes since no morphological differences could be detected every 20 minutes after that time). 300 minutes (Fig.13L) represented the last point since after 5 hours the analyzed cells were detached and appeared out of focus (images not shown). Separetely, we performed a FLIM analysis of DCF-exposed cells over the first 6 hours too. By fitting the FLIM values with a linear regression (Fig.14) we could find a linear increase (R^2=0.998) of the τ_1 values over the first 6 hours (Fig.14A) and a linear decrease for the α_1 (%) values (Fig.14B), even if the regression coefficient was in the second case worse (R^2=0.973).

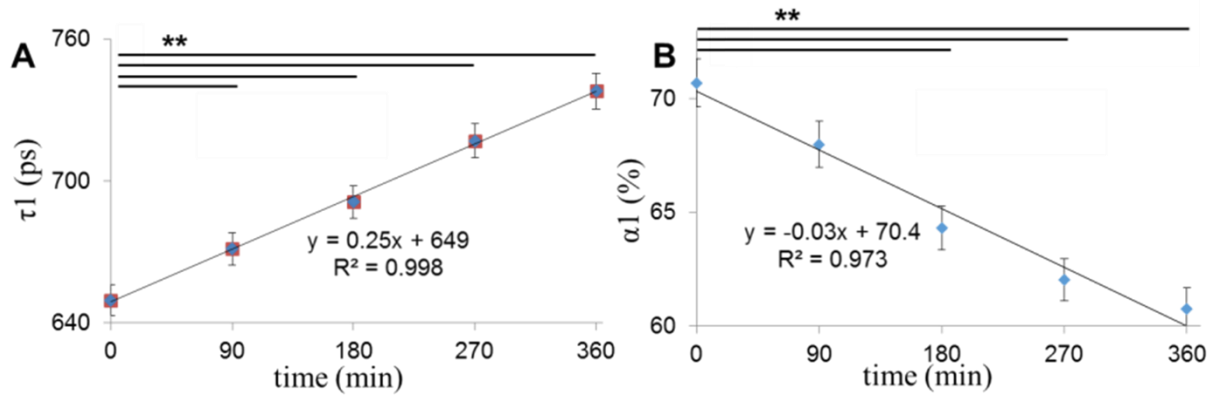

Fig.14. Linear regression fitting for the τ_1 (A) and α_1% (B) values of HDFs exposed to a DCF-loaded PLA scaffold for 6 hours.

τ_1 values significant increased already after 90 minutes DCF exposure (τ_1 (t=0): 649±4 ps *versus* τ_1 (t=90 minutes): 672±5 ps, p=0.0031, Fig.14A), while the α_1(%) significantly decreased first after 3 hours (α_1% (t=0): 70.4±1.6% *versus* α_1% (t=180 minutes): 64.2±1.3% ps, p=0.0016, Fig.14B). The better linear regression found by analyzing the τ_1 values (R^2=0.998, Fig.14A) in comparison to the one obtained for α_1% (R^2=0.973, Fig.14B) could be probably because the first refers to changes in the microenvironment, that is cell independent [109, 110], while the second to metabolic ones [110].

2.3. Discussion

Improved *in vitro* models are required to aid scientists in identificating and investigating candidate molecules for pharmaceutical development [111]. It is to time well accepted especially in the European Union that *in vitro* models will not be able to replace animal testing in the next future [111-113]. However, the scientific community agrees that animal studies are expensive, and it would be desirable to minimize this necessary part of drug testing, also because of the associated ethical issues [114-116]. *In vitro* studies are generally less expensive, faster and more flexible than regulated *in vivo* tests [111]. Nevertheless, the limited reliability and *in vivo* reproducibility of existing *in vitro* tests place great emphasis on

the need for more realistic models. Over the last decades, many investigators have been researching on *in vitro* assays that should enable informed strategic decisions already during screening processes, thus avoiding entire animal testing [113]. One of the biggest limits of the nowadays available *in vitro* systems by assessing the toxicity of drugs is the necessity to work with specific concentrations of the investigated substance. This approach is good to assess dangers and risks related to the hazards, but it doesn't really reproduce the therapeutic situation [111]. Controlled delivery over time can in this way better mimic the drug bioavailability after its administration, and can also help to reproduce the real daily dosages. Nano-delivery systems represent a great future perspective in this field, and are gaining a constantly growing interest among scientists [117]. In this thesis, we could effective encapsulate DCF in a PLA electrospun scaffold, finally having a system that allowed us to obtain a controlled drug delivery over 24 hours. Furthermore, we were able to enhance the initial release of DCF from our system by simply adding DMSO without changing neither the DCF content in the scaffold nor the drug-release profile. According to our results we believe that the encapsulated DMSO rapidly diffuses from the PLA scaffold carrying DCF as well. The effectiveness of the DCF/DMSO encapsulation and their subsequent release were proved by parallel using different analyses. The effective release of DCF from the electrospun scaffolds (either containing DMSO as well or not) was firstly proved with RP-HPLC. Besides, we investigated the release mechanism using Peppas equation, which offers a simple model to study drug-release mechanisms [37, 38], also from electrospun scaffolds [96, 97]. According to the obtained experimental release exponent the drug undergoes a controlled diffusion from the electrospun scaffolds [38]. Interestingly, the addition of DMSO doesn't alter the drug diffusion mechanism but only enhances the initial burst release of DCF. Nevertheless, the fibrous morphology of the scaffold appears clearly altered according to SEM observations, when having DMSO in the electrospun materials. The DMSO containing fibers seem crosslinked or merged [118]. However, no beads formed and the structure still appears

homogeneous. Moreover, after the release experiments, the DMSO containing samples regained the fibrous structure typical of electrospun scaffolds. The changes in the scaffolds morphology were related to the encapsulation of DMSO and its subsequent release according to our observations. To confirm our hypothesis we proved DMSO and DCF encapsulation with EDX, and their release with ^{1}H-NMR and EDX as well. EDX analysis has already been employed to investigate the elemental composition of electrospun scaffolds [119]. In our case, we used pure PLA as polymer, a polyester composed of only Carbon (C), Hydrogen (H) and Oxygen (O). On the other side, DMSO contains Sulphur (S) as well, while DCF Sodium (Na) and Chlorine (Cl). Thus, we could correlate the presence of DMSO with the presence of S peak on the EDX spectrum, and Cl and Na signals to the effective DCF encapsulation. Interestingly, after the release experiment (24 hours PBS immersion) only C and O signals could be detected from all the scaffolds, suggesting the diffusion of both DMSO and DCF from the starting functionalized materials, with a final content lower than 10% in weight, due to EDX detection limits [120]. Besides, with ^{1}H-NMR we could also demonstrate that DCF and DMSO were released unmodified from the electrospun scaffolds. This analysis was in our opinion necessary to prove that the encapsulated molecules effectively undergo a diffusion and not degradation or modification during the whole processing. This aspect is particularly important in this part of the thesis, since our final purpose was to prove DCF cytotoxicity towards HDFs. Before investigating the effects of DCF on HDFs, we characterized the mechanical properties of the electrospun scaffolds. We observed that the DCF encapsulation strongly affected scaffold elasticity, since the DCF containing electrospun scaffolds showed a much higher Young's modulus, as well as a lower elongation at break, than the ones not containing it. On the other hand, the hydrophobicity of the scaffolds was not affected when having DMSO and/or DCF, since the contact angle of all the modified scaffolds was not significant different when compared to pure PLA. After having characterized the mechanical properties of the scaffolds, we could demonstrate that cytotoxic effects were related to the

diffusion of the unmodified DCF according to the results of an accredited MTS assay. Instead, the presence of DMSO in the scaffolds did not affect PLA biocompatibility, probably because of its low amount [103-105]. This result is interesting, and suggests that DMSO could be effectively encapsulated in electrospun scaffolds to tune their properties, and enhance drug diffusion from the delivery systems. According to our idea, the drug-loaded scaffolds can be used as models to mimic the daily dosage, ensuring controlled drug diffusion over 24 hours. We believe that electrospinning offers in this way a broad spectrum of possibilities to encapsulate different drugs and ensure their controlled diffusion [3]. In the final part, thanks to MPM coupled with FLIM, we could analyze HDFs exposed to DCF and assess drug toxicity. A well-recognized effect of high concentrations of DCF is rapid and concentration-dependent cellular energy depletion [76]. Masubuchi et al. [76] have demonstrated that a relevant ATP depletion occurs in rat hepatocytes, when exposed to high DCF concentration (up to 100 µM). The ATP depletion is almost complete when working with DCF 500 µM [76]. Drug-induced oxidative stress can primarily recruit rescue pathways, but, if sustained, the stress can cause mitochondrial injury [80, 81]. Thus, the cells are usually not able anymore to repair the damage, and apoptotic or necrotic events mainly occur [82-84]. In this thesis, using MPM we could image changes in the morphology of the treated HDFs that allowed us to distinguish between necrotic and apoptotic cells [66, 123]. DCF induced cell death could be imaged even live over 5 hours, always analyzing the same cells. These morphological observations were confirmed with ImageStream® [92]. According to these data, we could prove that both apoptotic and necrotic events occurred in HDFs, when exposed to DCF. Besides, the FLIM analysis showed us changes in the cell metabolism of HDFs after DCF exposure, in terms of decrease in the contribution of free NAD(P)H (α_1%) to the glycolytic activity. At the same time the fluorescence lifetime of free NAD(P)H (τ_1) significantly increased. Free NAD(P)H is mainly located in the cytoplasm [124]. Thus, we believe that the significant change in its fluorescence lifetime is mainly to attribute to the changes in its

microenvironment, since especially in the necrotic cells the cytosol content is released after the disruption of the cell membrane [123]. The use of MPM coupled with FLIM by cell imaging and analysis, together with the choice of electrospun scaffolds as substrates for the drug delivery, could offer a new marker-free, not destroying method for the *in vitro* investigation of effects and mechanism of action of drugs. Actually, using this experimental setup we were able to image DCF induced cell death in HDFs thanks to MPM and analyze changes in the cell metabolism using FLIM. As a perspective, the here proposed model could be extended to longer studies where each 24 hours (or at specific time points) the target cells can be supplied with new culture medium and a new drug-loaded scaffold containing the desired drug amount. A big limit of many already existing *in vitro* systems is that the cells get damaged or die directly after the analysis, and so cannot be monitored over time [121]. Using MPM and FLIM, we were instead able to image and analyze the (same) cells at different time points. This aspect is of great interest since the here used approach could allow *in vitro* analysis over a long time that can represent, for example, the expected whole therapy in case of having adequate cell culture systems [122]. In the next future we aim to use the here proposed *in vitro* model also with other drugs and different cell lines in order to assess its reliability, and find new possible application fields. Furthermore, we aim to use the same setup with *in vitro* skin models instead of HDFs. These models would better represent the *in vivo* behavior than monolayer cell cultures. Moreover, we aim to further investigate how the use of DMSO affects the morphology and the drug-release profile of electrospun scaffolds. In particular, our challenge would be to find out if they can be predicted and controlled, by for example using different DMSO volumes, in order to tune the final properties of the scaffold.

2.4. Conclusions

In this part of the thesis we were able to effectively encapsulate DCF in a PLA scaffold, producing a system that allowed us to obtain a controlled drug release over 24 hours. HDFs were incubated together with the DCF-loaded electrospun PLA scaffold and then imaged with MPM. According to the observed morphological changes and the ImageStream® analysis, DCF trigger both apoptosis and necrosis in HDFs. Besides, metabolic changes in the treated cells were detected using FLIM. The model here proposed is marker-free and not destroying, and could represent a new interesting perspective for the *in vitro* testing of drugs or hazards. Moreover, we proved that the use of DMSO as co-solvent of HFIP alters the properties of electrospun PLA scaffolds. We found out that DMSO cannot be completely evaporated during the electrospinning process and remains retained within the fibers. Thus, the fiber size increases and this leads to lower tensile strength and E-modulus for the scaffold. However, after water immersion, DMSO diffuses and the fibers regain their normal morphology. When encapsulating DCF too, DMSO enhances its initial burst release from the PLA scaffold. These results suggest that DMSO could be used in small volumes as a co-solvent by electrospinning to module the properties of electrospun scaffolds without impacting on their biocompatibility.

CHAPTER 3. PRODUCTION AND CHARACTERIZATION OF AN ELECTROSPUN PLA SCAFFOLD LOADED WITH A SYNTHETIC DICLOFENAC PRODRUG FOR THE LOCAL TREATMENT OF ACTINIC KERATOSIS

3.1. Introduction

The medical term “actinic keratosis (AK)” identifies small skin lesions, which appear as round, rough spots between 5 mm and 1 cm in diameter. AKs are characterized as pre-cancerous or as early-stage tumors [125, 126]. This pathology is also known as "solar keratosis" or "senile keratosis" because it is more common to people over 50 with fair skin and is related to a prolonged sun-damage [125]. This process, also known as photoaging, leads to an accumulation of oncogenic changes [126]. Changes related to photodamage are most evident in the extracellular matrix (ECM) [127]. The accumulation of these changes leads to a pathological ECM mainly due to the degradation and fragmentation of its components such as elastic fibers [128]. As a result, the normal repair and regenerative capacity of the ECM is inhibited [128-130]. Skin ageing processes also have a significant impact on cellular mechanisms such as DNA repair, gene expression and immune response modulation [129]. AK is considered a key event in the progression from photoaged skin to the invasive squamous cell carcinoma (SCC) [43, 126]. SCC affects the keratinocytes of the epidermis layer and is the second most diffused skin cancer after the basal cell carcinoma (BCC) [125, 131]. However, there are many more AKs than SCCs and it is difficult to predict exactly which lesions will progress to invasive cancer [125, 126]. About 15% of the men and 6% of the women in Europe are affected by AKs. The percentages rise respectively to 34% and 18% in the European population over 70 years of age [131]. Since the average life expectancy is increasing, it is predicted that even more people will be affected by AKs in the next years [125, 126]. Although a number of treatments are already available [132-134], the development of effective, more targeted and well-tolerable therapies for the treatment of AKs

is still of great interest. The first therapy approved by the Food and Drug Administration (FDA) for the topical treatment of AKs was 5-Fluorouracil in 1962 [132] followed by Imiquimod in 1997 [132], Diclofenac sodium salt (DCF) in 2002 [133, 134] and Ingenol Mebutate in 2012 [134]. Among them, DCF is currently the therapy of choice in terms of costs, effectiveness, side effects and tolerability [135]. Diclofenac belongs to the class of non-steroidal anti-inflammatory drugs (NSAIDs) and is one of the most commonly used in the world [135]. It is still not clear how DCF affects AKs, but its activity seems to be related to anti-inflammatory and anti-angiogenic effects [136]. Induced apoptosis has been also proposed as a possible DCF mechanism of action in the treatment of AKs [137]. The absorption of a drug through the outermost layer of the skin, the *stratum corneum* (SC), is limited [138]. Thus, a specific formulation of DCF commercially known as Solaraze® is needed for the effective treatment of AKs. This formulation is supplied with hyaluronic acid that enables DCF accumulation in the epidermis [139]. Considering these aspects, a chemical modification of Diclofenac that enhances its permeation through the SC is of interest since it could improve its efficacy against AKs.

Over the last two decades, electrospinning has gained growing interest as a potential polymer processing technique for applications in tissue engineering [140, 141] and drug delivery [3]. Electrospinning is an easy way to fabricate fiber-containing scaffolds with a fiber diameter in the nano- to micrometer size scale that mimic the structure and morphology of the ECM components in the skin [140-142]. Biodegradable and natural materials can be electrospun, and a wide range of molecules like drugs and proteins can be incorporated in the scaffolds [3]. Polylactic acid is a biodegradable, biocompatible polymer with beneficial mechanical properties. Moreover, it is stable over a long time and its degradation proceeds through the hydrolysis of the ester linkage in the polymer's backbone resulting in a non-toxic degradation product called lactic acid [143, 144].

In this study, we aimed to encapsulate a chemical modified and synthetically produced Diclofenac prodrug in an electrospun poly-L-lactide (PLA) scaffold in order to obtain a suitable drug delivery system to locally treat AKs. Specifically, the prodrug was successfully synthesized by binding Diclofenac to a glycine residue via solid phase peptide synthesis (SPPS) and then incorporated in an electrospun PLA scaffold. The drug encapsulation was verified using multiphoton microscopy (MPM) and its release was monitored spectrophotometrically and confirmed with MPM as well. The scaffold was further characterized with scanning electron microscopy (SEM), tensile testing and contact angle measurements. Its biocompatibility was verified by performing a cell proliferation assay and compared to PLA scaffolds containing the same amount of DCF. Finally, the effect of the electrospun scaffolds on human dermal fibroblasts (HDFs) morphology and metabolism was investigated by combining MPM with fluorescence lifetime imaging microscopy (FLIM). The obtained results suggest that the obtained scaffold could be suitable for the controlled and targeted delivery of the synthesized prodrug for the treatment of AKs. A controlled and targeted drug delivery to the region of interest could reduce the undesired side-effects and enhance the efficacy of the therapy. The work described in this chapter and its final goal are schematized in Fig.15.

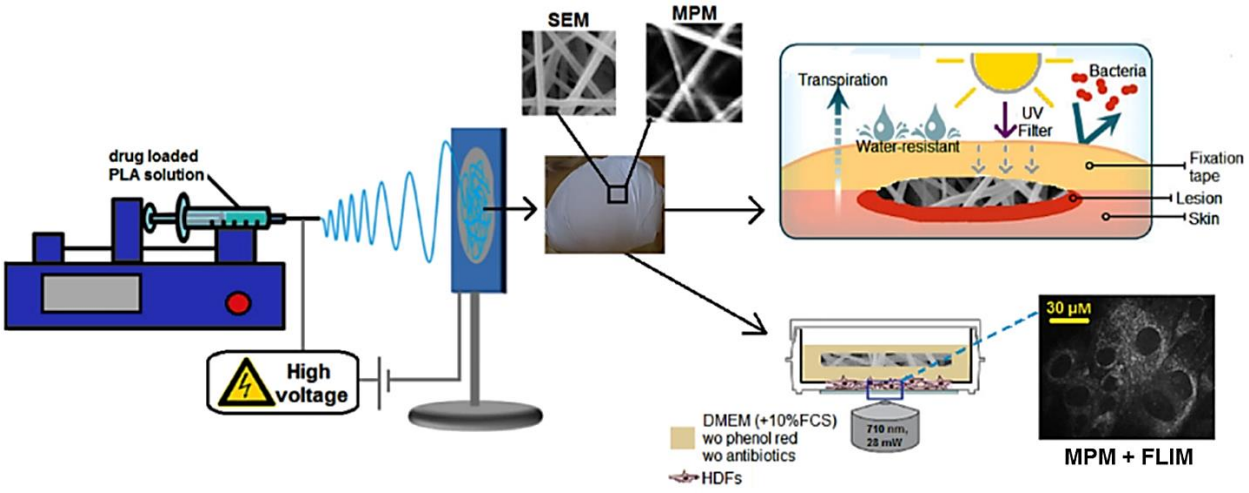

Fig.15. Graphical description of the production and characterization of the drug-loaded electrospun PLA scaffolds and their final application.

3.2. Results

3.2.1. Synthesis of a Diclofenac prodrug via SPPS

The DCF-Gly derivative was chosen according to the predicted values for its MW (=353.20 g/mol) and logP (=2.78), which were estimated using Molinspiration®, making it suitable for a transdermal delivery [138]. The synthetic scheme used for the DCF-Gly synthesis is shown in Scheme 5. The desired product was obtained with a high degree of purity (99%) according to NMR analysis (Fig.S6A, S6B) and was recovered in a high yield (98%).

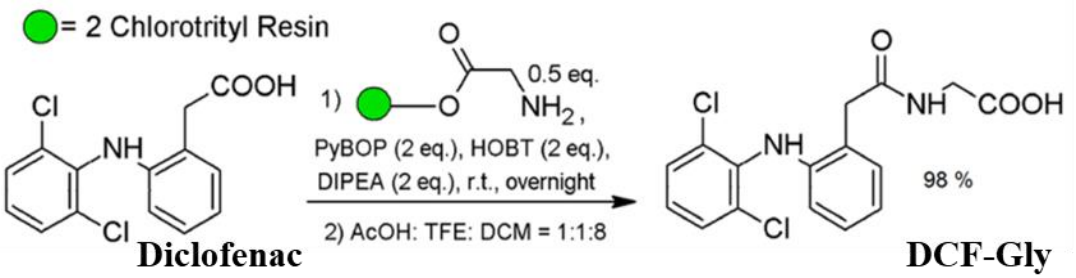

Scheme 5. Synthesis of DCF-Gly via SPPS with H-Gly-2ClTrt Resin

The final product was also characterized by MALDI-MS (Fig.S6C).

3.2.2. Production of the scaffolds by electrospinning

PLA was dissolved in HFIP either alone or in presence of DCF-Gly or DCF. Various electrospinning parameters were tested and those leading to a stable Taylor's cone and jet as well as to smooth and uniform fibers were then used throughout the study. The conditions were first defined for pure PLA and then adapted for the drug-loaded scaffolds.

3.2.3. SEM and fiber diameter analysis

Morphology and fiber size of the PLA scaffold and of the DCF-Gly loaded scaffold, before and after drug release (a.r.) were investigated using SEM (Fig.16). It was possible to generate scaffolds with a random fiber orientation. In all conditions, we obtained uniform nanofibers

with no beads (Fig.16 A-F). After drug release, morphological changes were visible; however, the fibers were still uniform and randomly oriented (Fig.16 G-I). Fiber sizes significantly increased by the incorporation of the drug (PLA: 148±9 nm *versus* PLA + DCF-Gly: 180±9 nm; p=0.001). Despite the change in morphology, there was no significant decrease in fiber size after drug release (PLA + DCF-Gly: 180±9 nm *versus* PLA + DCF-Gly a.r.: 170±8 nm; p=0.48).

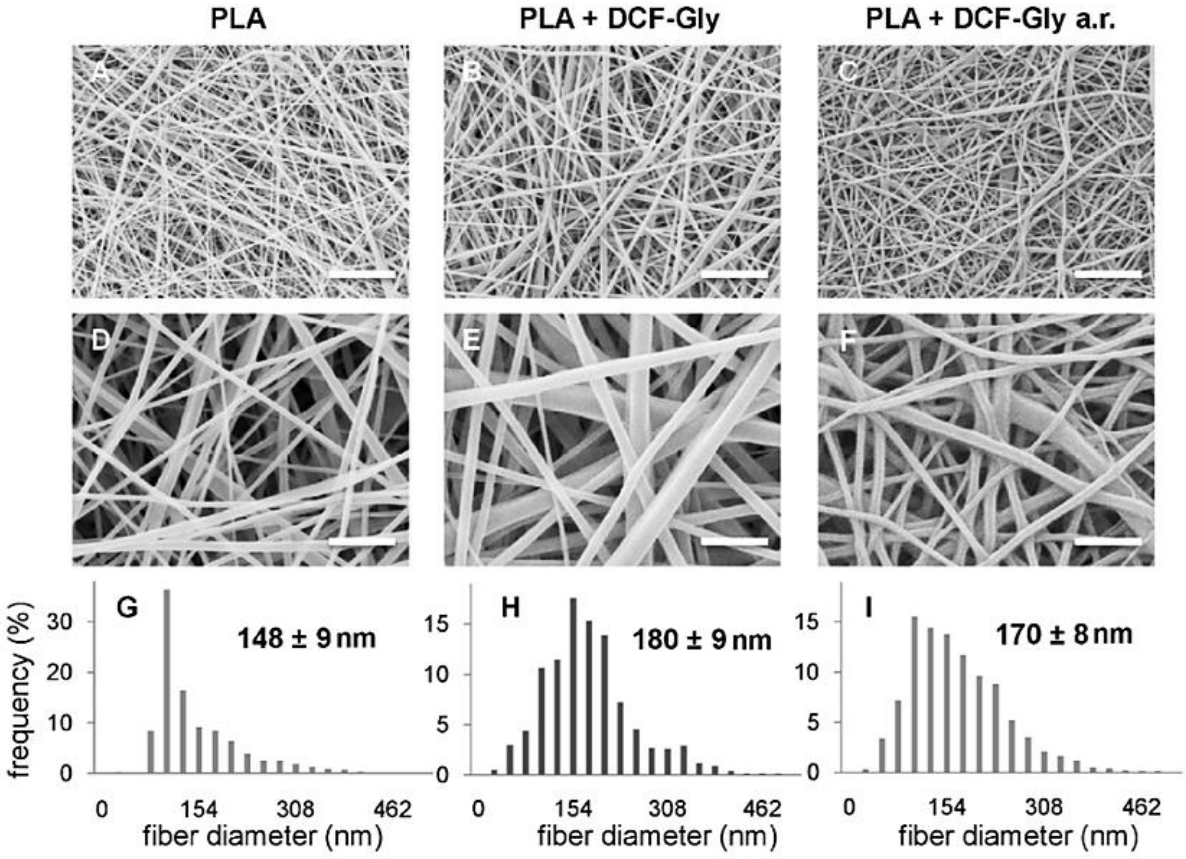

Fig. 16. Analysis of the morphology and fiber size of the electrospun scaffolds. A-F. SEM images of the electrospun scaffolds at different magnifications (a.r. = after release; scale bars: A-C= 5 µm; D-F= 1µm). G-I: Histograms of the fiber diameter distribution and average fiber size.

3.2.4. Contact angle measurements

Wettability of the scaffolds was determined using contact angle measurements (Fig.17 A-B). The analysis showed that the drug-loaded scaffolds remained highly hydrophobic (PLA + DCF-Gly: 130.1±8°) and no significant changes (p=0.81) were determined when compared with the pure PLA scaffolds (PLA: 131±7°).

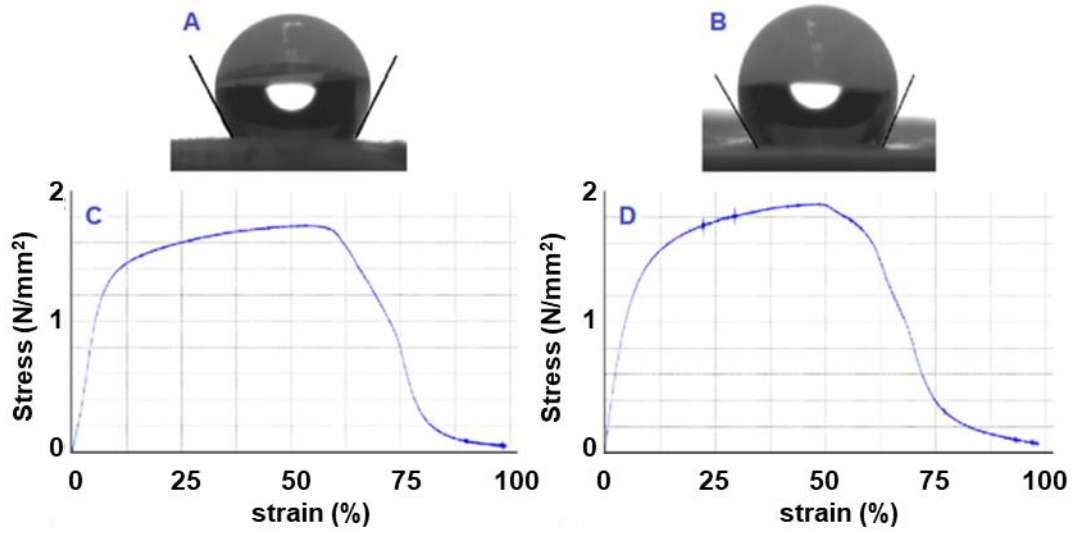

Fig.17. Analysis of the physical properties of the electrospun scaffolds. Drop shape analysis of the pure PLA (A) and the DCF-Gly containing PLA (B) scaffolds after water deposition. Representative stress-strain curves for pure PLA (C) and PLA + DCF-Gly (D).

3.2.5. Tensile tests

PLA is an elastic and electrospinnable polymer. No significant differences were observed in regards to tensile strength (PLA: 1.84±0.19 MPa [88] *versus* PLA + DCF-Gly: 1.91±0.18 MPa; p=0.67) and Young's modulus (PLA: 24.4±9.7 MPa [88] *versus* PLA + DCF-Gly: 25.4±1.2 MPa; p=0.48) when comparing the pure electrospun PLA with the drug-containing scaffold. Like the hydrophobicity, the elastic modulus and tensile strength were not influenced by the encapsulation of DCF-Gly. The experimental curves obtained for the PLA and the PLA + DCF-Gly scaffolds are shown in Fig.17C and 17D, respectively.

3.2.6. MPM analysis

MPM of the synthesized prodrug was employed for the visualization of the drug encapsulation profiting from the presence of an aromatic ring on the DCF molecule. Whereas there was no signal detectable for pure PLA scaffolds (Fig.S7), a strong signal was obtained for the drug-loaded PLA + DCF-Gly scaffolds (Fig.18A) demonstrating that drug encapsulation with electrospinning was successful. Furthermore, multiphoton laser-induced autofluorescence signals were detected from the entire scaffold. Every fiber is clearly visible, confirming that DCF-Gly is homogeneously distributed throughout the scaffold and the single fibers. After drug release, the signals significantly decreased or were absent (Fig.18B). Only a few fibers of the scaffold could be visualized suggesting that most of the encapsulated drug had been successfully released from the scaffold after the incubation in PBS. The obtained mean gray values (Fig.18C) were 82±12 and 8.1±1.1 before and after the drug release, respectively. According to these values the percentage of the not released drug was estimated to be approximately 10%.

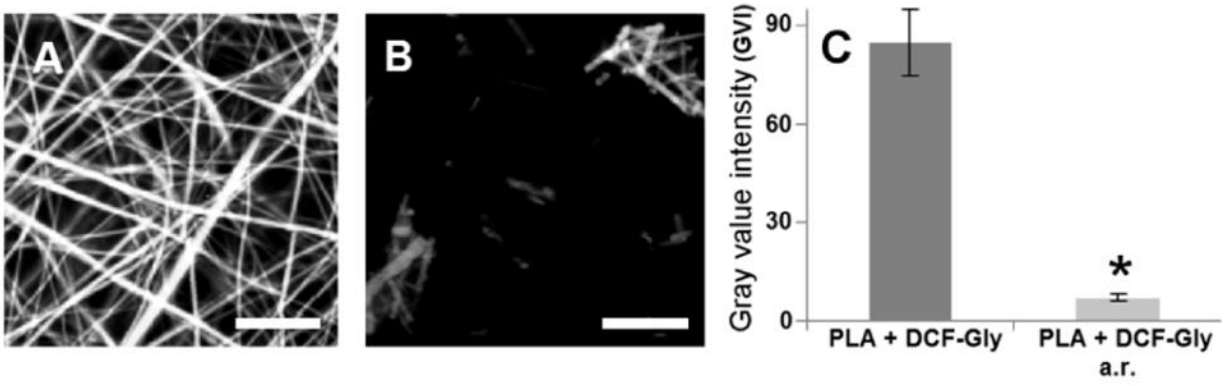

Fig.18. MPM imaging of the DCF-Gly loaded scaffolds. MPM images (scale bars=10µm) of the DCF-Gly loaded scaffold before (A) and after (B) the drug release. Gray values intensities obtained from the MPM images (C).

3.2.7. Drug release experiments

After demonstrating that the drug was successfully encapsulated within the PLA fibers, the ability of the scaffold to release the drug was investigated. The absorbance at 272 nm of the PBS solution, in which the scaffold was immersed, was constantly monitored for the first 7 hours (Fig.19A). Thereafter, it was measured again after 24, 48 and 72 hours. The absorbance value was constant after the first 24 hours. This time was therefore set as the end point measurement. According to a calibration curve and assuming that no loss of the drug occurs during the electrospinning process we could estimate that 89±2% of the encapsulated drug was released from the scaffold after 24 hours, which agrees with the results obtained by the GVI analysis of MPM images (Fig.18). The obtained data were also plotted in a logarithmic form (Fig.19B) using the equation developed by Peppas et al. [37], that offers a simple model to study the release mechanism of incorporated molecules from polymers. According to the value obtained for the slope (0.29±0.03), which is lower than 0.45, Peppas model suggests that drug-release undergoes a controlled diffusion [38].

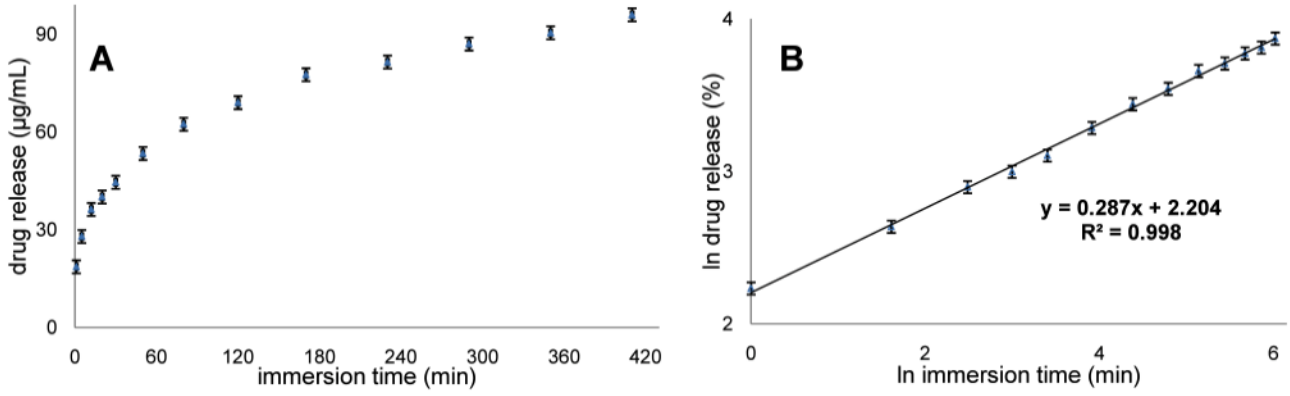

Fig.19. Release profile of DCF-Gly from the PLA scaffold. Drug release analysis (A) and logarithmic fitting of the drug release data with Peppas equation (B).

The effectiveness of the release of DCF-Gly from the PLA scaffold was verified by RP-HPLC too (Fig.S8A and S8B). A binary gradient of CH_3CN/ddH_2O from 5 to 70% over 30 minutes (5→40% over the first 10 min followed by 40→50% over the next 15 min and 50→70% over

the last 5 min) was used allowing a good separation for pure DCF-Gly in PBS (retention time: 18 min by 45.3% CH_3CN/ ddH_2O, Fig.S8A). The same conditions were then used also for the elution of the supernatant of the drug-loaded scaffold extract in PBS. The unmodified DCF-Gly released from the PLA scaffold could be eluted with a high degree of purity (Fig.S8B).

3.2.8. In vitro cytotoxicity

The biocompatibility of the modified scaffold was assessed with a MTS assay using a standardized protocol and HDFs (Fig.20E). A material is non-cytotoxic when the proliferation is higher than 80% relative to the NC [145]. Accordingly, we determined that the PLA scaffolds, either with or without the encapsulated DCF-Gly, showed no cytotoxic effects (cell proliferation: PLA = 104±6%; PLA + DCF-Gly = 105±7%). The assay was also performed with a PLA scaffold containing the unmodified DCF as a positive cytotoxic control [146]. In this case, a severe cytotoxicity (cell proliferation = 16±3% *versus* NC, $p=5e^{-6}$) was observed.

3.2.9. FLIM analysis

FLIM was performed to analyze endogenous NAD(P)H in HDFs as a measure for metabolic changes in the target cells due to the incubation together with the drug-loaded scaffolds. For FLIM analyses, a biexponential decay was employed assuming to have two different fluorescence lifetimes for the free (τ_1) and the protein-bound (τ_2) NAD(P)H [42], respectively. The α_1 (%) represents the free NAD(P)H relative contribution to the final lifetime values. Moreover, we aimed to correlate the obtained data directly with the results that arose from the MTS assay since the rate of tetrazolium reduction reflects the general metabolic activity/rate of glycolytic NAD(P)H [41]. No changes in the cell morphology could be observed for the DCF-Gly loaded and pure PLA scaffolds when compared to the controls (Fig.20 A-C). The cells were elongated and showed the typical shape of fibroblasts [147].

However, when exposed to DCF, a significant morphological change was observed in the MPM images (Fig.20D) due to induced necrosis / apoptosis [147]. Here, the cytoplasm and the nucleus were clearly altered. This morphological change correlated to a metabolic change according to the α_1% values of FLIM measurements. A significant decrease in the free NAD(P)H level (α_1 (%); Fig.20F) was observed for the PLA + DCF treated HDFs when compared to the control (NC), but not for PLA or PLA + DCF-Gly exposed cells (PLA + DCF: 63.9±0.9% *versus* NC: 67.5±0.8%; p=0.001). No significant changes in τ_1 and τ_2 were detectable (Fig.S9).

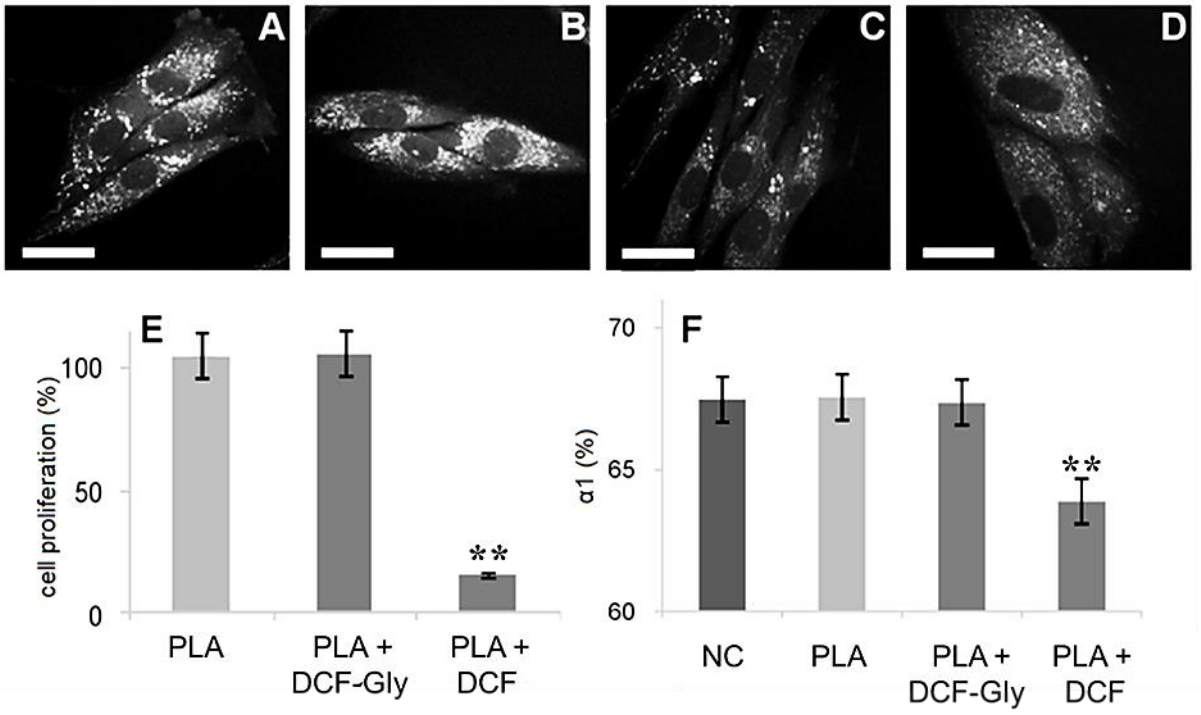

Fig.20. Cytotoxicity assessment using HDFs. MPM images of HDFs (A-D). HDFs treated with cell culture medium only as negative control (A) or in presence of PLA (B), PLA + DCF-Gly(C) and PLA + DCF (D) scaffolds. Scale bars equal 20 µm. Results of the accredited MTS assay (E) and the FLIM analysis of α_1% using a biexponential decay (F).

3.3. Discussion

Three dimensional scaffolds are of growing interest among scientists for applications in the field of tissue engineering or as drug delivery systems [148, 149]. Among the currently employed polymers, polylactide may be the most suitable material for the production of slowly biodegradable scaffolds for biomedical applications [150]. Thus, polylactide is also a suitable material to produce systems for a controlled drug delivery [151]. DCF is one of the most potent NSAIDs [152, 153]. It has been used for the treatment of many different diseases such as osteoarthritis [154] and AKs [155, 156]. Since its approval, a number of different DCF containing products have been developed with the goal of improving efficacy, tolerability, and patient convenience [157-160]. However, no new formulations of DCF for the treatment of AKs have been proposed since its FDA approval in 2002 [133]. The Diclofenac formulation proposed in this thesis should offer a new option for the local treatment of AKs. DCF has unique chemical features. For example, the amine function is a very weak base when compared to other secondary amines [161]. This feature was utilized in this study to handle Diclofenac as an amino acid analogue with protected amine function in SPPS. In particular, it was linked to a glycine residue by forming an amidic bond to obtain a derivative (DCF-Gly) with a lower logP when compared to DCF (estimated logP: DCF-Gly= 2.78 *versus* DCF= 4.96). This is necessary in order to be suitable for a transdermal delivery [138]. The formation of an amidic bond is a well-used strategy for the synthesis of prodrugs since it may be easily cleaved by enzymatic hydrolysis [162, 163]. Solid phase synthesis represents a clean, versatile and efficient way to avoid the use of large amounts of solvents and reagents [163]. Amide prodrugs of DCF have already been synthesized by Kumar et al. [164]. However, the synthetic scheme that was proposed allowed them to reach only yields about 60% [164]. Here, we obtained a quantitative yield of 98%. Moreover, we obtained the free amino acid derivative instead of the protected ester [164], which is crucial when aiming for obtaining a synthesized prodrug with proper hydrophobicity. For the synthesis of the DCF-

Gly prodrug, a 2-Chloro Trityl Chloride (2-CTRL-Cl) resin was employed. The 2-CTRL-Cl resin allows the synthesis of peptides with a carboxylic group at the C-terminus [165], and is compatible with the Fluorenyl-9-methoxycarbonyl protecting group chemistry [166, 167]. Compared to the other resins, the 2-CTRL-Cl one has not only the advantage to produce peptides free from diastereomeric side-products [165-167], but offers the possibility to operate the cleavage under mild acidic conditions (either 1% TFA/DCM [166] or AcOH/TFE/DCM [167]), which is required when handling protected or modified peptides. The opportunity of binding DCF to different amino acid residues and even to longer peptide chains without the need of further purification could be employed to obtain many different DCF derivatives. This is potentially very useful considering the variety of medical applications of DCF [152-155]. The results obtained in this study by binding Diclofenac to a glycine residue are promising since we achieved a high yield and a great degree of purity. However, the versatility of this synthesis has to be further investigated. The synthesized DCF-Gly prodrug was successfully incorporated in a PLA scaffold using electrospinning. The obtained electrospun scaffold was then characterized in order to demonstrate that it is a suitable system for the topical treatment of AKs. In particular, the morphology of the scaffold was investigated using SEM. This technique is the often used for the investigation of nanostructures. It is reliable and allows high magnifications with a good resolution [168]. Thus, this analysis was necessary to investigate the scaffold morphology, analyze the diameter distributions and compare them. The SEM investigation showed a homogeneous fibrous structure of the generated electrospun scaffolds. For the drug-loaded scaffolds, a significant increase in the fiber diameters could be observed. This may be due to the increase in viscosity of the electrospun solution and also the presence of the drug molecules within the polymeric fibers [169]. Nevertheless, the mean values of the fiber diameter remained still lower than 200 nm, and a regular fibrous structure with no beads was maintained. The increased fiber diameters after drug encapsulation did not affect the mechanical properties such as the Young's modulus or the tensile strength of the

electrospun scaffold. Soliman et al. [170] and Milleret et al. [171] showed in previous studies that fiber diameter and orientation, as well as scaffold porosity can impact the mechanical properties of the scaffolds. In particular, they both proved that an increase in the fiber diameter leads to a significant increase in the Young's modulus [170, 171]. However, they analyzed differences in the diameter values that were in the µm range [170, 171]. In our case the variation in the fiber diameters is probably too low to significantly impact the investigated mechanical properties. By adding DCF-Gly, the wettability of the scaffolds was also not affected. The scaffolds remained highly hydrophobic as it is described for pure PLA [141]. We have chosen PLA as the drug carrier, since hydrophobicity is important to ensure the drug diffusion from the scaffold into the lesion [172, 173]. DCF-Gly encapsulation could be easily visualized using MPM due to the ability to selectively induce DCF autofluorescence [174]. One of the advantages of the MPM technique is the ability to image non-invasively and thus without destroying or modifying the samples [175, 176]. This enables a simple, *in situ* quality control. MPM has already been used to image scaffolds with and without a fibrous structure [177, 178]; however, a good contrast or resolution could not be achieved thus far. Interestingly, we obtained a good contrast using a very low laser power (3.2mW). This approach is promising and could be potentially extended to different substrates since a great number of drugs and endogenous molecules are autofluorescent when excited at defined wavelengths. Here, we used MPM to show successful encapsulation and release of the prodrug. By calculating the GVI, it was possible to estimate the amount of non-released DCF-Gly. After 24 hours, 10% of DCF-Gly remained in the scaffold, which is comparable to values from literature described by Sidney et al. for previously developed DCF eluting systems [158]. However, the initial burst release was ~ 60% [158], and in our study only ~20%. Initial burst of drug release is related to drug type, drug concentration, polymer hydrophobicity and scaffold nanostructure [179-181]. In contrast to the previously described eluting system, the one described in this study utilized a fibrous structure since it was obtained via

electrospinning. Moreover, hydrophobic PLA was used as the only polymer while Sidney et al. used a mixture of the hydrophobic polyester PLGA (poly-lactic-co-glycolic acid) with the more hydrophilic PEG (poly-ethylene glycol) [138]. In addition, the synthesized DCF-Gly prodrug was used as free acid instead of the Diclofenac sodium salt (DCF). Carboxylic acids have lower water solubility than the correspondent sodium salts, thus showing a slower and more controlled diffusion over the time [182]. Due to these features, the formulation that is proposed here helps to reduce the initial burst release and to have a sustained drug diffusion from the scaffold over the first 24 hours. Furthermore, we investigated the amount of the released drug in the supernatant. It has been shown before, that drug release can be controlled and influenced by changing various parameters such as hydrophobicity, fiber size or drug concentration [183]. The encapsulated DCF-Gly was effectively released from the scaffold following a controlled diffusion according to the spectrophotometric measurements and the Peppas equation. This equation has already been employed as a simple model to investigate the drug release from electrospun scaffolds [183-185]. For the here characterized scaffold, the release mechanism undergoes a controlled diffusion due to a very low release exponent of 0.29. The encapsulated drug is mostly (~90%) released within the first 24 h. Such a behavior is suitable for the aim of this thesis considering that DCF is used as a daily treatment to cure AKs [134]. Furthermore, the *in vitro* biocompatibility of the drug-containing scaffold was tested by performing a MTS cell proliferation assay. This test allows for a quantitative evaluation of cytotoxicity [183] and satisfies the international standard requirements of ISO 10993-5. In contrast to DCF, DCF-Gly was non-cytotoxic, after release from PLA scaffolds. It is well known that DCF induces cell death [146, 187], suggesting that the newly synthesized molecule is a promising non-cytotoxic prodrug for treating AK. In addition, we investigated the effect of DCF on HDFs after its release from the PLA scaffold employing MPM coupled with FLIM. For the analysis NAD(P)H was chosen as a target [42]. This approach allows the monitoring of changes in cell morphology and metabolism without the

need of staining or the interruption of cell culture. The MPM analysis allowed us to image morphological changes in HDFs after the DCF treatment. It is known that DCF induces cell death due to a mitochondrial injury [184]. Specifically, either apoptosis or necrosis is induced depending on how many mitochondria are affected [146]. In this thesis we aimed to correlate the observed morphological changes to the induced cell death as previously described by Seidenari et al. [147]. In particular, cells that showed a nuclear and cytoplasmic condensation were assessed as apoptotic while cells showing both swelling and vacuolation of the cytoplasm were considered to undergo necrosis [147]. According to the morphological observations obtained with MPM, we suggest that both apoptotic and necrotic events occur after the DCF treatment. Besides, FLIM allowed the detection of metabolic changes after the DCF treatment. In particular, a significant decrease in the rate of glycolytic NAD(P)H [42] could be detected. FLIM data supported the results obtained from the MTS assay. Our results show that employing a drug-loaded PLA scaffold as a drug-releasing wound dressing to treat AKs could be a very useful and promising alternative to current treatment strategies. It would help to control the daily dosage, thus significantly reducing side-effects, and be applicable as targeted therapy. In addition, the here proposed formulation could be very useful after surgical procedures, photodynamic- and cryotherapy because it would ensure a protection of the treated area and favor the wound healing [188-190]. It has been reported that the application of drug-free electrospun PLA nanofibrous scaffolds as wound dressing materials already enhance the recovery process [190-193], indicating that the here presented combination of PLA and DCF-Gly is a highly interesting candidate for AK treatment. In order to confirm an enhanced transdermal delivery of the synthesized DCF-Gly prodrug compared to DCF [194], further experiments are necessary. Particurarly, the effective DCF-Gly absorption through the skin and its activation by enzymatic hydrolis have to be verified [195]. 3D *in vitro* skin models would offer a closer to in vivo system to test these aspects compared to monolayer cell

cultures [196]. Finally, the effectiveness to treat AK needs to be further investigated in adequate *in vivo* models.

3.4. Conclusions

In this study, an electrospun PLA scaffold loaded with a synthetically obtained DCF prodrug was generated and characterized. The proposed DCF-Gly synthesis based on the use of SPPS is novel and promising. Compared to unmodified DCF, DCF-Gly is non-cytotoxic and therefore potentially a more suitable drug to treat AK. The electrospun PLA + DCF-Gly scaffold represents an interesting drug releasing system that enables a controlled and targeted delivery of DCF-Gly for the topical treatment of AKs.

CHAPTER 4. HYBRID GELATIN/POLYLACTIDE ELECTROSPUN SCAFFOLDS WITH CONTROLLED HYDROPHOBICITY AND WETTABILITY

4.1. Introduction

Blend nanofibrous electrospun scaffolds represent an emerging class of nanostructures that can mimic the native tissue, and besides interact with the local microenviroment [197-199]. By combining two or more polymers, they can behave cooperatively to finally provide hybrid scaffolds with unique mechanical, biochemical and structural properties [200]. Blend electrospun scaffolds have already found application in a wide range of tissue engineering and drug delivery systems [198, 201]. To this end, many scientists have already demonstrated that nanofibrous scaffolds are capable of mimicking and reorganizing the extracellular matrix (ECM) to sustain damaged or pathological areas [202-206]. Besides, they can also favor tissue regeneration and healing processes [207-210]. The electrospinning process leads to final 3D structures with a high surface to volume ratio, composed of nanofibers and pores with variable sizes [211-215]. Electrospun scaffolds also have strong mechanical properties while maintaining a very low density [216, 217]. Moreover, their degradation profile can be predicted before being implanted in the human body or even modified later *in situ* [218, 219]. Thus, the implanted scaffolds slowly break down into non toxic fragments in the foreseen way, while the native tissue gradually grows replacing them [218, 219]. To date, many different synthetic and naturally derived polymers have been electrospun into nanofibers [220, 221]. Among the most widely electrospun synthetic polymers there are the linear aliphatic polyesters polylactic acid [222-224], polyglycolic acid [225] and their copolymer, poly(lactic-co-glycolic) acid (PLGA) [226-228]. All of these materials are biocompatible, can be easily obtained starting from cheap raw material sources [222-228], and have already been widely used in soft tissue regeneration [229, 230]. Although synthetic materials are strong, cheap and reliable, they unfortunately share no biochemical signatures and cannot interact with the

human body. This aspect can be sometimes highly desirable but in other cases a specific interaction with the target tissue is required. To obtain biomimetic nanofibers, an appealing approach has been the direct electrospinning of naturally derived polymers [231- 233]. To date, collagen, gelatin, fibrinogen, chitosan and alginate have all been used as starting polymers to obtain nanofibrous structures by electrospinning [233]. Many of these macromolecules retain cell-binding sites and biomolecular signatures that can favor cell-material interactions [234]. The harvesting and processing of natural polymers, however, is not as straightforward as for synthetic ones, since their unique and specific properties are strongly influenced by temperature and solvent interaction, among others [234, 235]. Thus, a greater attention should be paid when working with them in order not to alter or even denaturate the starting polymer [235]. In the last years, growing attention has been paid to the advantages of hybrid scaffolds over single-component systems [197-202]. These structures can be obtained starting from solutions of mixtures of both synthetic and naturally derived polymers [197-199]. By blending two or more polymers together the final scaffolds can combine the characteristic properties of different polymers or even have new unique features [197-200]. While each single polymer unlikely shares the chemical composition and the structural properties of the native tissue, polymers used in combination can take mutual advantage, and better emulate the complexity of the ECM. Moreover, some (natural) polymers cannot be electrospun alone, while by blending them together with other materials they can be more easily solubilized and processed [236-238]. Not least, the direct production of blend scaffolds by electrospinning offers advantages over copolymerization and physical coating, alternative techniques employed to obtain hybrid structures [239-241]. Indeed, both processes require a generally irreversible chemical modification of the starting polymers, and are in most cases also solvent and material consuming [240, 241]. However, the development of well-blended hybrid scaffolds by electrospinning does not occur effortless due to the poor miscibility of the different polymers [242]. Badly blended polymeric nanofibers exhibit weak

mechanical strength, and have unpredictable material properties as a result of inhomogeneity [243]. Thus, the production of hybrid electrospun nanostructures that can profit from the favorable biological properties of the natural polymer (-s) and the mechanical of the synthetic one (-s) still remains a great challenge in tissue engineering and regenerative medicine.

In this part of the thesis, we present the development and characterization of different hybrid electrospun (hyaluronic acid containing) scaffolds comprised of well-blended gelatin (GE) and poly-L-lactide (PLA), a natural and a synthetic polymer, respectively (Fig.21). Gelatin consists of a mixture of water-soluble protein fragments, with the same amino acid composition as collagen from which it is obtained through partial hydrolysis [244]. GE has already been successfully employed in the production of biomaterials profiting from its biodegradability, biocompatibility and commercial availability at low cost [245]. GE shows to have advantages over collagen, which include lower immunogenicity [246-248] and better solubility in aqueous systems [249]. Unmodified GE is also a good material to let cells adhere and proliferate, but has unfortunately low mechanical properties [250]. Not least, its high water solubility, representing an advantage by its processing, makes it necessary to cross-link GE before any use for biomedical applications. The cross-linking can strongly alter the material properties and its biocompatibility, even if, nowadays, different not destroying, clean methodologies are available [251-253]. To time, carbodiimide based cross-linking strategies represent the first choice [251-255]. Though being a limitation on one side, the cross-linking reaction offers, nevertheless, the possibility to (specific) bind other molecules to the amino acid residues in order to functionalize or modify GE [256-259]. GE can be obtained starting from different animal collagens [260-263]. The most commonly used forms in tissue engineering are derived from porcine [260, 261], fish [262] and bovine [263] tissues. Gelatin final properties depend not only on its source [260-263] but also on pH, temperature, and extraction time used for the collagen hydrolysis [264]. Depending on the processing conditions, GE with different molecular weight, Bloom strength and isoelectric point (IEP)

can be obtained [263, 265-269]. Collagen hydrolysis under acidic and alkaline conditions gives rise to type A GE (IEP at pH 8–9) and type B GE (IEP at pH 4–5), respectively [264, 265]. Mammalian gelatin is rich in domains able to bind to cell-surface receptors and to other ECM proteins, such as fibronectin, thus offering an excellent substrate for attachment and proliferation of adherent cells [270]. In addition, gelatin can undergo collagenase mediated hydrolysis, which allows *in vivo* biologically driven remodeling of GE-based scaffolds [271] and, at the end, the material resorption without having any toxic residuals [272]. Cell adhesion for polylactide is instead sometimes not high, probably due to its hydrophobicity [273], but its mechanical strength and elasticity are much greater than GE [274, 275]. Thus, the combination of GE and PLA could provide composite materials with good cell adhesion and mechanical resistance as well. Polylactide is a widely used aliphatic polyester [276]. It can be chemically synthesized either by poly-condensation of lactic acid or by ring-opening polymerization of lactide, a cyclic dimer of lactic acid [277]. The preparation of polylactide fibers by electrospinning requires the use of high molecular weight polymers (~100kDa) [278]. Different configurations of the monomer units have a great influence on the thermal and mechanical properties of the polymer [112, 277]. For example, homopolymers produced from optically pure L,L- or D,D-lactide (PLLA or PDLA) have isotactic structure and are semi-crystalline with a glass-transition temperature (T_g) in the range of 55–60°C and a melting temperature (T_m) around 175°C [275]. The high T_m of isotactic PLLA and PDLA is of great importance when the thermal sterilization of the polymers is required, which is often the case in pharmacy, medicine and food industry [279, 280]. Polymerization of a racemic mixture of L- and D-lactic acid produces a copolymer (PDLLA), which is essentially atactic and amorphous. PDLLA has a T_g around 60°C but no T_m [275, 279]. PLLA has very good mechanical properties [281-285], while the amorphous PDLLA shows lower tensile strength and higher elongation at break compared to PLLA [275]. One of the very attractive properties of polylactide is that it can be resorbed in the human body after hydrolytic or enzymatic

digestion like many natural polymers, even if it is a synthetic one [286]. *In vivo* polylactide hydrolysis occurs by the cleavage of its ester bonds to give the non-toxic lactic acid which is finally eliminated as CO_2 and H_2O via Krebs cycle [287, 288]. Polylactide bioresorption is also influenced by its crystallinity degree [289]. It has been demonstrated that the *in vivo* hydrolysis of implants of high molecular weight PLLA requires a period of over a year, while their full resorption takes an even longer time [290, 291]. Amorphous PDLLA undergoes instead a faster complete bioresorption [292]. Thus, PLLA is the polymer of choice for the preparation of biomaterials when a longer exploitation time is required.

Hyaluronic acid (HA) is a glycosaminoglycan (GAG) found within the ECM of human connective tissue consisting of the repetition of two alternating glycoside linkages of α-1, 4-D-glucuronic acid and β-1, 3-N-acetyl-D-glucosamine (Fig.21) [293]. HA is involved in tissue repair, wound healing, and cellular adhesion and proliferation as well [294-297]. The unique viscoelastic and rheological properties together with its antibacterial and anti-inflammatory properties make HA an attractive material for biomedical applications [297]. In addition, HA has an essential role in the regenerative process for both the dermal and epidermal layers of the skin, and thus is considered of great potential as scaffold component to sustain healing processes [298]. In addition, various proteins that influence ECM interactions are able to bind to HA, and thus it can regulate how the cells will interact with the surrounding microenvironment [299, 300].

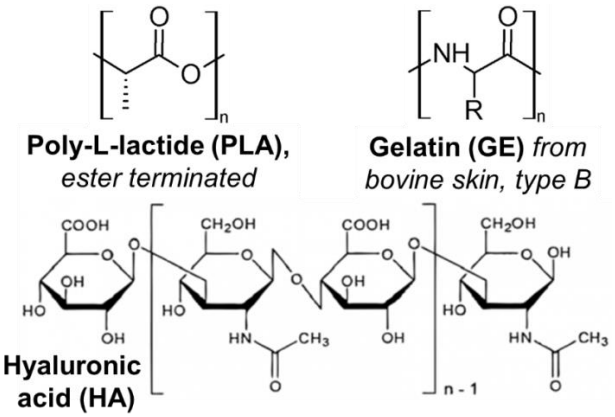

Fig.21. Structure of the polymers used for the production of the hybrid electrospun scaffolds.

In this introduction, an overview is given about the many different chemical and biological properties of gelatin, polylactide and hyaluronic acid and about the advantages that can be achieved by blending them in ECM-like nanofibrous scaffolds. The ECM represents a complex structure whose composition and properties vary from tissue to tissue, and is responsible for cell proliferation, communication and differentiation [300]. We believe that polylactide and gelatin represent two completely different polymers that, however, share many similarities. For example, they are both bioresorbable and their mechanical properties strongly depend on the polymer molecular weight and how they are obtained and isolated, too. Thus, they offer a broad spectrum of possibilities and frontiers in the production of electrospun blend scaffolds for tissue engineering with unique features, depending on composition and ratio of the single components, and how they are processed (together). Finally, we also believe that HA, a GAG present in the ECM, and playing a key-role in its complex action, represents a good substrate to further functionalize hybrid GE/PLA electrospun scaffolds. Herein, we aimed to produce and characterize hybrid GE/PLA scaffolds with controlled wettability and hydrophobicity. These two purposes could be achieved by using blend electrospun scaffolds containing different GE:PLA w:w ratios (4:1, 5:2 and 1:1) and by binding different HA amounts to the hybrid GE:PLA in 1:1 w:w ratio scaffolds, respectively.

4.2. Results

4.2.1. HYBRID GELATIN/POLY-L-LACTIDE *SCAFFOLDS WITH CONTROLLED POROSITY AND WETTABILITY*

4.2.1.1. Production of the scaffolds by electrospinning and cross-linking

For the production of the scaffolds, various electrospinning parameters were tested and those leading to a stable Taylor's cone and jet, as well as to smooth and uniform fibers, were then used throughout the study. The conditions were first defined for pure PLA (chapter 2) and GE, and then adapted for the hybrid scaffolds. Generally, we noticed that when using a concentration higher than 10% w/v for GE the electrospinning process was not stable and the solution jellified at room temperature. Actually, when using the two highest GE:PLA ratios (4:1 and 5:2), the relative GE concentration was 10% w/v, which is the threshold value that, according to our observations, avoided its jellification during the electrospinning experiment. On the other side, when having PLA we noticed that a final polymer concentration higher than 15% led to instable electrospinning processes with inhomogeneous final electrospun scaffolds. After the cross-linking, all the scaffolds shrank, but this effect was more evident when having a higher GE content. After having verified that no significant weight loss occurred for the pure PLA electrospun scaffolds when handling them according to the cross-linking procedure used throughout this thesis, we were able to determine the final GE:PLA (w:w) ratio and the final scaffold diameter for all the hybrid scaffolds, after the cross-linking (Table 2).

Initial GE:PLA w:w ratio	Initial scaffold diameter (cm)	GE:PLA final w:w ratio	Final scaffold diameter (cm)
4:1	*9*	*18(±2):5*	*5.5±0.5*
5:2	*9*	*9(±1):4*	*6.6±0.4*
1:1	*9*	*9 (±1):10*	*8.0±0.2*

Table 2. Composition of Polymers expressed as ratio (w:w) and dimensions of the hybrid GE:PLA scaffolds, before and after cross-linking.

The lower final GE content in the hybrid scaffolds is due to the cross-linking that leads to a water loss after intramolecular reaction between GE aspartic (L-Asp)/glutamic (L-Glu) acidic residues and the free amines of GE lysines (Fig.S10). Besides, a little GE solubilization could occur as well, due to water presence in the cross-linking solution. Nevertheless, this GE loss is not significant, and so we decided to always refer to the initial GE:PLA w:w ratio when characterizing the hybrid scaffolds, considering this value as the most reliable one.

4.2.1.2. SEM and fiber diameter analysis

All the electrospun scaffolds were characterized by SEM in order to assess the goodness of the electrospinning experiments (Fig.22 and Fig.23) and of the cross-linking reactions (Fig.22 and Fig.24). Pure GE appeared good electrospun, showing a homogeneous random-oriented fiber distribution (Fig.22), with the fibers normally distributed around the mean value (Fig.22B, 334±35 nm). After the cross-linking, the porous-like structure of GE typical of electrospun scaffolds got lost, and no considerations about the fiber distribution could be done (Fig.22 C, D).

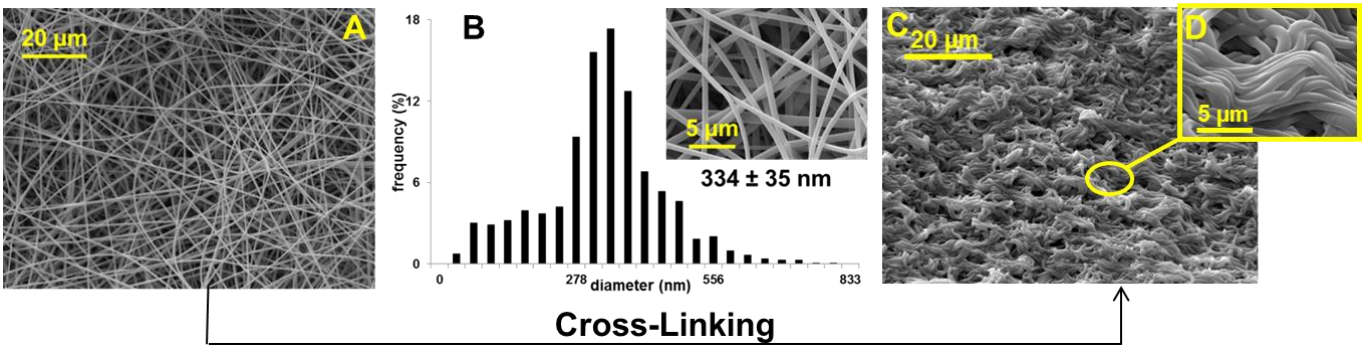

Fig. 22. A, B. SEM images at different magnifications of electrospun gelatin and fiber diameter distribution. C, D. SEM images at different magnifications of cross-linked electrospun GE.

Blend electrospun scaffolds often lack of homogeneity, and the cross-linking reaction can instead strong alter their porous structure. Nevertheless, when blending GE together with PLA in different ratios (4:1, 5:2 and 1:1) we were able to generate scaffolds with a random fiber orientation. In all conditions, we obtained uniform fibers with no beads showing a normal distribution (Fig.23). When increasing the PLA content, the mean fiber diameter of the uncross-linked hybrid scaffolds significantly increased (GE:PLA 4:1, 243±25 nm *versus* GE:PLA 5:2, 344±22 nm, p=0.007; GE:PLA 4:1 *versus* GE:PLA 1:1, 420±38 nm, p=0.003; GE:PLA 5:2 *versus* GE:PLA 1:1, p=0.008, Fig.25) probably due to higher final polymer concentration and blend solution viscosity [197, 198].

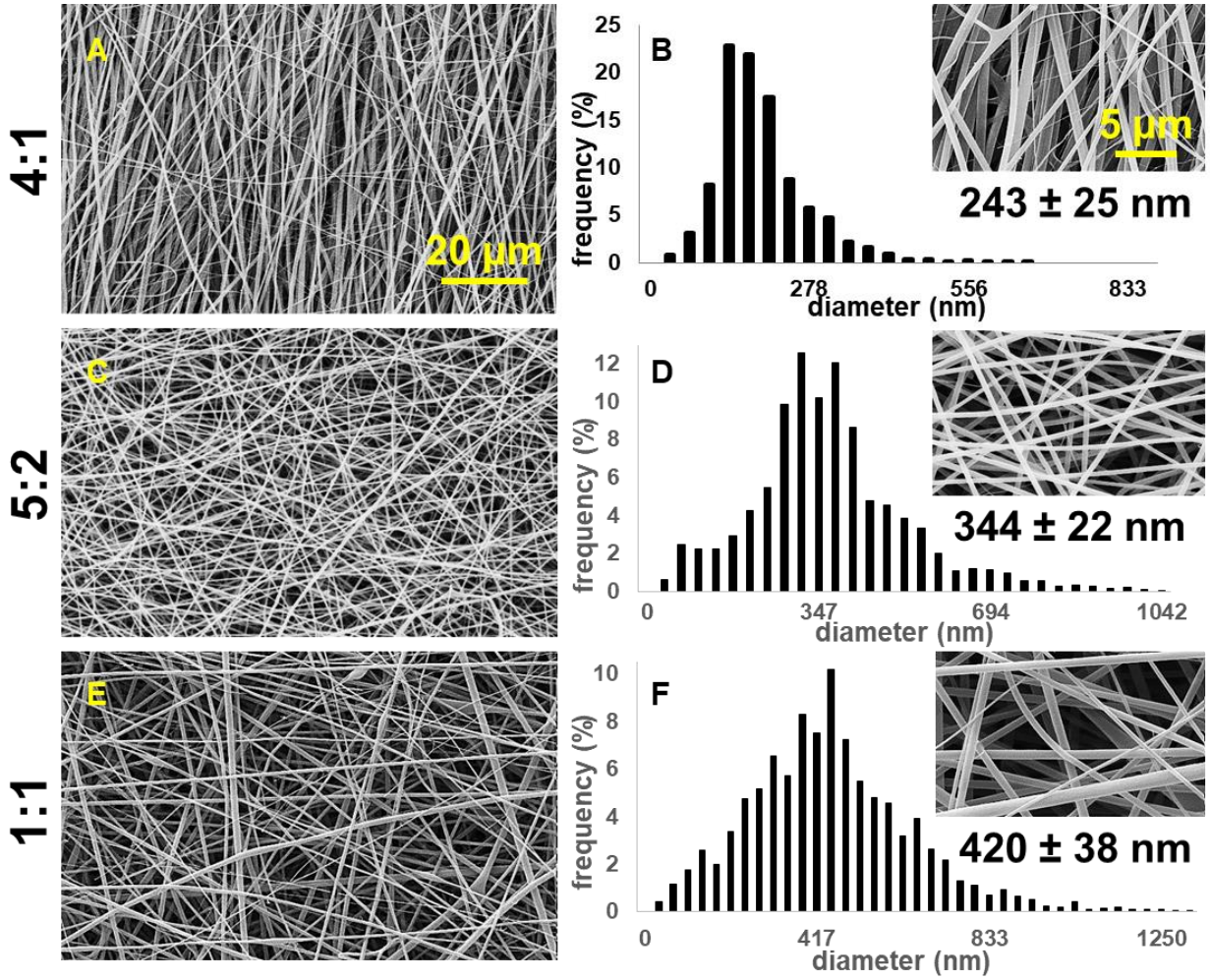

Fig. 23. A, B. SEM images at different magnifications of electrospun GE:PLA 4:1 scaffold and fiber diameter distribution. C, D. SEM images at different magnifications of electrospun GE:PLA 5:2 scaffold and fiber diameter distribution. E, F. SEM images at different magnifications of electrospun GE:PLA 1:1 scaffold and fiber diameter distribution.

After the cross-linking, the mean fiber diameter generally increased (Fig.24) but no significant differences could be found when comparing the values obtained for the same hybrid scaffolds before and after cross-linking, respectively (Fig.25).

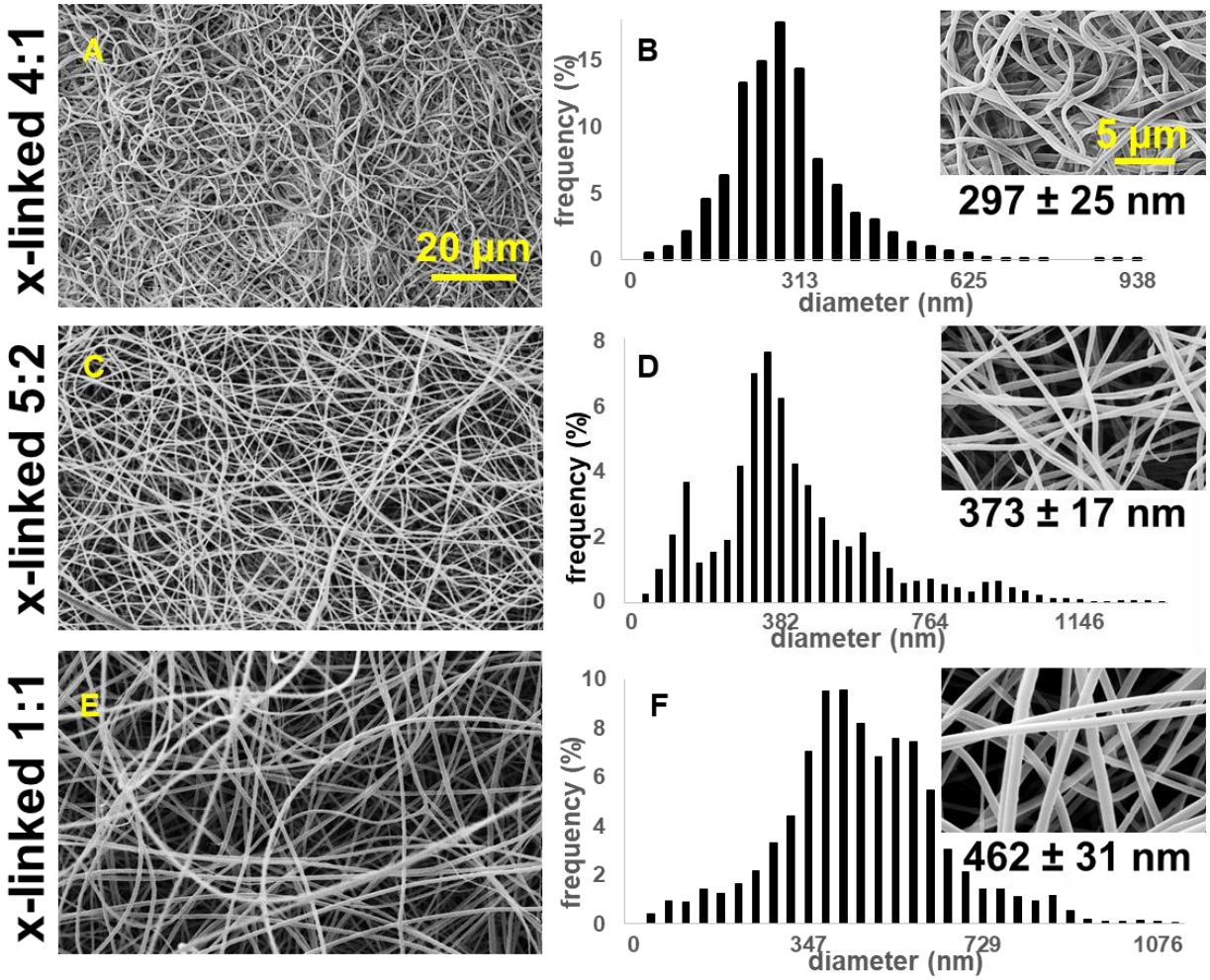

Fig. 24. A, B. SEM images at different magnifications of electrospun GE:PLA 4:1 scaffold and fiber diameter distribution after cross-linking. C, D. SEM images at different magnifications of electrospun GE:PLA 5:2 scaffold and fiber diameter distribution after cross-linking. E, F. SEM images at different magnifications of electrospun GE:PLA 1:1 scaffold and fiber diameter distribution after cross-linking.

However, a significant increase in the mean fiber diameter due to the increasing PLA content could still be detected when comparing the hybrid scaffolds among them, even after the cross-linking (cross-linked GE:PLA 4:1, 297±25 nm *versus* cross-linked GE:PLA 5:2, 373±17 nm, p=0.007; cross-linked GE:PLA 4:1 *versus* cross-linked GE:PLA 1:1, 462±31 nm, p=0.003; cross-linked GE:PLA 5:2 *versus* cross-linked GE:PLA 1:1, p=0.009, Fig.25).

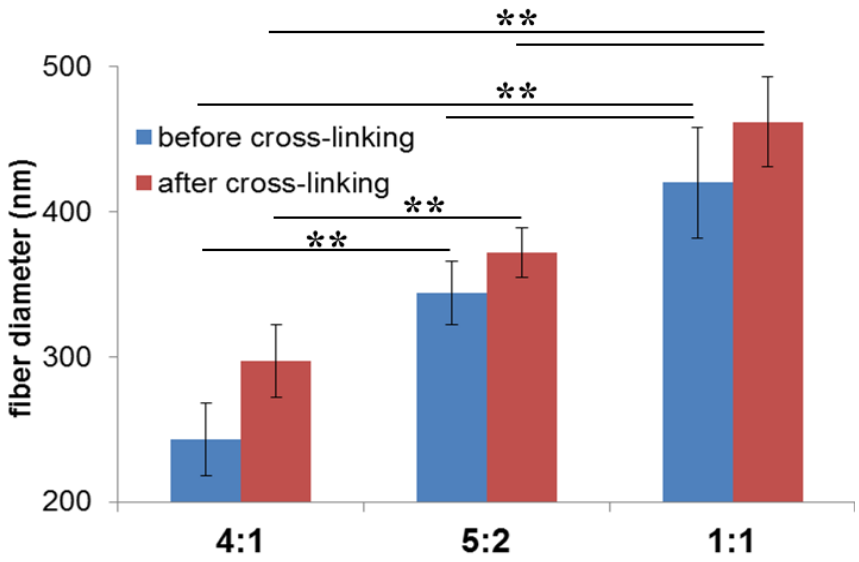

Fig.25. Fiber diameter comparison among the hybrid GE:PLA electrospun scaffolds before (blue) and after (red) cross-linking.

4.2.1.3. Porosity, swelling properties and contact angle measurements

According to the scaffold morphology (Fig.24) the cross-linked hybrid scaffolds having a higher GE content showed a higher porosity. This observation could be confirmed with DiameterJ analysis of the SEM images. According to this analysis, the mean pore size increased with the increasing PLA percentage (Fig.26A), while the number of pores (expressed as number of pores/ μm^2, Fig.26B) decreased with the increasing PLA content. These microscopical properties of the hybrid cross-linked scaffolds correlated with the results obtained with the swelling test and the liquid displacement method to determine their wettability (Fig.26C) and porosity (Fig.26D), respectively.

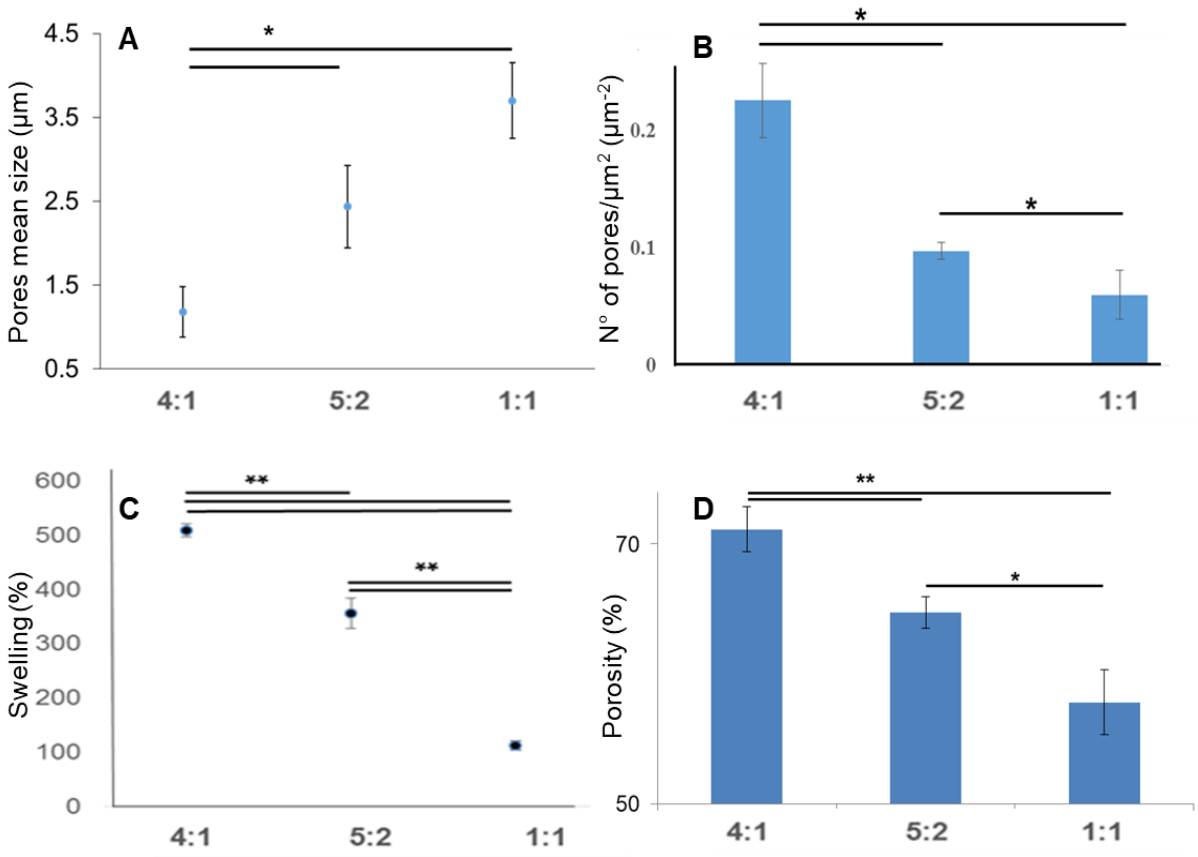

Fig.26. Comparison of the properties of the cross-linked hybrid GE:PLA scaffolds. A. Pores mean size. B. Mean number of pores divided per the scaffold surface. C. Swelling properties. D. Porosity percentage according to the liquid displacement method.

According to our observations, the scaffolds having a higher GE percentage and a greater number of pores retained more water (cross-linked GE:PLA 4:1, 507±15% *versus* cross-linked GE:PLA 5:2, 362±34%, p=0.004; cross-linked GE:PLA 4:1 *versus* cross-linked GE:PLA 1:1, 121±9%, p=0.0008; cross-linked GE:PLA 5:2 *versus* cross-linked GE:PLA 1:1, p=0.004, Fig.26C). Besides, the higher GE percentage correlated with higher porosity as well (cross-linked GE:PLA 4:1, 71±3% *versus* cross-linked GE:PLA 5:2, 65±2%, p=0.003; cross-linked GE:PLA 4:1 *versus* cross-linked GE:PLA 1:1, 58±4%, p=0.0019; cross-linked GE:PLA 4:1 *versus* cross-linked GE:PLA 5:2, p=0.024, Fig.26D). The scaffolds wettability was evaluated by measuring the contact angle too. Both 4:1 and 5:2 GE:PLA cross-linked scaffolds were highly hydrophilic, while the 1:1 GE:PLA blend was highly hydrophobic. The

obtained contact angle values were of 0° for the first two cross-linked scaffolds (4:1 and 5:2) and 129°±3° for the cross-linked 1:1 GE:PLA blend.

4.2.1.4. Tensile tests

The tensile strength and the E-modulus for pure PLA were already evaluated [88]. Besides, we investigated the same properties for hybrid GE:PLA and pure GE cross-linked scaffolds, before and after swelling (Fig.27). The swollen scaffolds showed a higher elongation at break when compared to the dry ones (Fig. 27 A-H), and our instrument was even not able to break down the wet hybrid samples (elongation (%) > 100%). However, no significant differences could be found in both Young's modulus and tensile strength when comparing the same hybrid scaffolds, before and after swelling, respectively. Only pure cross-linked gelatin was significantly more elastic after swelling (dry cross-linked GE: 26.6±2.2 MPa *versus* swollen cross-linked GE: 1.22±0. 34 MPa). Thus, only the values obtained for the dry scaffolds were used for comparison and are reported. Interestingly, no significant differences in the ultimate tensile strength could be found when comparing the different cross-linked scaffolds among them (cross-linked GE, 2.5±0.4 MPa; cross-linked GE:PLA 4:1, 2.7±0.4 MPa; cross-linked GE:PLA 5:2, 2.2±0.5 MPa; cross-linked GE:PLA 1:1, 2.6±0.2 MPa, Fig.27I). In all cases, we were instead able to obtain hybrid scaffolds showing a significant lower Young's modulus (E-modulus) when compared to pure cross-linked GE (cross-linked GE:PLA 4:1, 16.4±2.4 MPa *versus* cross-linked GE, p=0.006; cross-linked GE:PLA 5:2, 13.0±2.4 MPa *versus* cross-linked GE, p=0.004; cross-linked GE:PLA 1:1, 8.6±0.8 MPa *versus* cross-linked GE, p=0.003, Fig.27J). Nevertheless, the scaffold showing the highest elasticity was that in 1:1 GE:PLA ratio since it was significantly more elastic when compared to the other hybrid cross-linked scaffolds (cross-linked GE:PLA 1:1 *versus* cross-linked GE:PLA 4:1, p=0.0016; cross-linked GE:PLA 1:1 *versus* cross-linked GE:PLA 5:2, p=0.009, Fig.27J).

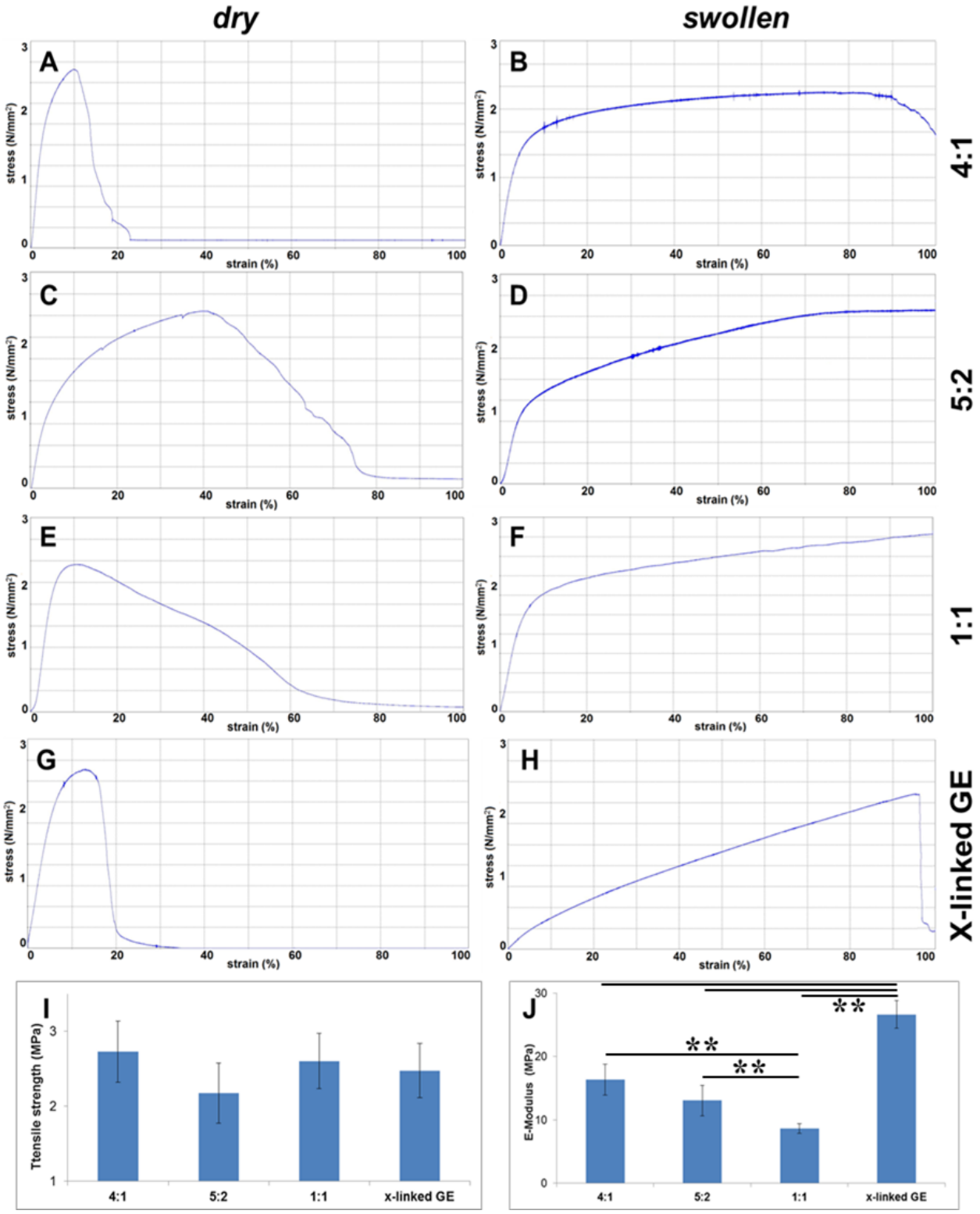

Fig.27. A-H. Representative stress-strain curves of: cross-linked hybrid GE:PLA 4:1 before (A) and after swelling (B); cross-linked hybrid GE:PLA 5:2 before (C) and after swelling (D); cross-linked hybrid GE:PLA 1:1 before (E) and after swelling (F); pure cross-linked GE

before (G) and after swelling (H). I, J. Comparison of Young's modulus (I) and tensile strength (J) among the scaffolds in dry state.

4.2.1.5. Raman spectra and principal component analysis (PCA)

The different hybrid GE:PLA scaffolds were analyzed by Raman microspectroscopy, both before and after cross-linking. Raman analysis has the advantage of allowing the measurement of the unmodified samples in solid state without the need to pre-treat them, when compared for example to Fourier-transformed infrared spectroscopy (FTIR) [40, 43]. All the spectra are shown in Fig.28. According to the obtained spectra, the region of interest was found to be between 740 and 920 cm^{-1}. In particular, the signals at 743 cm^{-1} (Fig.28, green arrow) and at 876 cm^{-1} (Fig. 28, red arrow) were attributed to vibrations of the free carboxylic groups of L-Glu [301, 302] and L-Asp [301, 303], respectively. Both signals could be found only in the spectra of the uncross-linked GE containing scaffolds. After the cross-linking both signals disappear, since L-Glu and L-Asp are involved in the formation of new amide bonds after the reaction [251-253]. The signal at ca. 895 cm^{-1} (Fig. 28, blue arrow) was instead assigned to the C-COO stretching [304-306] of the polyester PLA, and so used to identify the increasing PLA content in the hybrid scaffolds. Moreover, after the cross-linking, this signal appears more narrow and with a higher relative intensity, reflecting the higher final PLA content in the scaffolds after the cross-linking.

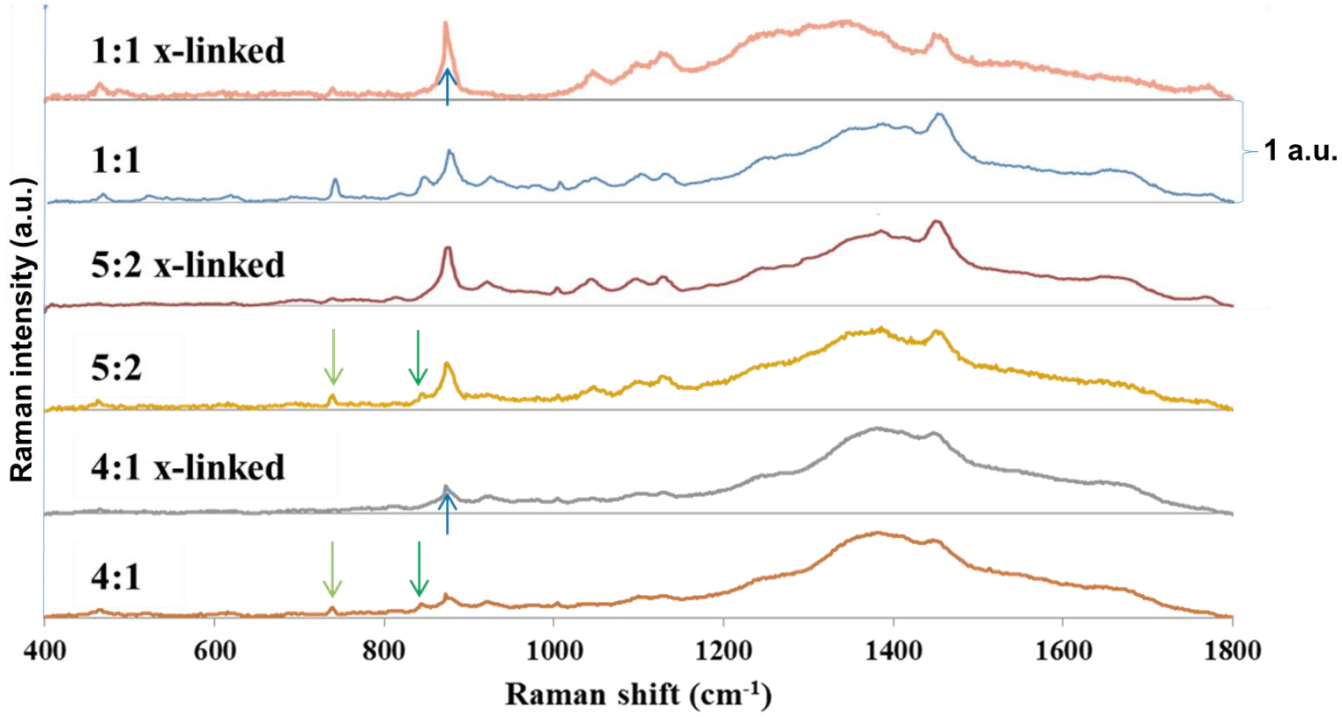

Fig.28. Raman spectra of different hybrid electrospun scaffolds. Starting from the top: cross-linked 1:1 GE:PLA; uncross-linked 1:1 GE:PLA; cross-linked 5:2 GE:PLA; uncross-linked 5:2 GE:PLA; cross-linked 4:1 GE:PLA; uncross-linked 4:1 GE:PLA.

The principal component analysis (PCA) was performed as well to compare the obtained spectra and detect differences in the samples. This analysis allows distinguishing samples with significant differences in the contribution of single peaks to the final spectrum. Herein, it allowed us to group the different samples, and to detect spectral differences due to the cross-linking and the increasing PLA content in the samples as well. Actually, we were able to detect the effect of the cross-linking for each single hybrid scaffold (Fig.29 A-C), separating the samples according to the contribution of the signals at 743cm^{-1}, 876 cm^{-1} and 895 cm^{-1} which represent the peaks of interest as already observed in the Raman spectra (Fig.28). Besides, the PCA analysis allowed us to group and distinguish the different hybrid scaffolds as well, when comparing them all together and mainly considering the contribution of the signals at 743cm^{-1}, 876 cm^{-1} and 895 cm^{-1} (Fig. 29D).

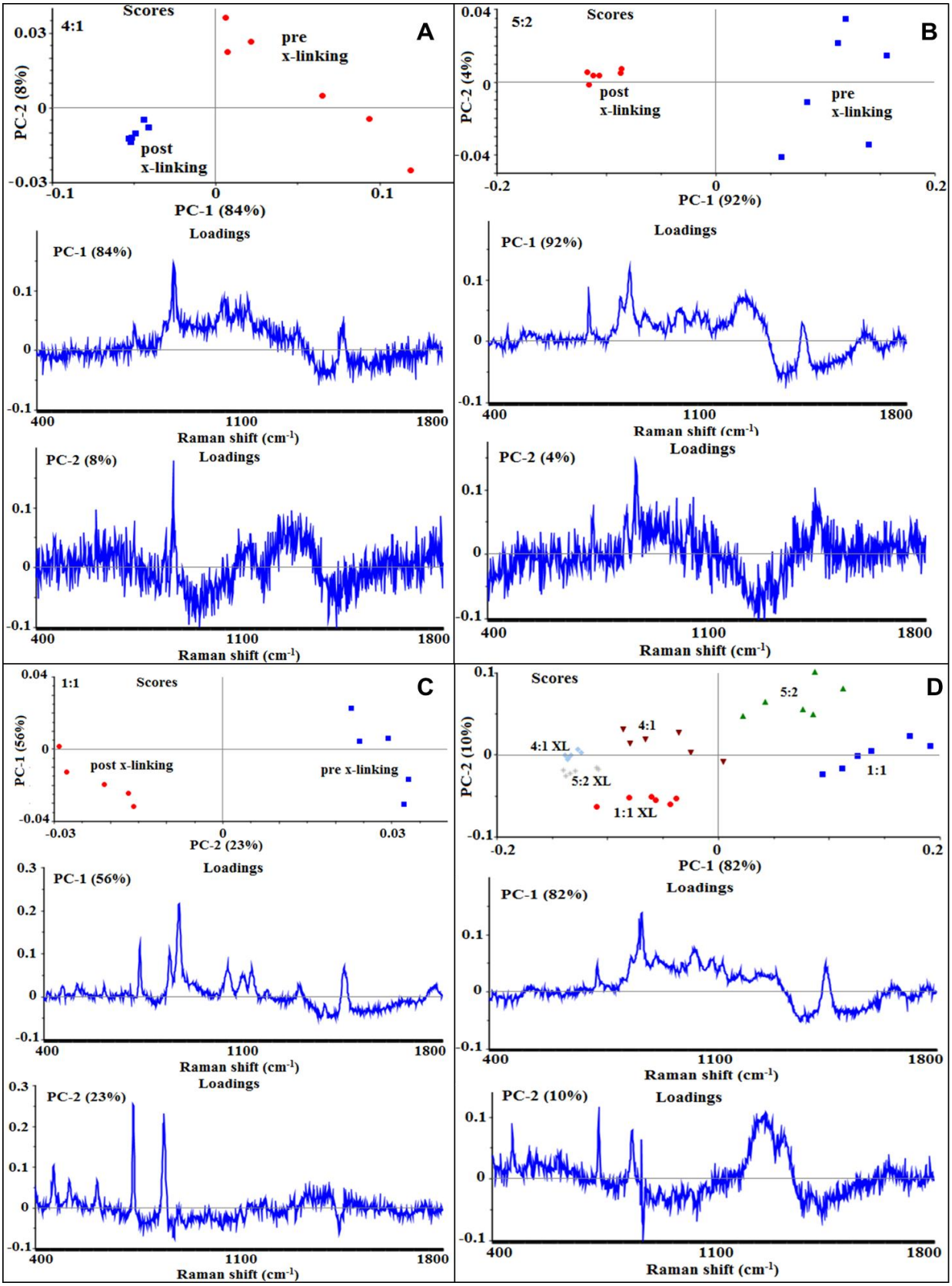

Fig.29. PCA analysis of the RAMAN spectra of: GE:PLA 4:1 with the relative PCs (A); GE:PLA 5:2 with the relative PCs (B); GE:PLA 1:1 with the relative PCs (C); all the hybrid GE:PLA scaffolds (XL=after cross-linking) with the relative PCs (D).

4.2.1.6. Scaffolds biocompatibility

The biocompatibility of all cross-linked hybrid GE:PLA scaffolds containing different ratios of the two polymers was verified performing a cell proliferation assay (Fig.30).

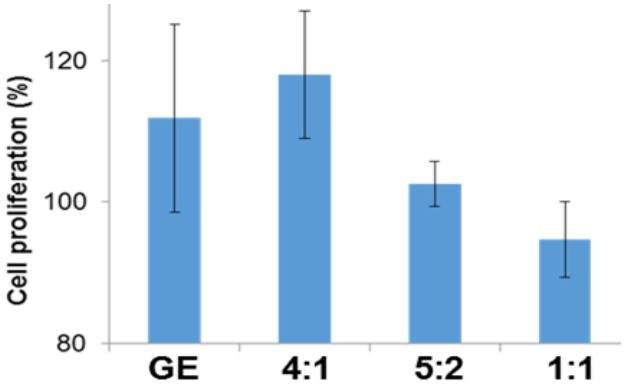

Fig.30. Results of the MTS assay for all the hybrid cross-linked scaffolds, as well as for pure cross-linked GE.

According to the results of the MTS assay all the scaffolds showed a high biocompatibility, since their extracts after 72 hours incubation didn't exhibit any cytotoxic effect towards HDFs. The test was performed also for the pure cross-linked GE. Biocompatibility of pure PLA was previously verified [88]. According to the results neither the cross-linking reaction nor the polymers have cytotoxic effects on HDFs.

4.2.2. HYBRID GELATIN/POLY-L-LACTIDE IN 1:1 RATIO SCAFFOLDS WITH CONTROLLED HYDROPHOBICITY

4.2.2.1. Functionalization of the scaffolds with hyaluronic acid

Cross-linking of the scaffolds was performed in presence of HA or not. The hybrid GE:PLA 1:1 electrospun scaffold was in this case chosen because it showed greater elasticity in comparison with the other hybrid scaffolds after cross-linking. Moreover, it was the only hydrophobic scaffold (section 4.2.1.3.). Therefore, the HA functionalization could also help to increase scaffold hydrophilicity and, thus, to enhance cell adhesion [307, 308]. The highest

HA concentration in the cross-linking solution was 0.03% w/v, since when going over this value we were not able anymore to solubilize HA which instead jellified in the reaction mixture. Besides, a simple HA coating was performed as well, using the same experimental conditions, but not having any cross-linking reagent in the HA containing solution. In this case, only one HA concentration was used (0.025% w/v).

4.2.2.2. SEM and fiber diameter analysis

All the electrospun scaffolds were characterized by SEM in order to investigate the morphology of the electrospun scaffolds after the cross-linking or after the coating in presence of HA (Fig.31). The scaffolds which did not contain HA (GE:PLA 1:1, before and after cross-linking) were previously characterized (section 4.2.1.2.). When the hybrid GE:PLA 1:1 scaffold was cross-linked in presence of HA, we were still able to obtain scaffolds with a random oriented fiber distribution. Moreover, the mean fiber diameter did not significantly change when compared to the cross-linked hybrid GE:PLA 1:1 scaffold ($p>0.7$ in all cases), and we could still obtain a normal diameter distribution (Fig.31). Nevertheless, when using the highest HA concentration (0.03% w/v) the initial fibrous structure of the scaffold appeared altered (Fig.31G, H), probably due to a not complete HA solubilization in the cross-linking solution. Therefore, we decided to not further characterize the scaffold cross-linked in presence of the highest HA concentration, since by losing the initial structure it is not more possible to profit from the advantages of the electrospinning technique by processing the polymer(-s). Finally, when analyzing the hybrid GE:PLA 1:1 cross-linked scaffold after having coated it with HA, the fibrous structure did not appear homogeneous. Instead, a HA film formed on the scaffold surface and no normal diameter distribution could be found (Fig.31 I, J).

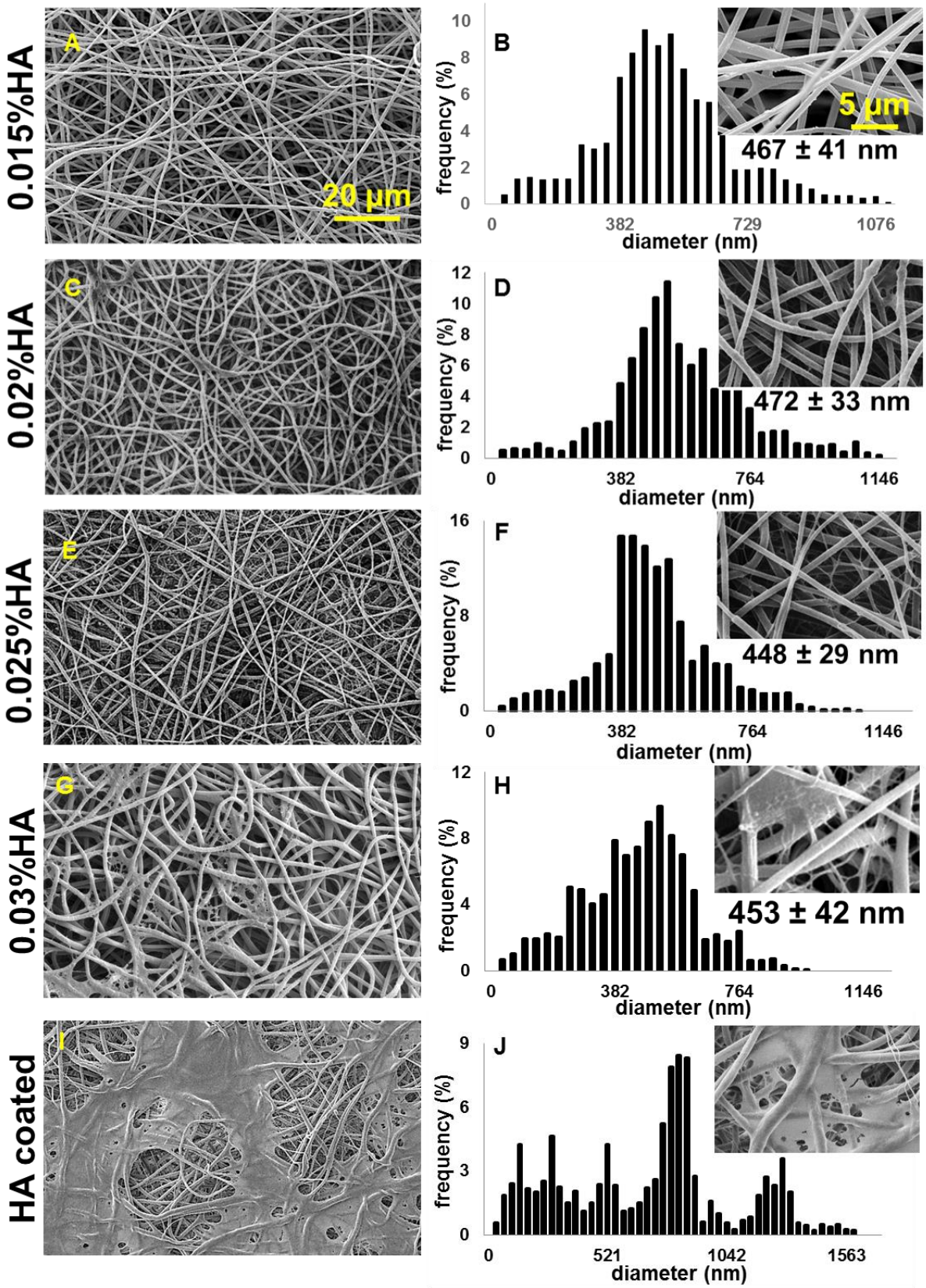

Fig. 31. A, C. SEM images at different magnifications of HA containing electrospun GE:PLA 1:1 blend scaffolds and fiber diameter distribution. A, B. SEM images at different magnifications of electrospun GE:PLA 1:1 cross-linked in presence of 0.015% w/v HA and

fiber diameter distribution. C, D. SEM images at different magnifications of electrospun GE:PLA 1:1 cross-linked in presence of 0.02% w/v HA and fiber diameter distribution. E, F. SEM images at different magnifications of electrospun GE:PLA 1:1 cross-linked in presence of 0.025% w/v HA and fiber diameter distribution. G, H. SEM images at different magnifications of electrospun GE:PLA 1:1 cross-linked in presence of 0.03% w/v HA and fiber diameter distribution. I, J. SEM images at different magnifications of electrospun cross-linked GE:PLA 1:1 coated in presence of 0.025% w/v HA and fiber diameter distribution.

4.2.2.3. Porosity, swelling properties and contact angle measurements

The porosity and the wettability of the HA containing hybrid GE:PLA scaffolds were not significantly different (data not shown) from the values obtained for the cross-linked GE:PLA 1:1 scaffold (section 4.2.1.3). Scaffold hydrophilicity instead increased when the hybrid GE:PLA 1:1 scaffolds were cross-linked or coated in presence of HA (Fig.32). Generally, all the HA containing scaffolds were significantly more hydrophilic than the pure cross-linked GE:PLA 1:1 scaffold not containing HA (no HA) which was highly hydrophobic (Fig.32G. no HA: 129°±3° *versus* 0.015%HA: 87±10 ° , $p=3e^{-7}$; no HA *versus* 0.02%HA: 68±11°, $p=7e^{-9}$; no HA *versus* 0.025%HA: 53±9°, $p=4e^{-9}$; no HA *versus* HA coated: 36±3°, $p=2e^{-10}$). The increasing HA concentration also led to a signicantly higher scaffold hydrophilicity (Fig.32G. 0.015%HA *versus* 0.02%HA, p=0.032; 0.015%HA *versus* 0.025%HA, p=0.004; 0.02%HA *versus* 0.025%HA, p=0.027). Besides, when washing the HA coated scaffold according to the normal experimental procedure (described in section 1.5), the cross-linked GE:PLA 1:1 scaffold regained the initial hydrophobicity. Indeed, the contact angle was not significantly different if compared to the uncoated scaffold (HA coated (post washing): 126±3° *versus* no HA, p=0.21). Thus, the chemical cross-linking of HA seems to show advantages compared to a simple coating, since if performing biological tests, scaffolds are usually incubated together

with cells in culture medium for at least 24 hours. As a result, the HA film deposited on the electrospun fibers after the coating may be washed away.

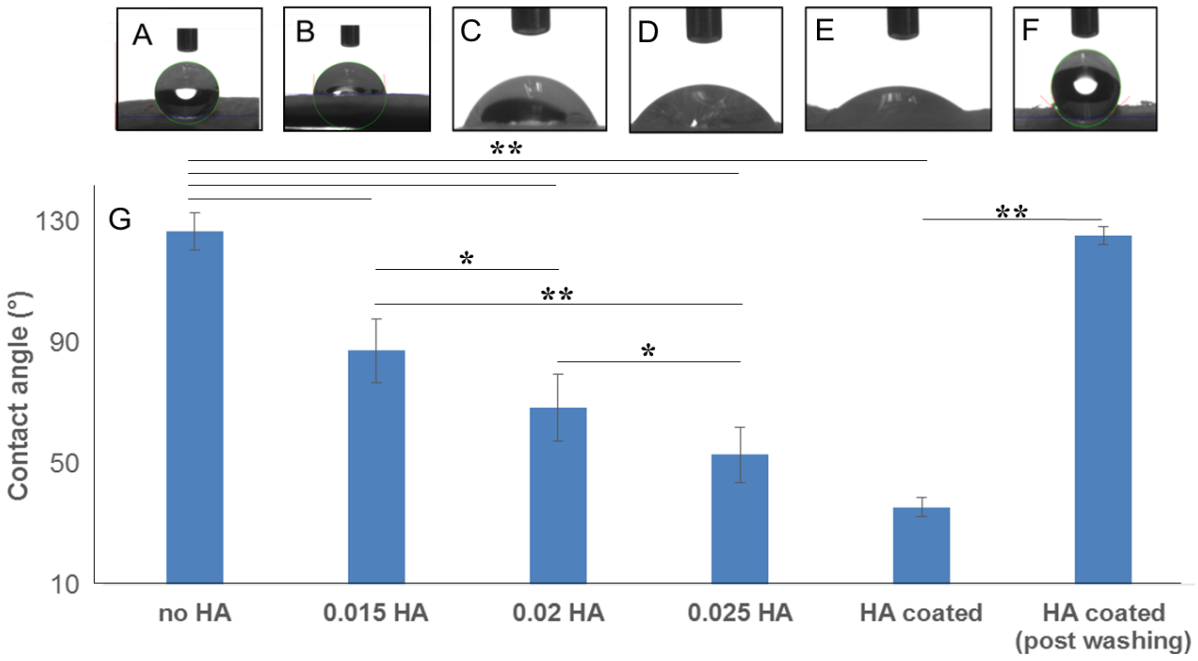

Fig. 32. A-F. Frames of the contact angle evaluation of the hybrid GE:PLA scaffolds cross-linked in presence of 0.00% w/v HA (A), 0.015% w/v HA (B), 0.02% w/v HA (C), 0.025% w/v HA (D), coated with HA (E) and coated with HA after standard washing procedure (F). G. Statistical comparison of the average contact angles for the different hybrid GE:PLA 1:1 scaffolds.

4.2.2.4. Tensile tests

The mechanical properties of the different hybrid GE:PLA 1:1 scaffolds were analyzed. Representative stress-strain curves for the hybrid GE:PLA scaffolds cross-linked or coated in presence of specific HA amounts, before or after swelling, are shown in Fig.33A-H. No significant differences could be detected regarding the tensile strength (Fig.33I) and the Young's modulus (Fig.33J) when comparing the cross-linked scaffolds among them, as well as in comparison to the hybrid GE:PLA 1:1 scaffold cross-linked without HA, previously characterized in section 4.2.1.4. (Fig.27).

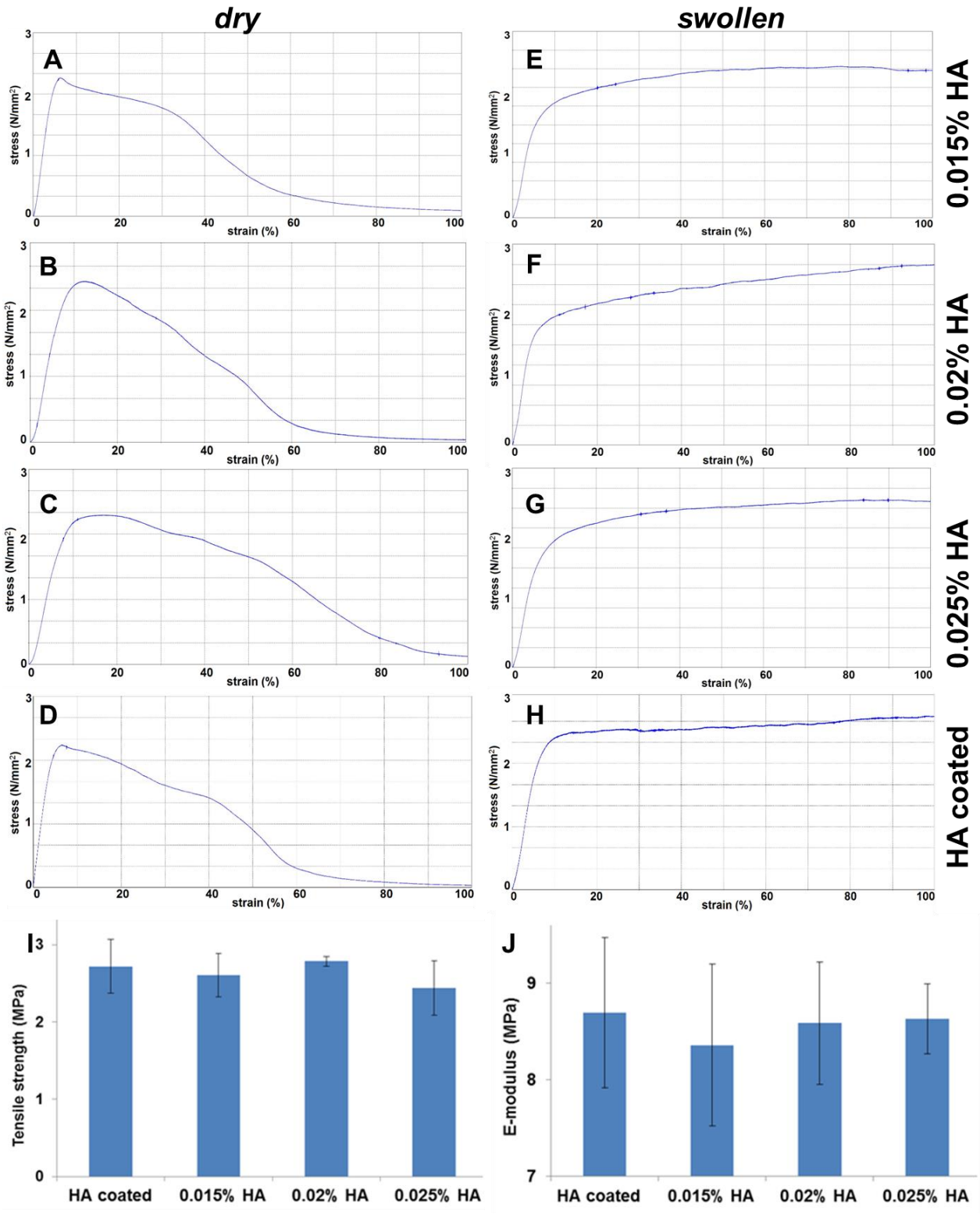

Fig.33. A-D. Representative stress-strain curves of hybrid GE:PLA 1:1 scaffolds cross-linked in presence of 0.015% w/v HA (A), 0.02% w/v HA (B), 0.025% w/v HA (C), or coated with HA (D). E-H. Representative stress-strain curves after swelling of hybrid GE:PLA 1:1 scaffolds cross-linked in presence of 0.015% w/v HA (E), 0.02% w/v HA (F), 0.025% w/v

HA (G), or coated with HA (H). I. Comparison of the tensile strength among the HA containing cross-linked GE:PLA 1:1 scaffolds. J. Comparison of the Young's modulus among the HA containing cross-linked GE:PLA 1:1 scaffolds.

Furthermore, when comparing the swollen and dry HA containing scaffolds among them no significant changes in both Young's modulus and tensile strength could be found (data not shown). However, all the swollen scaffolds showed a greater elongation at break than the dry samples. According to our results, the addition of HA does not affect the mechanical properties of the hybrid GE:PLA 1:1 cross-linked scaffold, differently from literature data by Yang et al. working on silk fibroin [33].

4.2.2.5. Raman spectra and principal component analysis (PCA)

Raman microspectroscopy was used to investigate HA presence in the scaffolds. The only two signals in the Raman spectrum of the pure HA, in powder, (Fig.34, first spectrum from the top) that do not appear in the Raman spectrum of GE:PLA 1:1 scaffold (Fig.28), are those related to vibrations of the β-linkages of the polysaccharide and skeletal C-O-C stretchings, which have a Raman shift of 900cm^{-1} (Fig.34 first spectrum from the top, blue arrow) and 945cm^{-1} (Fig.34 first spectrum from the top, red arrow), respectively [309]. In the HA coated scaffold the signal related to the C-O-C stretchings appears to be shifted to a lower wavenumber of 897 cm^{-1} (Fig.34 first spectrum from the bottom, red arrow), probably due to the interaction of HA with the scaffold. The signal related to the stretching of the β-glucuronidic linkages which is significant for the maintaining of the glycoside structure [309] appears instead not shifted (Fig.34 first spectrum from the bottom, blue arrow). The same signals found in the Raman spectrum of the HA coated scaffold could be found in the hybrid GE:PLA 1:1 scaffold cross-linked in presence of 0.025% w/v HA (Fig.34 second spectrum from the top, blue and red arrows). When using lower HA concentrations only the signal

related to skeletal C-O-C linkage stretching could be detected (Fig.34 third and fourth spectrum from the top, red arrow). Finally, after washing the HA coated cross-linked scaffolds both signals significant for the HA presence could not be detected anymore, confirming our hypothesis that the HA deposited film is washed away.

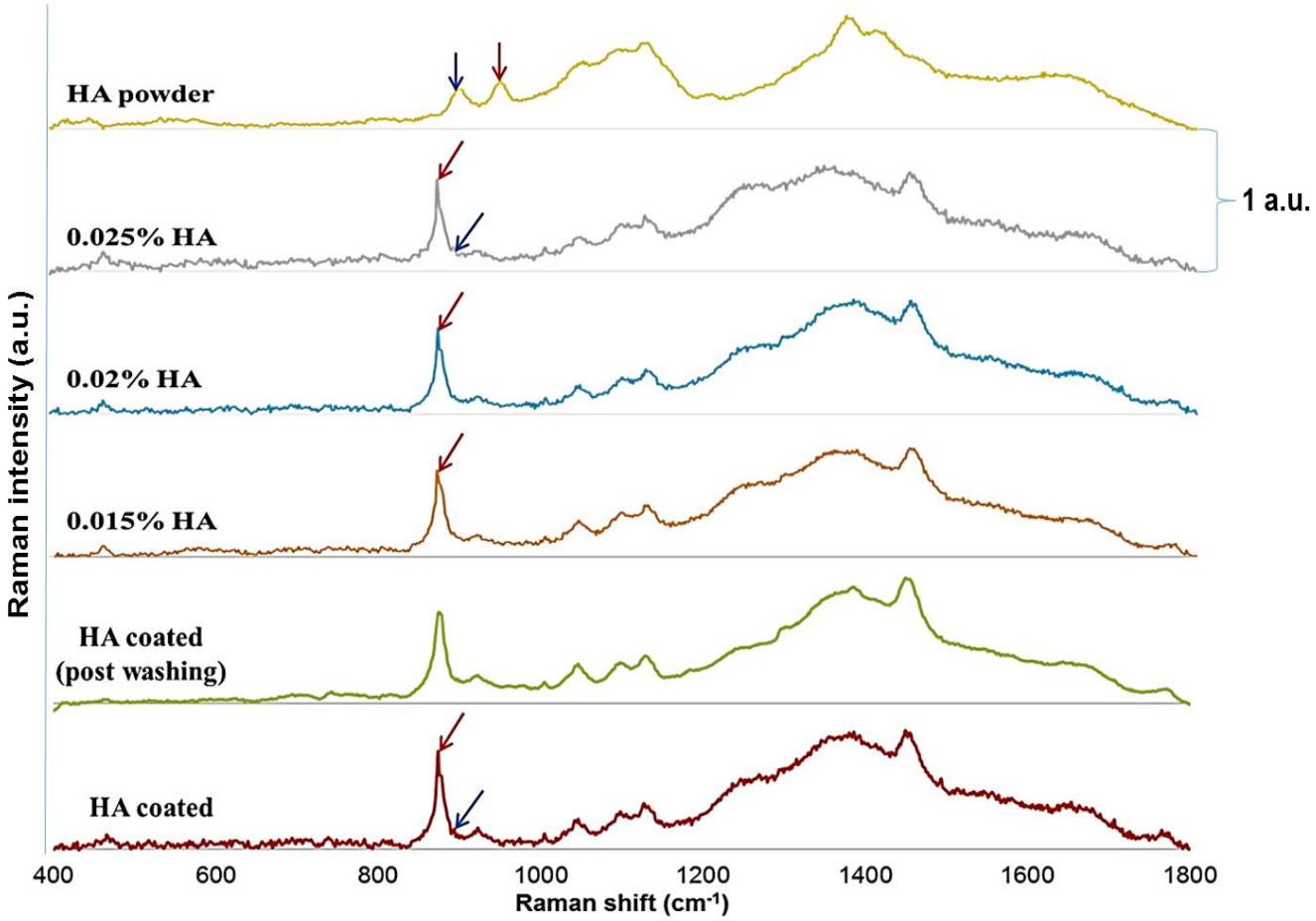

Fig.34. Raman spectra. Starting from the top: HA as powder; GE:PLA 1:1 scaffold cross-linked in presence of 0.025% w/v HA; GE:PLA 1:1 scaffold cross-linked in presence of 0.02% w/v HA; GE:PLA 1:1 scaffold cross-linked in presence of 0.015% w/v HA; HA coated cross-linked GE:PLA 1:1 scaffold after standard washing procedure; HA coated cross-linked GE:PLA 1:1 scaffold.

Besides, we also performed a PCA analysis comparing the scaffolds cross-linked in presence of HA among them (Fig.35A), and, separately, the coated one, before and after washing (Fig.35B). In all cases the hybrid GE:PLA 1:1 scaffold cross-linked without HA (no HA), previously characterized in section 4.2.1.5., was used as a control.

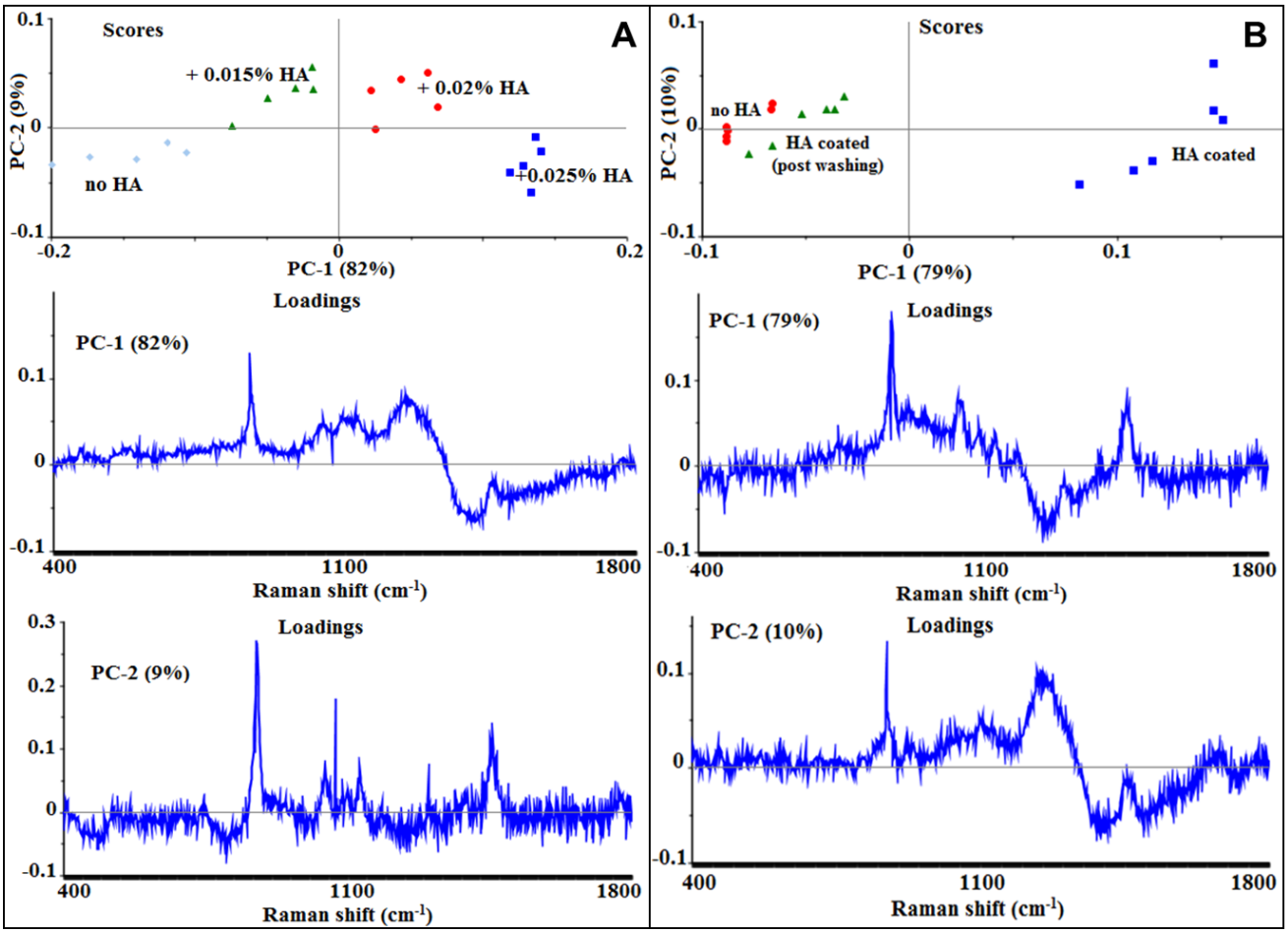

Fig.35. PCA analysis with the relative PCs of the Raman spectra of: A. hybrid GE:PLA 1:1 scaffold cross-linked either in presence of different HA w/v% (+0.015% HA; +0.02% HA; +0.025% HA) or without HA (no HA); B. hybrid cross-linked GE:PLA 1:1 scaffold before (no HA), after HA coating (HA coated) and after HA coating followed by washing (HA coated (post washing)).

According to the PCA analysis we could detect the increasing HA content in the cross-linked scaffolds, mainly taking into account the contribution of the signal at 897 cm^{-1} to the final spectra (Fig.35A). On the other side, the PCA analysis allowed us to distinguish the HA

coated scaffold from the starting hybrid cross-linked GE:PLA scaffold, while after the washing procedure the coated scaffold was similar to the uncoated (Fig.35B). These results confirm the advantages of using the cross-linking procedure instead of a simple coating when aiming to obtain HA containing scaffolds for *in vitro* cell-culture.

4.2.2.6. Scaffolds biocompatibility

The biocompatibility of all cross-linked hybrid GE:PLA 1:1 scaffolds containing HA was verified performing a cell proliferation assay (Fig.36).

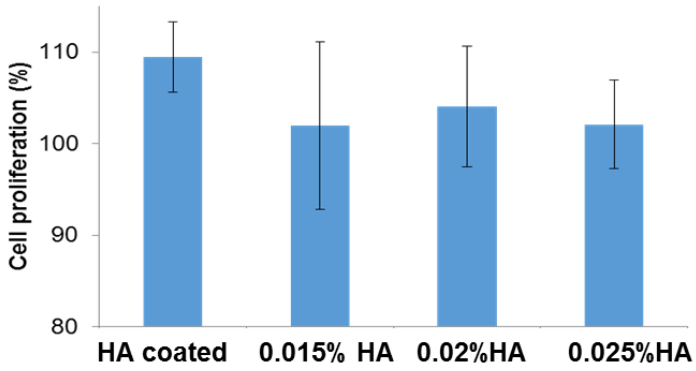

Fig.36. Results of the MTS assay for all the hybrid HA containing cross-linked GE:PLA 1:1 scaffolds.

According to the results of the MTS assay all the scaffolds showed a high biocompatibility, since the scaffold extracts after 72 hours incubation did not show any cytotoxic effect towards HDFs. These results suggest that neither the cross-linking reaction nor the presence of HA affect the biocompatibility of the hybrid electrospun scaffolds.

4.2.3. MPM AND FLIM ANALYSIS OF HDFs ON HYBRID GELATIN/POLY-L-LACTIDE SCAFFOLDS

4.2.3.1 MPM imaging

In the last part of the work, we verified cellular adhesion and cellular growth properties of human dermal fibroblasts (HDFs) on the different hybrid electrospun scaffolds using multiphoton microscopy (MPM) which represents a not invasive, marker-free methodology [94-97]. All the cross-linked hybrid GE:PLA scaffolds with a different ratio between the two polymers, as well as the GE:PLA 1:1 hybrid scaffold cross-linked in presence of 0.025% w/v HA were investigated. Gelatin is reported to exhibit autofluorescence at an excitation wavelength of 355 nm [310], and in our case we could detect this autofluorescence signal (Fig.37A-H) using a two-photon excitation at a wavelength of 710 nm. However, we were also able to image HDFs within the scaffolds by inducing NAD(P)H autofluorescence at the same wavelength (Fig.37 A-H). For easier cellular visualization also a control represented by HDFs seeded on glass is shown in Fig.37I and Fig.37J. Furthermore, images where HDFs are labeled with yellow arrows (Fig.37 B, D, F, H, J) are reported.

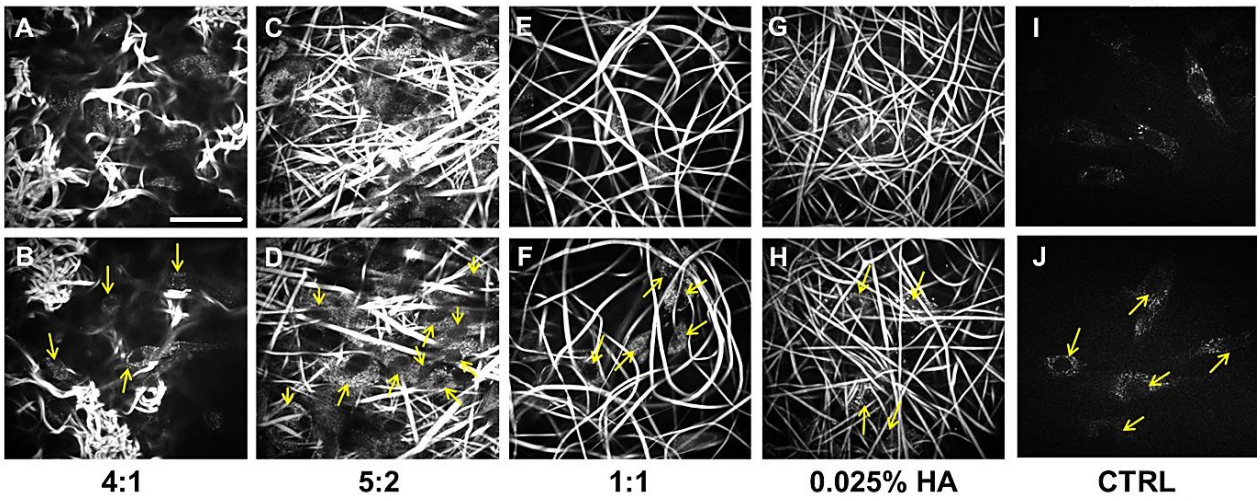

Fig.37. A-J. MPM images of HDFs seeded on hybrid GE:PLA scaffolds (A,B. 4:1; C,D. 5:2; E,F. 1:1; G,H. 1:1 + 0.025% w/v HA) or on glass (I,J). Scale bar equals 40µm.

Interestingly, we were able to image both cells and scaffolds at the same time using MPM, showing that HDFs adhere not only on the scaffold surface but mainly within the fibrous structure which is a must when aiming to produce a 3D *in vitro* model. According to morphological observations, the hybrid cross-linked GE:PLA 5:2 scaffold seems to be the one where more HDFs adhered and proliferated (Fig.37 C, D). However, cells could be imaged in all the other hybrid GE:PLA scaffolds as well (Fig.37 A,B, E-H), showing proliferation and adhesion properties similar to those of HDFs seeded on glass (Fig.I, J) according to morphological observations.

4.2.3.2 FLIM analysis

After MPM imaging of HDFs within the fibrous hybrid GE:PLA scaffolds we investigated the same samples using fluorescence lifetime imaging microscopy (FLIM, Fig.38), which allows the analysis of the metabolism of the target cells, parallel to their imaging, having NAD(P)H as a target [42]. Interestingly, even if having a strong autofluorescence from the gelatin, using a biexponential decay curve fitting, we were able to distinguish the cells from the scaffolds by a false colour coding, based on a 2D-correlation. As a matter of fact, the cells show a much shorter τ_1 than the scaffolds, due to the free NAD(P)H fluorescence lifetime [42]. This value also leads to a shorter mean fluorescence lifetime (τ_m) which directly depends on the τ_1 values [29]. We believe that a discrimination between cells and scaffolds using two variables could be an interesting way to separate the single contributions, and thus analyze the cells alone. Actually, when having cells within the fibrous scaffolds (Fig.38 A-L) they could be coulored in yellow/light green (Fig.38 B, E, H, K) due to shorter τ_1 and τ_m values when compared to the scaffold fibers which were instead coloured in blue due to longer τ_1s and τ_ms (Fig.38 B, E, H, K).

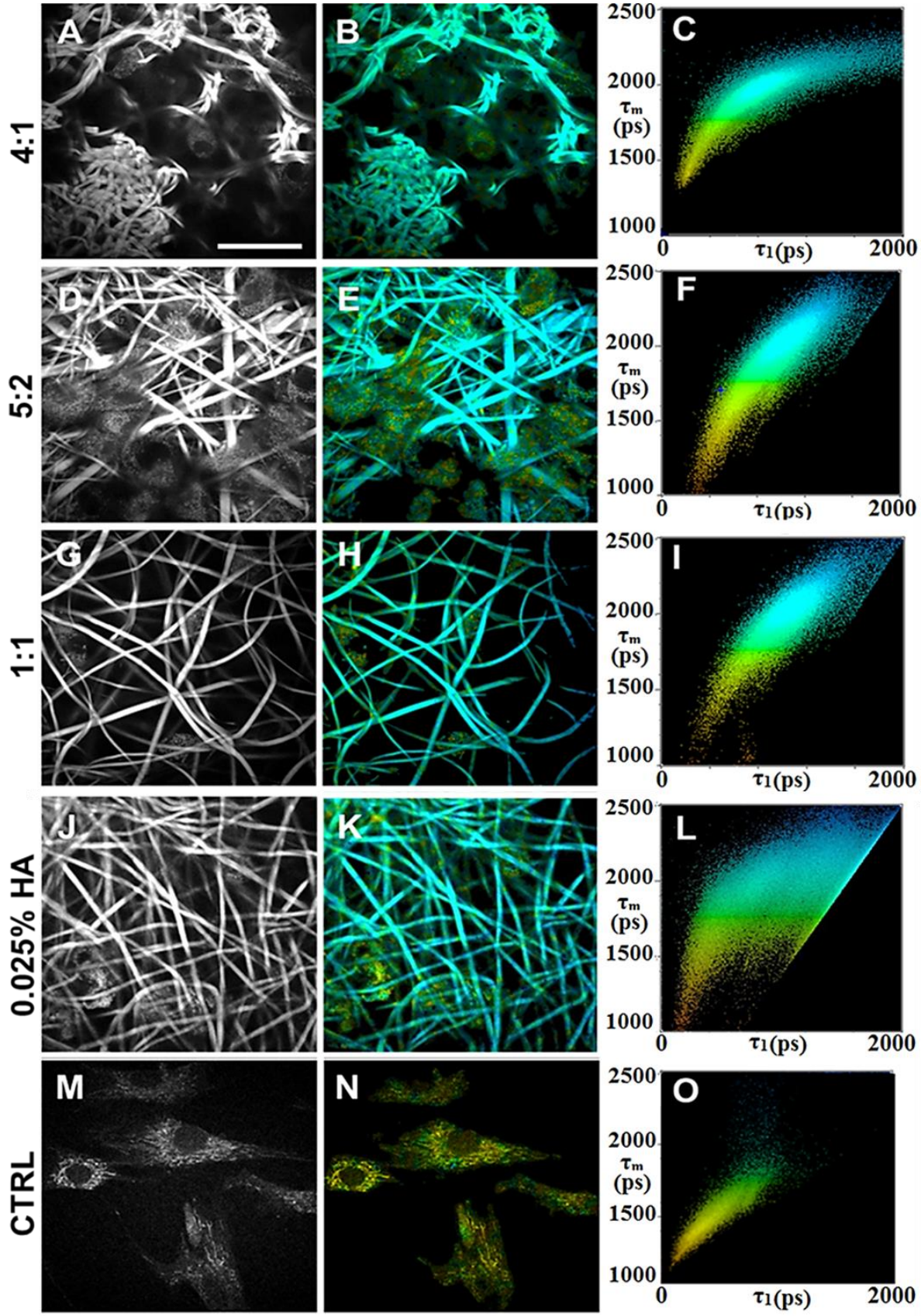

Fig.38. FLIM analysis of HDFs seeded on hybrid GE:PLA scaffolds (A-L) or on glass (M-O).

Scale bar equals 25µm.

Looking at the 2D-correlation having τ_1 and τ_m as variables on the x and y axes, respectively (Fig.38 C, F, I, J), the pixels obtained from the cells lay in the south-west part of the plot, while those due to scaffold contribution in the north-east one. To confirm our hypothesis, when analyzing HDFs on glass (CTRL, Fig.38 M-O), all the values lay in the south-west part of the plot, with more than the 95% of the points having τ_1<1000ps and τ_m<1750ps (Fig.38O). According to these observations we developed a spreadsheet using Microsoft Excel™ that allowed us to isolate all the pixels satisfying at the same time these two conditions (τ_1<1000ps and τ_m<1750ps) in the FLIM images. Once isolated these pixels, we could compare the α_1 (%) values for the HDFs, to evaluate the relative glycolysis/oxidative phosphorylation contribution to their metabolism (Fig.39). According to the results, only the cells in the hybrid scaffold having the highest GE content showed a lower glycolytic activity when compared to HDFs seeded on glass (α_1 (%) 4:1= 54±8% *versus* CTRL α_1 (%) = 73±6%). No significant differences could be instead found when comparing the other cross-linked hybrid GE:PLA scaffolds with the control (CTRL), or when comparing the different GE:PLA scaffolds among them (Fig.39).

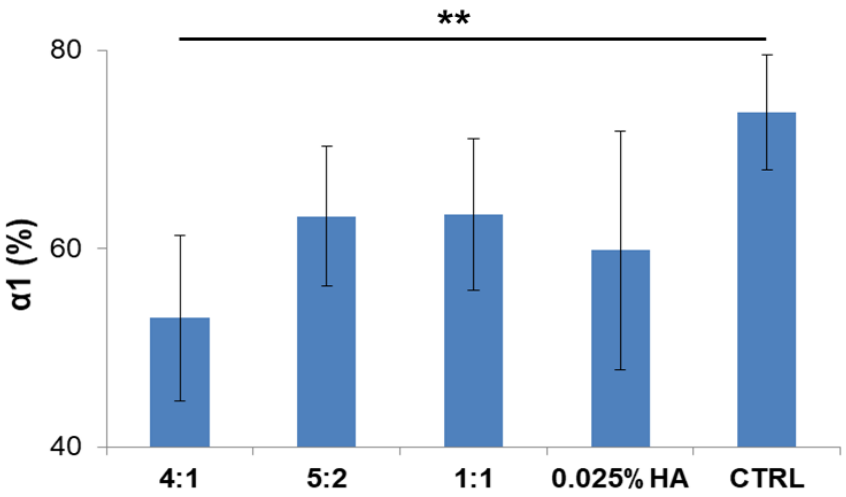

Fig.39. Comparison of the α_1 (%) values for HDFs seeded on different hybrid GE:PLA scaffolds. Results arise from a biexponential fitting of the FLIM data.

4.3. Discussion

Blend electrospun nanofibrous scaffolds are of growing interest as biomimetic structures with unique properties resulting from the combination of naturally derived and synthetic polymers [197, 198]. In this thesis, different hybrid GE/PLA electrospun scaffolds were produced and characterized with the final aim of obtaining biomimetic porous structures with tunable physical and mechanical properties. To time, some attempts have already been made to produce well-blended GE/PLA scaffolds [311-315]. The best electrospun hybrid scaffolds composed of GE and PLA have been so far obtained using HFIP as solvent for polymers processing [312, 313, 315]. Thus, throughout this thesis we used HFIP, since it ensured us to dissolve both GE and PLA, either alone or together (in different ratios too), and to process the resulting blend solutions by electrospinning. In the first part, hybrid GE/PLA scaffolds having different relative polymers ratios were characterized. Three different GE:PLA w:w ratios (4:1, 5:2 and 1:1) were chosen for scaffolds production, characterization and comparison. All the scaffolds were homogeneous, even after cross-linking, showing a high porous structure with random oriented fibers, according to the SEM analysis. In all cases, the mean fiber diameter was in the hundred nanometers scale, but this value generally increased with the increasing PLA percentage. These results are in agreement with the data by Moon et al. [311] and Wang et al. [314]. A different behavior could be instead found by Kim et al. [313]. However, Kim et al. [313] used 2,2,2-trifluoroethanol as solvent for the electrospinning experiments, while in this work HFIP was employed like Moon et al. [311] and Wang et al. [314]. The chosen solvent plays an important role for polymers processing which reflects on the final morphology of the electrospun scaffolds [100, 316, 317]. The hybrid scaffolds with the highest GE content showed a greater porosity, due to a higher number of pores, even with a lower mean size. These results agree with previous studies [318-320]. Moreover, we could also infer that, the higher the porosity is the more water is retained by the cross-linked hybrid scaffolds. These swelling properties are also directly related to the GE content [321, 322]. It is

well known that hydrogels and foam or sponge scaffolds have a higher porosity than the electrospun ones [323]. However, electrospinning allows the production of fibrous 3D nano-structures which better mimic the ECM, still remaining highly porous [202]. Not least, we also demonstrated that by blending GE and PLA, we could obtain final cross-linked scaffolds with improved elasticity if compared to pure cross-linked GE, due to the lower Young's modulus shown in the dry state. According to these results, we also belive that the stiffness of hybrid GE/PLA scaffolds could be tuned. However, pure cross-linked GE Young's modulus may represent a threshold value when aiming to increase scaffold stiffness. It has already been proved that mechanical properties of electrospun cross-linked GE strongly change after water uptake [324], even when blended together with other polymers [324-327]. As already observed by Kharaziha et al. [324] we could find a higher elasticity and a better elongation at break for pure cross-linked GE after swelling when compared to the dry scaffolds. However, in our case, when blending GE together with PLA the elastic modulus of the wet samples was not significant different from the values obtained for the dry scaffolds. A similar behavior could be found by Jing et al. when blending GE together with poly (propylene carbonate) [327]. Nevertheless, as previously shown [324, 326, 327] all the scaffolds showed a much greater elongation at break after swelling (elongation (%) > 100%), and our instrument was even not able to break down the scaffolds. Moreover, changes in the Raman spectra of the hybrid scaffolds due to the cross-linking reaction were found, suggesting a new non-destructive approach to detect the effectiveness of this reaction. Finally, all the different hybrid scaffolds showed a high biocompatibility towards HDFs according to the results of the MTS cell proliferation assay. The MTS assay results prove that no toxic reagents or solvent residuals remain in the scaffolds after the whole processing ranging from electrospinning to cross-linking.

In the second part of the work described in this chapter, hybrid GE:PLA 1:1 scaffolds cross-linked in presence of different HA concentrations according to the method described by Yang

et al. [33] were produced and characterized. In this case, the final aim was to obtain hybrid scaffolds with a tunable, enhanced hydrophilicity. It is well known that surface hydrophilicity of 3D electrospun scaffolds better favor cell attachment and proliferation [307-308, 328-332]. Besides, we could also introduce HA, an essential component of the ECM, involved in many biological or physiological functions [333-335]. Many different attempts have already been made to produce HA containing electrospun scaffolds [336-340]. To time, the best results in directly electrospinning HA have been achieved either using NH_4OH/DMF as solvent for its processing [338, 339] or using the thiolated HA as starting substrate [340]. However, the usage of a strong basic system as well as of chemically modified HA have been questioned since the final HA properties may be altered [341]. Considering these literature data, in this thesis, we decided to bind HA to previously electrospun hybrid GE:PLA scaffolds using the procedure recently described by Yang et al. [33]. The cross-linking chemistry used by Yang et al. is based on the simultaneous use of 1-ethyl-3-(3-dimethylaminopropyl) carbodiimide (EDC) and N-hydroxysuccinimide (NHS), which is a widely exploited and well-approved approach [33, 253-256]. According to this procedure, HA is firstly bound to electrospun scaffolds when cross-linking them (Fig.S10). Cross-linking is a necessary step when working with water-sensitive polymers like gelatin, and thus it doesn't represent a further step in the scaffolds production. Firstly, we investigated the structure of the scaffolds using SEM. We could notice, that the addition of HA didn't affect the fiber diameter distribution of the electrospun scaffolds, still having a normal distribution with an average diameter of ca. 500 nm. However, when increasing the HA concentration to 0.03% w/v the fibrous structure of the final scaffold was altered and different from the one typical of good electrospun scaffolds. According to these observations and the chosen methodology [33], we believe that the 0.025% w/v concentration represents a threshold value when aiming to cross-link HA to hybrid GE:PLA scaffolds in 1:1 ratio, and still obtain ECM-like final structures. To prove that the hydrophobicity of the hybrid cross-linked GE:PLA blend could be reduced by increasing

the HA percentage, the contact angle of all the different scaffolds was measured. As already observed by Yang et al. [33], the scaffolds became the more hydrophilic the higher was the HA concentration used by the cross-linking reaction. Moreover, we could also demonstrate that the addition of HA did not modify the mechanical properties of the hybrid GE/PLA scaffold. Besides, we showed the advantages offered by the chemical cross-linking of HA to the hybrid electrospun scaffolds over a simple HA coating of the materials. According to our observations the HA film deposited on the cross-linked hybrid scaffolds due to the coating is washed away from the materials after 24 hours incubation in an aqueous environment. Thus, this kind of functionalization is not useful for the most biological tests [41, 160, 317]. The biocompatibility of all the scaffolds was verified too by a cell proliferation test in order to prove that no toxic reagents and solvents were retained in the scaffolds after their modification. To check the HA presence in the hybrid electrospun scaffolds Raman analysis was performed. This technique allowed us to detect the increasing HA content in the electrospun scaffolds even if the peaks used for HA detection were shifted in the spectra of the hybrid GE/PLA functionalized materials. These findings suggest, that this analysis allows the HA detection also in electrospun scaffolds as previously demonstrated [342]. However, the detection of HA in so low percentages may be confirmed with more sensitive and specific analyses [343-345]. In the last part of this work, the proliferation of HDFs on the hybrid cross-linked scaffolds could be imaged and analyzed using MPM coupled with FLIM. According to our results it is also possible to distinguish the specific cellular NAD(P)H contribution to the final fluorescence lifetime, even if a strong autofluorescence was detected from the scaffold fibers during the FLIM analysis. This separation could allow analysis of cellular metabolism of HDFs besides their imaging even in a complex matrix using an innovative, non-invasive approach. Nevertheless, cell proliferation on the hybrid scaffolds and the cell-material interactions have to be investigated using already established methodologies [330, 331, 346, 347].

4.4. Conclusions

In this part of the thesis, different hybrid GE/PLA electrospun scaffolds were produced and characterized. By changing the ratio between the two polymers we were able to obtain scaffolds with different porosities, which directly correlate with their swelling properties. In particular, the porosity and the swelling properties of the scaffolds increased when using a higher GE content. Besides, we were also able to obtain hybrid GE/PLA electrospun scaffolds whose hydrophilicity could be enhanced by introducing increasing amounts of HA. In all cases, we were able to characterize the scaffolds with Raman microspectroscopy which is a non-destructive, non-invasive methodology when compared to FTIR. Moreover, all the scaffolds showed no cytotoxic effects towards HDFs. Afterwards, cell adhesion in the different scaffolds could be imaged and analyzed by MPM coupled with FLIM without any staining. On resuming, we were able to tune the properties of hybrid GE/PLA electrospun scaffolds without changing the nature of used polymers, and to characterize them in a non-destructive, marker-free way. Both aspects are of great interest when aiming to develop new versatile *in vitro* models that could be potentially used for *in vivo* applications.

SUMMARY AND CONCLUDING REMARKS

In the first part of the thesis (chapters 2 and 3), pure poly-L-lactide (PLA) scaffolds were obtained and characterized as delivery systems for Diclofenac sodium salt (DCF) and a synthetically obtained prodrug of it for the treatment of actinic keratosis. The effective drug encapsulation, as well as the release could be demonstrated in all cases. When working with the unmodified DCF we were also able to control the release profile by adding small amounts of dimethyl sulfoxide. The DCF-loaded scaffold was used as a delivery system to induce *in vitro* cell death in human fibroblasts. The target cells were observed using MPM coupled with fluorescence lifetime imaging microscopy (FLIM), using a non-invasive, marker-free *in vitro* model to investigate drug effects. The Diclofenac prodrug was obtained via solid phase using a versatile, clean, high yielding procedure. Besides, as a novelty, the drug encapsulation and its release from the scaffold could be imaged using multiphoton microscopy (MPM). Moreover, the synthesized DCF prodrug showed no cytotoxic effects towards human dermal fibroblasts when compared to the unmodified DCF. Thus, we believe that DCF-Gly could be an interesting DCF precursor for the treatment of actinic keratosis and other diseases. In the last part of the thesis (chapter 4), we produced and characterized different hybrid gelatin/PLA scaffolds. In this case, the goal was to obtain well-blended scaffolds with tunable properties, such as porosity, stiffness, hydrophobicity and wettability. This aspect is of great interest since one of the main problems in tissue engineering is the difficulty of reproducing *in vitro* properties that *in vivo* usually differ from tissue to tissue. We were instead able to control them even without changing the employed polymers, by simply modifying few experimental processing conditions. Not least, the hybrid scaffolds were spectroscopically characterized with Raman microspectroscopy, while cellular interaction was analyzed with MPM coupled with FLIM, with all of them being non-invasive, non-destructive and marker-free approaches.

SUPPLEMENTARY MATERIALS

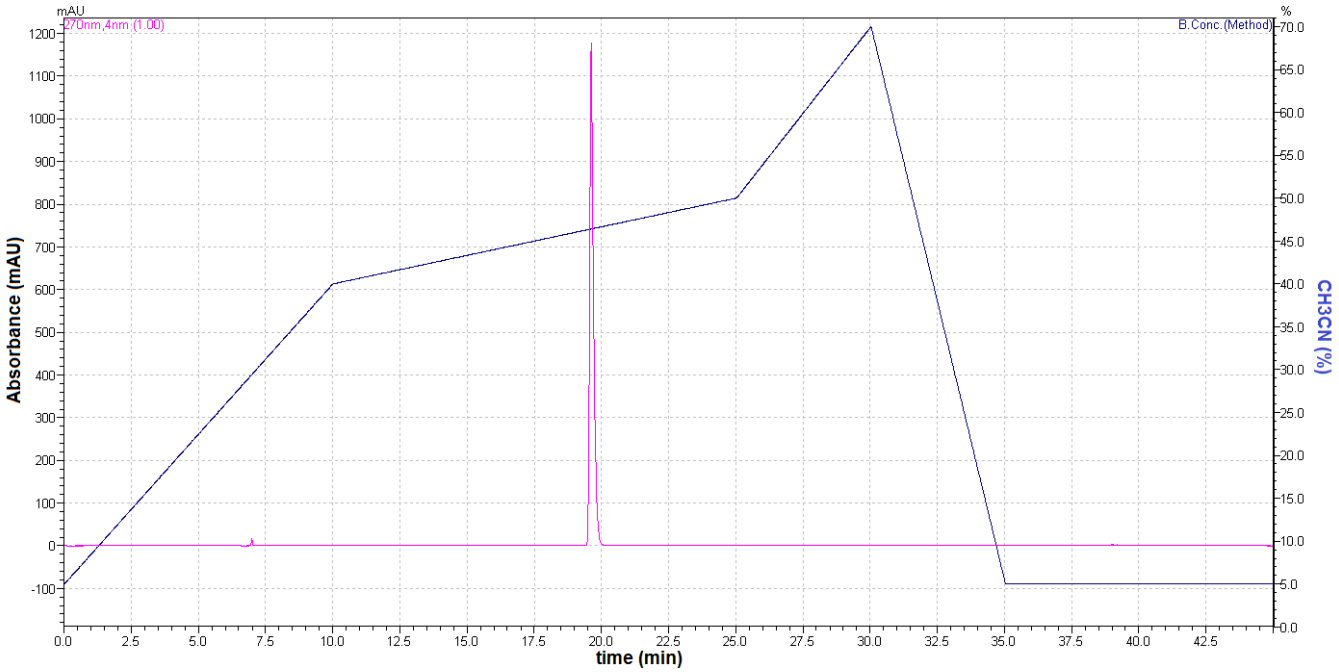

Fig.S1A. RP-HPLC chromatogram of DCF 1mg/mL in PBS.

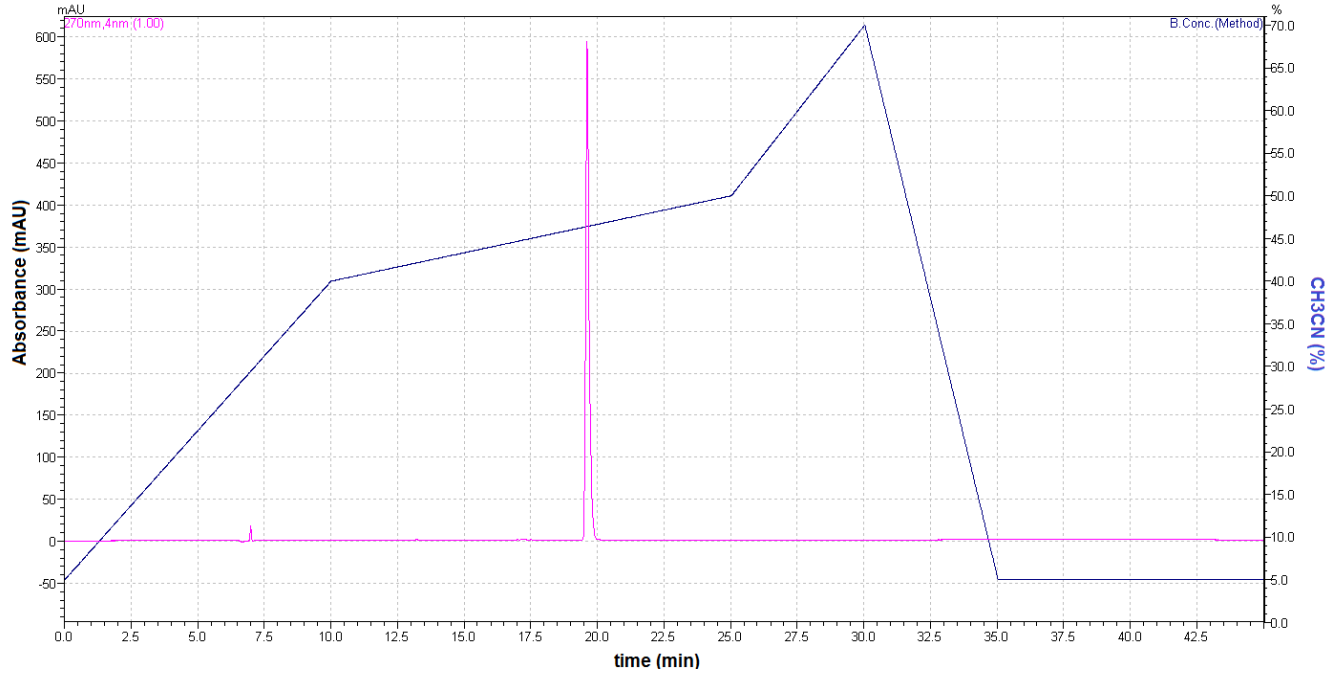

Fig.S1B. RP-HPLC chromatogram of DCF in PBS after its release from a PLA scaffold.

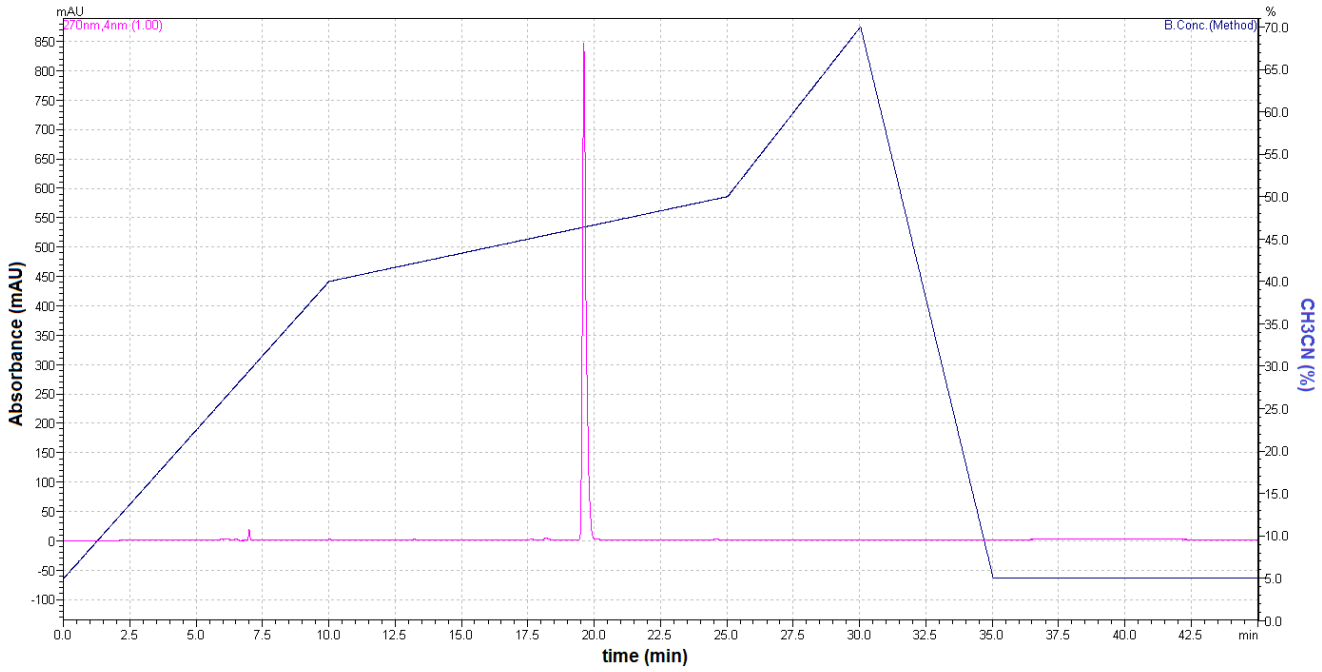

Fig.S1C. RP-HPLC chromatogram of DCF in PBS after its release from a DMSO containing PLA scaffold.

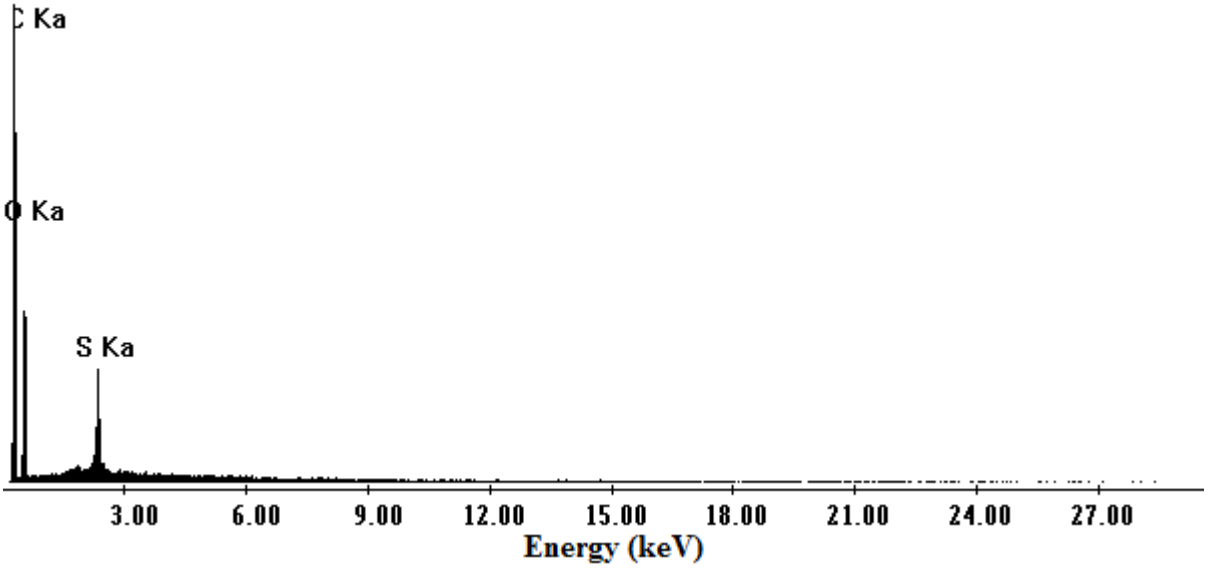

Fig.S2A. Full EDX spectrum of a PLA scaffold electrospun using DMSO as a co-solvent.

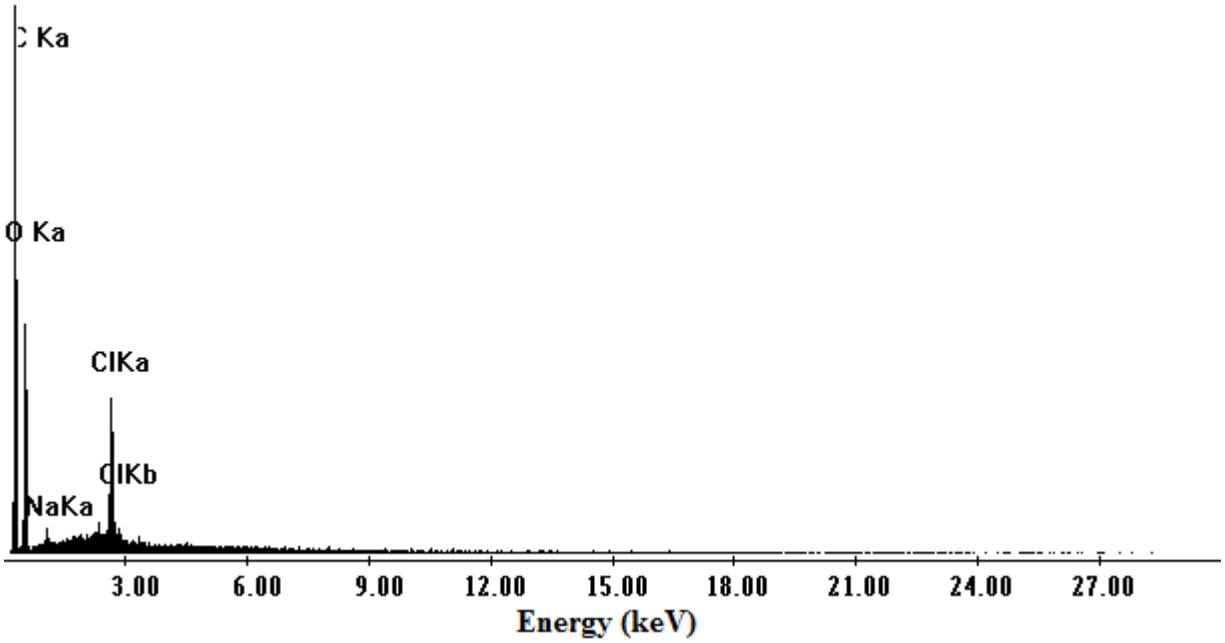

Fig.S2B. Full EDX spectrum of a DCF-loaded PLA electrospun scaffold.

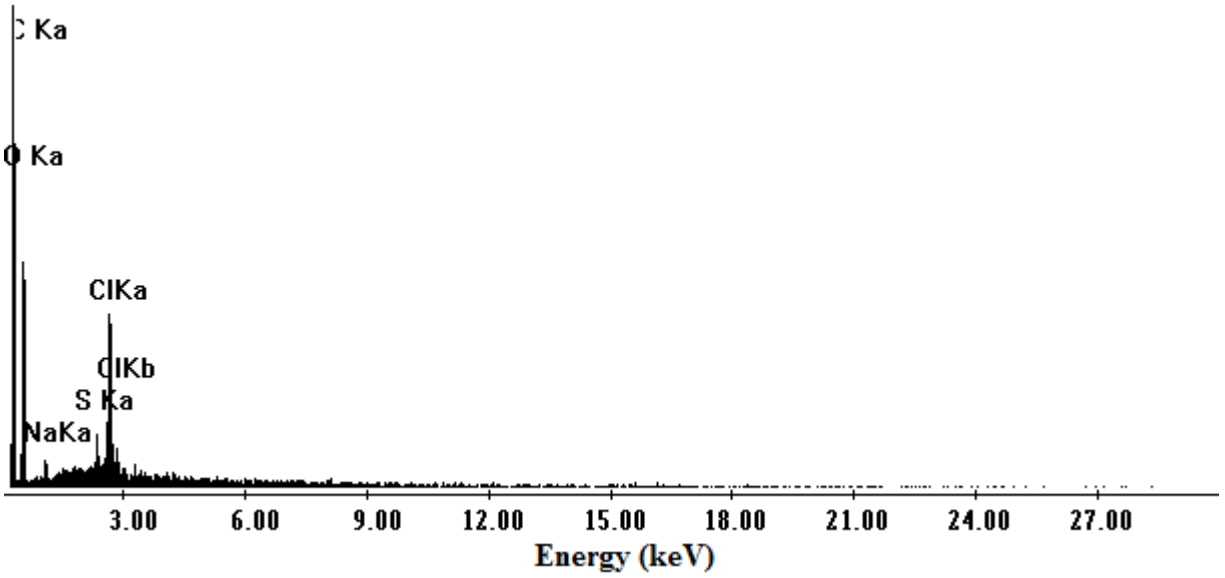

Fig.S2C. Full EDX spectrum of a DCF-loaded PLA scaffold electrospun using DMSO as a co-solvent.

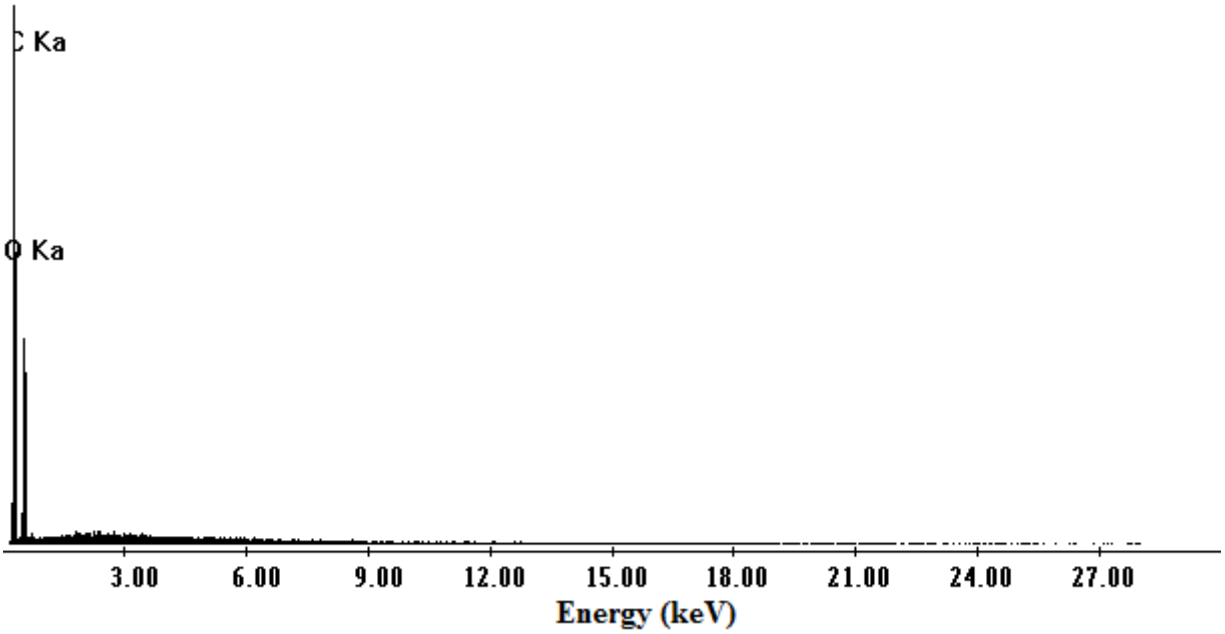

Fig.S2D. Full EDX spectrum of a PLA scaffold electrospun using DMSO as a co-solvent after 24h PBS immersion and washing.

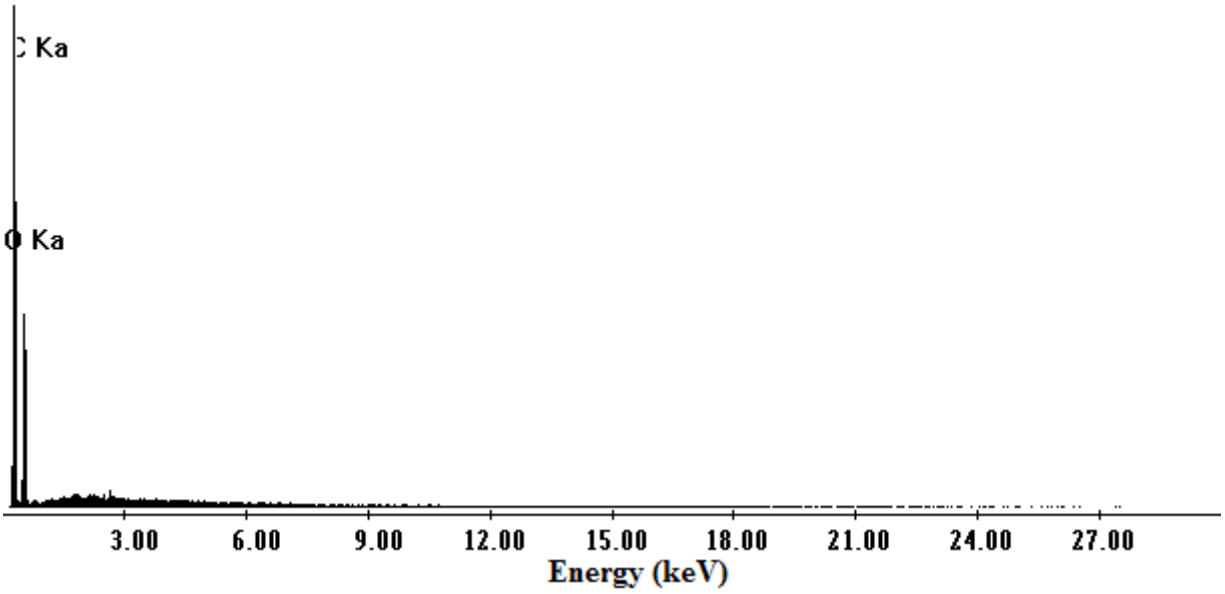

Fig.S2E. Full EDX spectrum of a DCF-loaded PLA electrospun scaffold after 24h PBS immersion and washing.

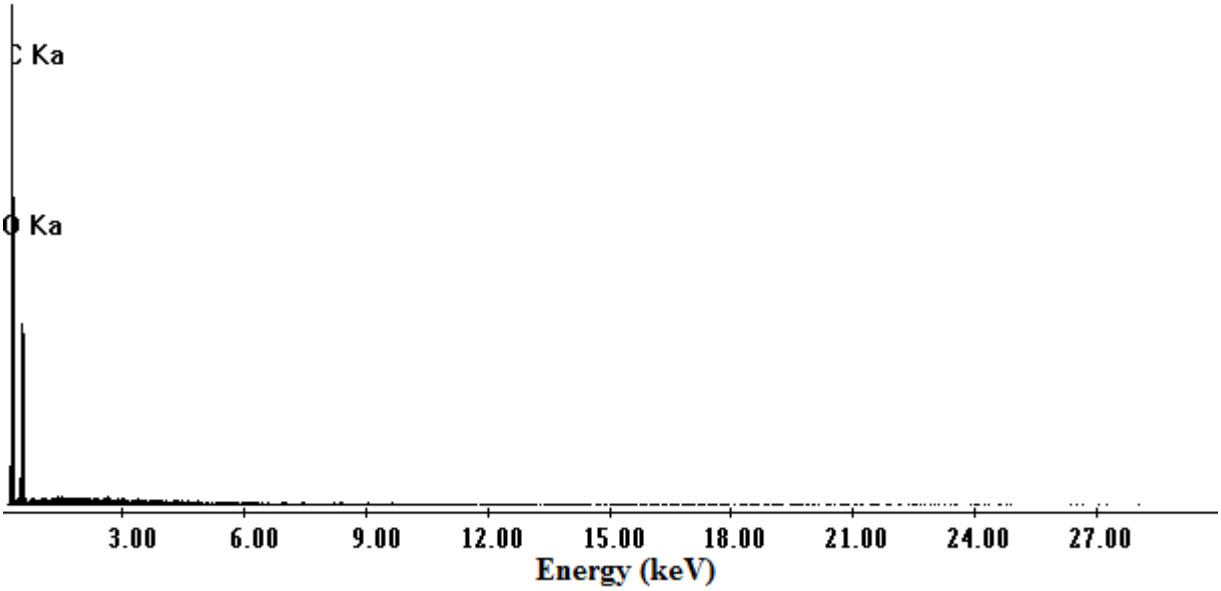

Fig.S2F. Full EDX spectrum of a DCF-loaded PLA scaffold electrospun using DMSO as a co-solvent after 24h PBS immersion and washing.

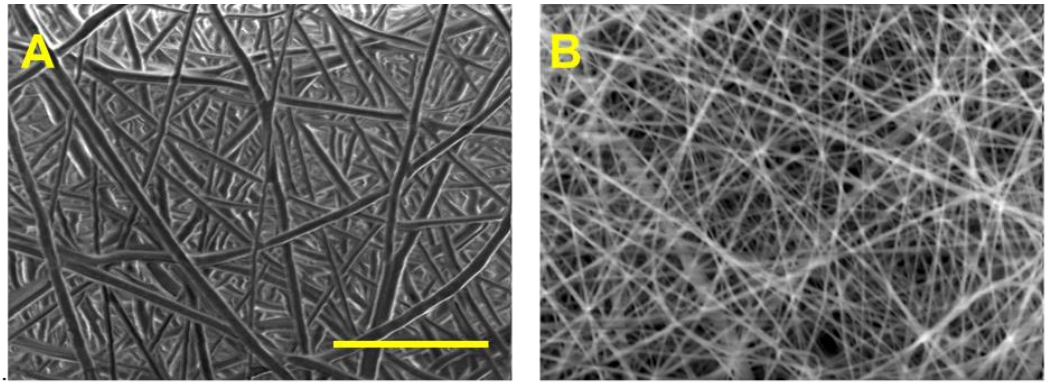

Fig.S3. SEM images of un-coated scaffolds acquired before making EDX analysis on the samples. **A.** Images of PLA + DCF (w DMSO) acquired using a voltage of 4 kV. **B.** Images of PLA + DCF (w DMSO) acquired using a voltage of 10 kV. Scale bar equals 10 µm.

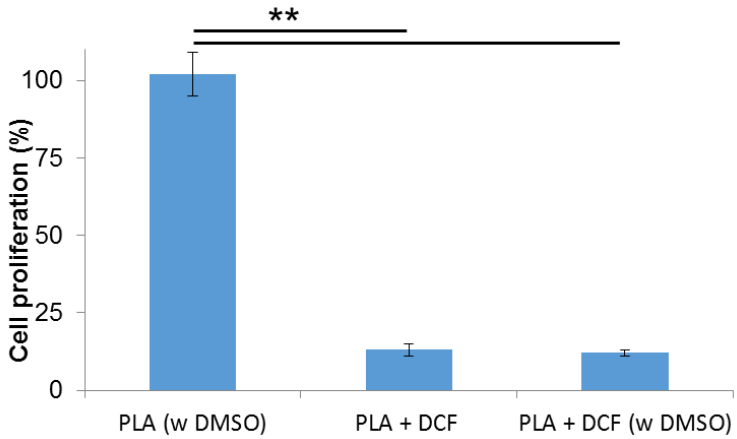

Fig.S4. Results of the MTS cell proliferation assay for PLA electrospun scaffolds containing DCF and/or DMSO.

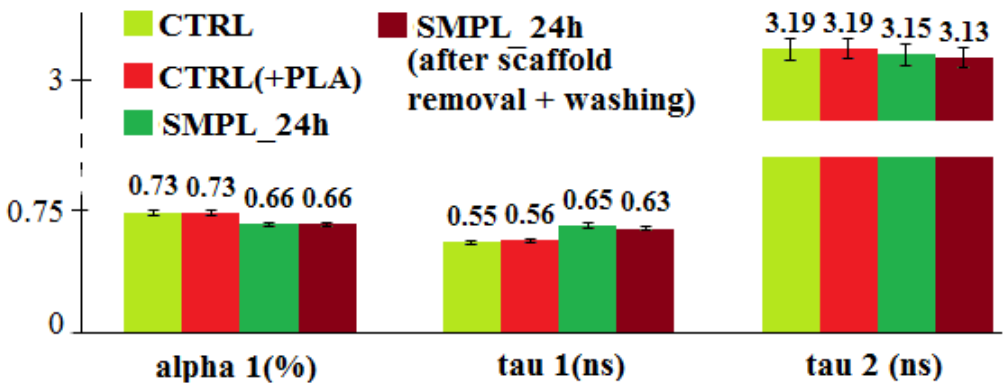

Fig.S5. FLIM results of the control samples. HDFs (control, CTRL) *versus* HDFs in presence of a PLA scaffold (CTRL+PLA); treated HDFs in presence of DCF-loaded PLA scaffold (SMPL) *versus* treated HDFs after scaffold removal.

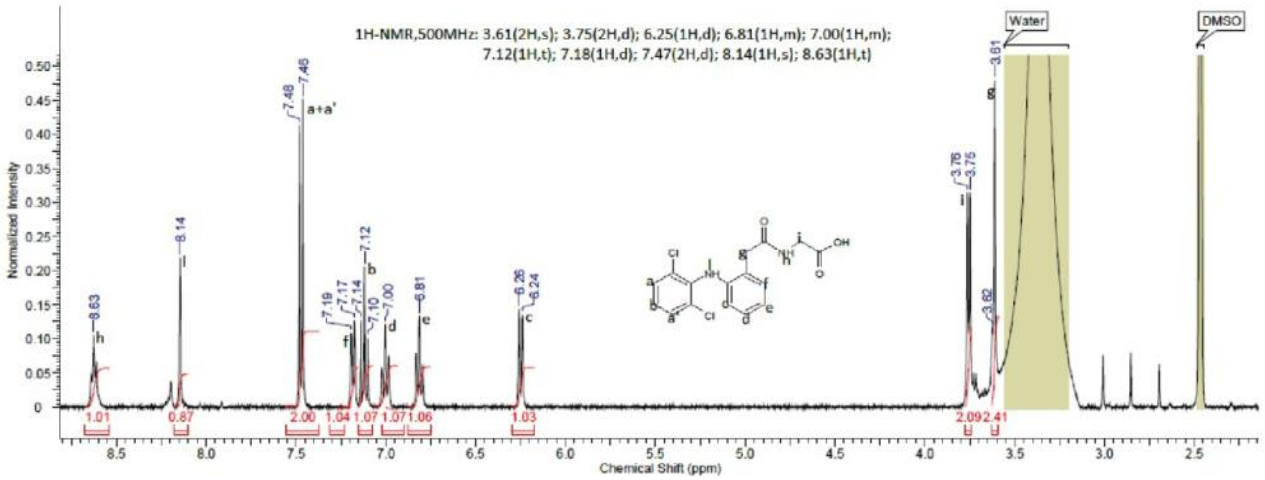

Fig.S6A ^{1}H-NMR of DCF-Gly in DMSO-d_6.

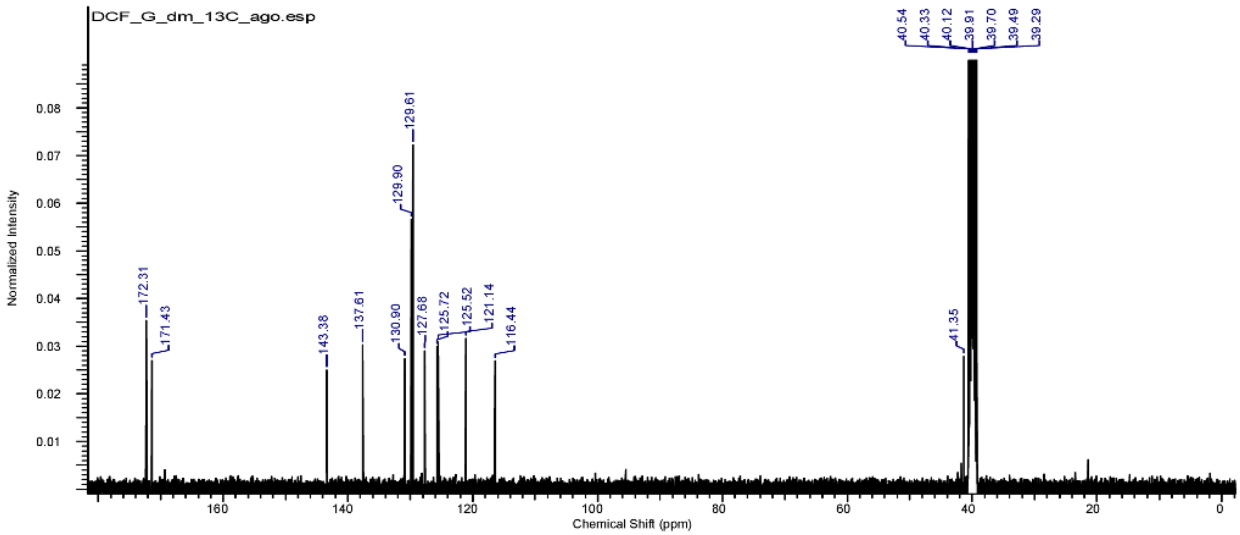

Fig.S6B ^{13}C-NMR of DCF-Gly in DMSO-d_6.

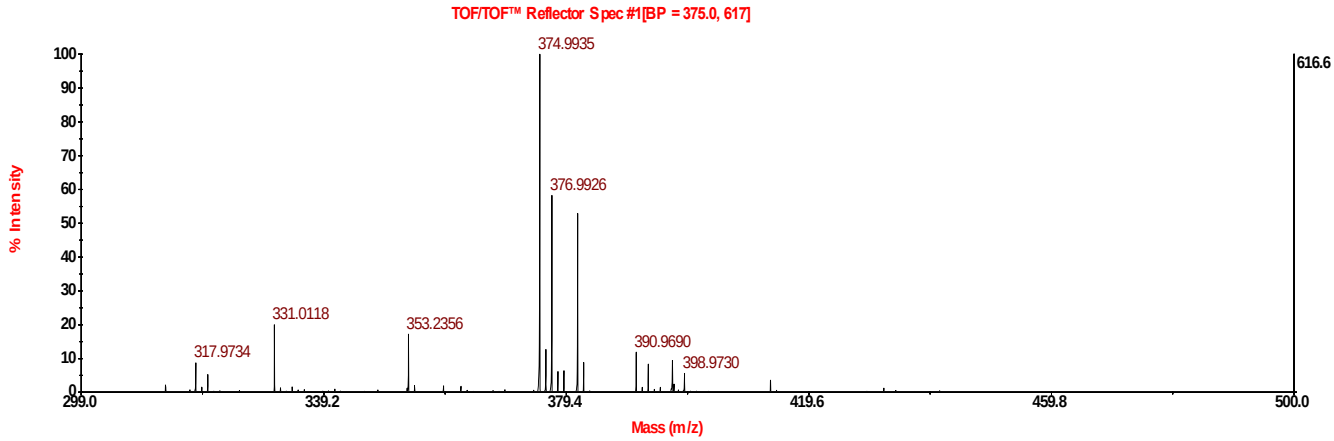

Fig.S6C. MS-MALDI spectrum of DCF-Gly.

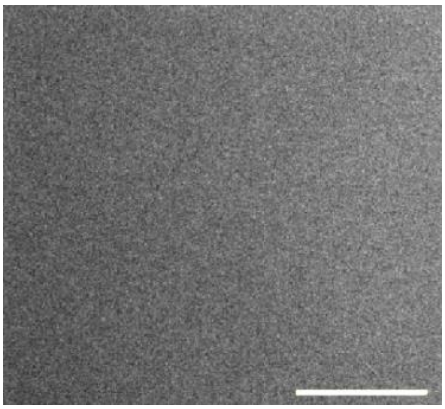

Fig.S7. MPM image of pure electrospun PLA (scale bar: 10µm, excitation wavelength:710 nm, laser power: 3.2 mW, acquisition time: 26s).

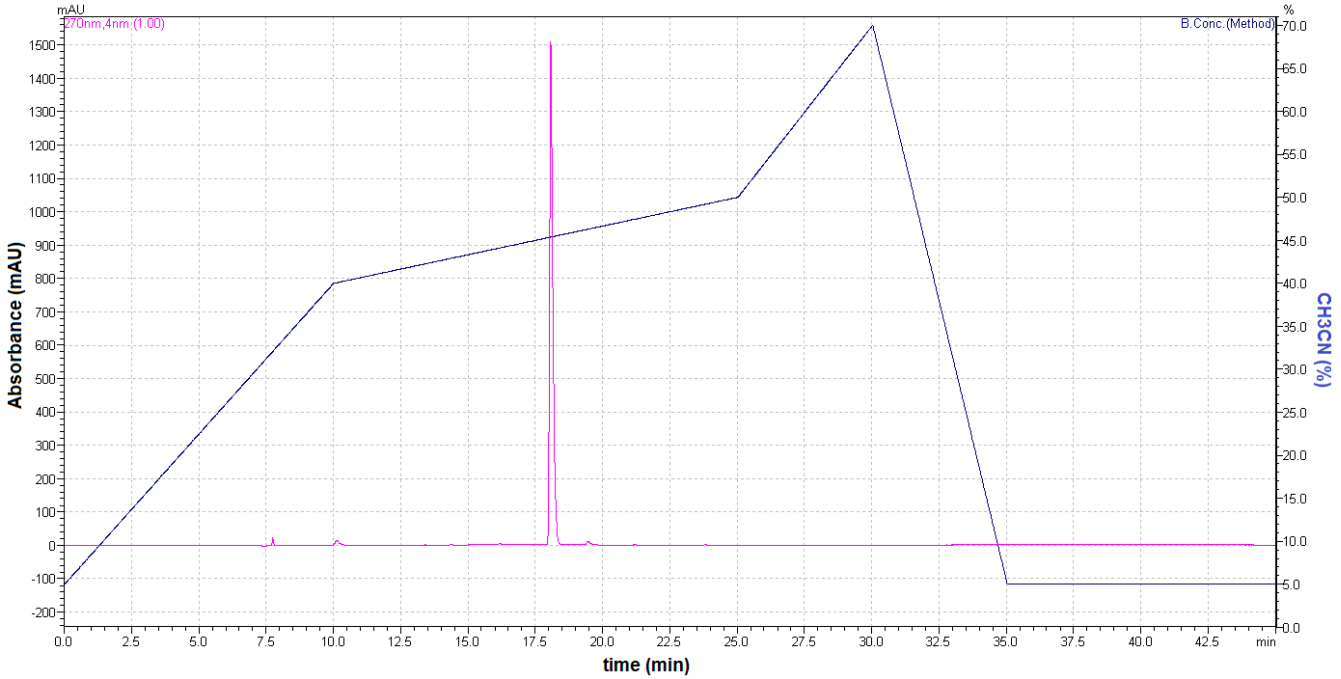

Fig.S8A. RP-HPLC chromatogram of DCF-Gly 1mg/mL in PBS.

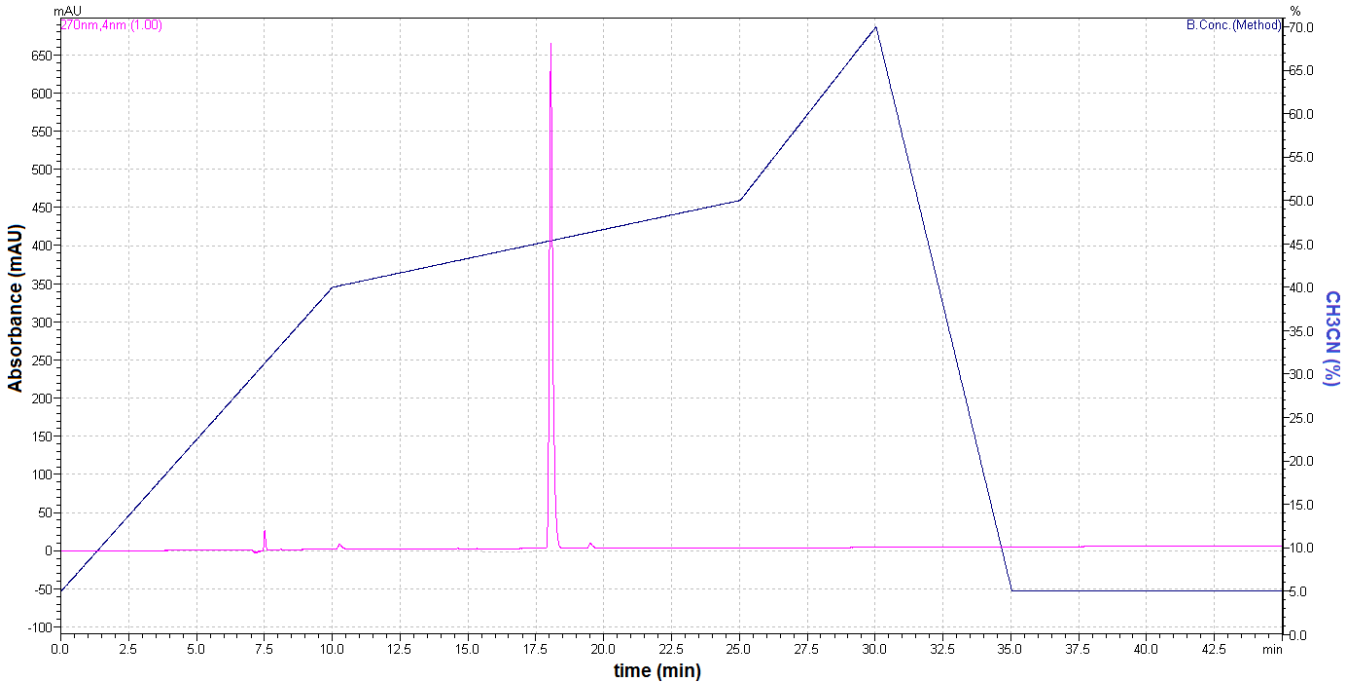

Fig.S8B. RP-HPLC chromatogram of DCF-Gly in PBS after its release from a PLA scaffold.

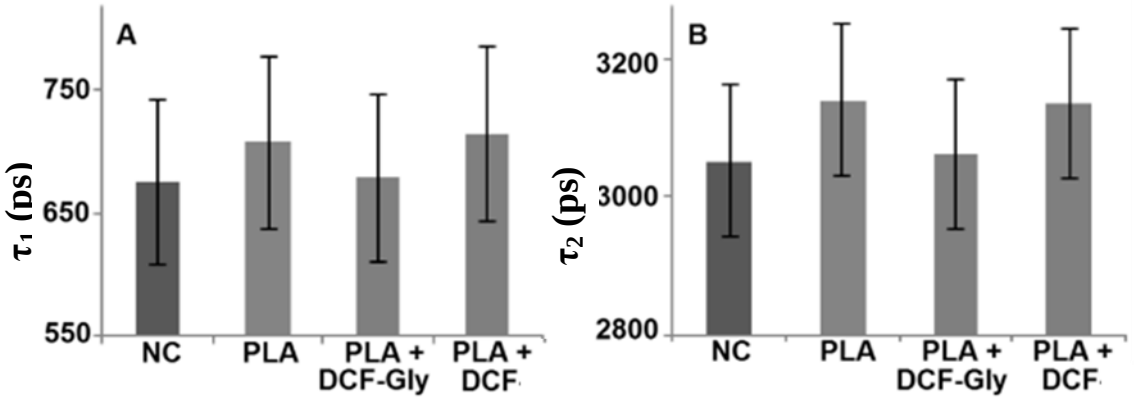

Fig.S9. FLIM analysis using a biexponential decay of τ_1 (A) and τ_2 (B) of HDFs seeded on glass (NC) alone or incubated together with different electrospun scaffolds.

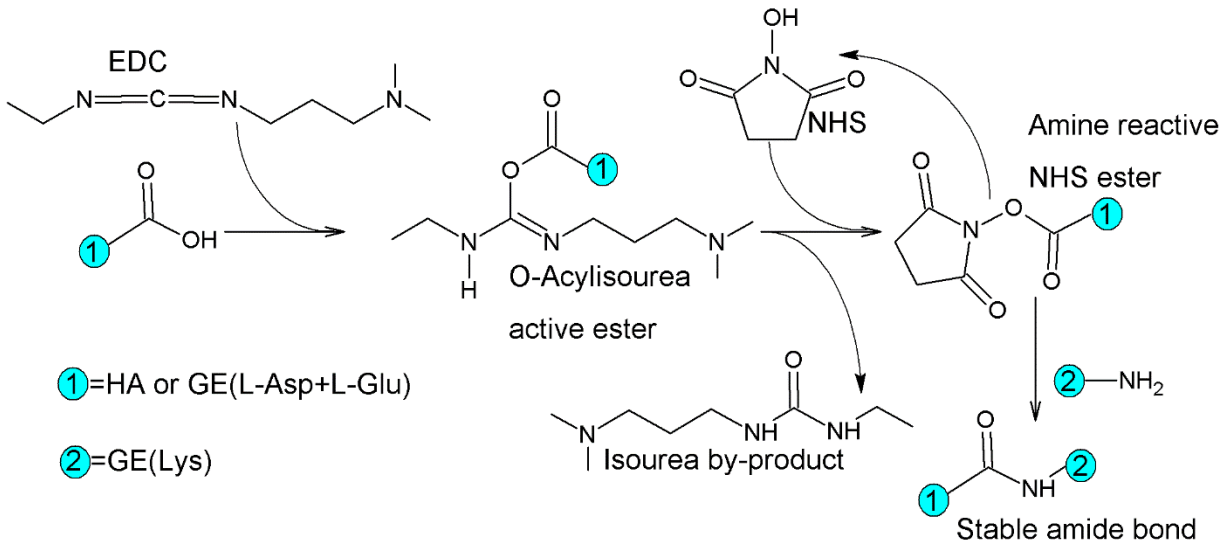

Fig.S10. Reaction scheme for the EDC/NHS-based cross-linking. First, EDC reacts with carboxylic acid groups (from HA glucuronic acid or from GE L-Asp and L-Glu) to form an active O-acylisourea intermediate. Addition of NHS to EDC reactions increases efficiency and enables molecule that is easily displaced by nucleophilic attack from primary amino groups (Lys of GE) in the reaction mixture to give stable amide bonds.

REFERENCES

[1] Edmondson R, Broglie JJ, Adcock AF, Yang L, Three-Dimensional Cell Culture Systems and Their Applications in Drug Discovery and Cell-Based Biosensors, Assay and Drug Development Technologies 12 (2014) 207-218. doi:10.1089/adt.2014.573.

[2] Lu Y, Kim S, Park K, In vitro–in vivo correlation: Perspectives on model development, International Journal of Pharmaceutics 418 (2011) 142-148. doi:10.1016/j.ijpharm. 2011.01.010.

[3] Sill TJ, Von Recum HA, Electrospinning: Applications in Drug Delivery and Tissue Engineering, Biomaterials 29 (2008) 1989-2006.

[4] Nishimura I, Garrell RL, Hedrick M, Iida K, Osher S, Wu B, Precursor tissue analogs as a tissue-engineering strategy, Tissue Eng 9 (2003); S77–S89.

[5] Larsen M, Tremblay ML, Yamada KM, Phosphatases in cellmatrix adhesion and migration, Nat Rev Mol Cell Biol 4 (2003) 700–711.

[6] Iivanainen E, Kahari VM, Heino J, Elenius K, Endothelial cellmatrix interactions, Microsc Res Tech 60 (2003) 13–22.

[7] Frame MC, Fincham VJ, Carragher NO, Wyke JA, v-SRC's hold over actin and cell adhesions, Nat Rev Mol Cell Biol 3 (2002) 233–245.

[8] Suzuki K, Saito J, Yanai R, Yamada N, Chikama T, Seki K, Nishida T, Cell-matrix and cell-cell interactions during cornea epithelial wound healing, Prog Retin Eye Res 22 (2003) 113–133.

[9] Vasita R, Katti DS, Nanofibers and their applications in tissue engineering, International Journal of Nanomedicine 1 (2006) 15-30.

[10] Zamani M, Prabhakaran MP, Ramakrishna S, Advances in drug delivery via electrospun and electrosprayed nanomaterials, International Journal of Nanomedicine 8 (2013) 2997-3017. doi:10.2147/IJN.S43575.

[11] Cui W, Zhou Y, Chang J, Electrospun Nanofibrous Materials for Tissue Engineering and Drug Delivery, Sci Tech Adv Mater 11 (2010) 14108–14118.

[12] Yu D, Zhu L, White K, Branford-White C, Electrospun nanofiber-based drug delivery systems, Health 1 (2009) 67-75. doi:10.4236/health.2009.12012.

[13] Sawicka KM, Gouma P, Electrospun composite nanofibers for functional applications, J Nanopart Res 8 (2006) 769-781. doi:10.1007/s11051-005-9026-9.

[14] Weng L, Xie J, Smart Electrospun Nanofibers for Controlled Drug Release: Recent Advances and New Perspectives, Current pharmaceutical design 21 (2015) 1944-1959.

[15] Katti DS, Robinson KW, Ko FK, Laurencin CT, Bioresorbable nanofiber-based systems for wound healing and drug delivery: optimization of fabrication parameters, J Biomed Mater Res 70B (2004) 286–296.

[16] Hoboken NJ, Poly(Lactic Acid): Synthesis, Structures, Properties, Processing, and Applications edited by Auras R, Lim L, Selke SEM, Tsuji H, Wiley-VCH, Weinheim, Germany (2010). doi:10.1002/9780470649848.

[17] Boland ED, Wnek GE, Simpson DG, Pawlowski KJ, Bowlin TL, Tailoring tissue engineering scaffolds using electrostatic processing techniques: a study of poly(glycolic acid) electrospinning, Journal of Macromolecular Science Part A 38 (2001) 1231-1243. doi:10.1081/MA-100108380.

[18] Khil MS, Cha DI, Kim HY, Kim IS, Bhattarai N, Electrospun nanofibrous polyurethane membrane as wound dressing, J Biomed Mater Res 67B (2003) 675–679.

[19] Azimi B, Nourpanah P, Rabiee M, Arbab S, Poly (lactide -co- glycolide) Fiber: An Overview, Journal of Engineered Fibers and Fabrics 9 (2014) 47-66.

[20] Wayne JS, Mcdowell CL, Shields KJ, Tuan RS, In vivo response of polylactic acid-alginate scaffolds and bone marrow-derived cells for cartilage tissue engineering, Tissue Eng. 11 (2005) 953-963. doi:10.1089/ten.2005.11.953.

[21] Yoo HS, Lee EA, Yoon JJ, Park TG, Hyaluronic acid modified biodegradable scaffolds for cartilage tissue engineering, Biomaterials 26 (2005) 1925-1933. doi:10.1016/j.biomaterials.2004.06.021.

[22] Pavlov MP, Mano JF, Neves NM, Reis RL, Fibers and 3D mesh scaffolds from biodegradable starch based blends: production and characterization, Macromol. Biosci. 4 (2004) 776-784. doi:10.1002/mabi.200400002.

[23] Agarwal S, Wendorff JH, Greiner A, Use of electrospinning technique for biomedical applications, Polymer 49 (2008) 5603-5621. doi:10.1016/j.polymer.2008.09.014.

[24] Kherlopian AR, Song T, Duan Q, Neimark MA, Po MJ, Gohagan JK, Laine AF, A review of imaging techniques for systems biology, BMC Systems Biology 2 (2008) 74-92. doi:10.1186/1752-0509-2-74.

[25] Denk W, Strickler JH, Webb WW, Two-photon laser scanning fluorescence microscopy, Science 248 (1990) 73-76. doi:10.1126/science.2321027

[26] Hoover EE, Squier JA, Advances in multiphoton microscopy technology, Nature photonics 7 (2013) 93-101. doi:10.1038/nphoton.2012.361.

[27] Benninger RKP, Piston DW, Two-Photon Excitation Microscopy for the Study of Living Cells and Tissues, Current protocols in cell biology Unit-4 (2013). doi:10.1002/0471143030.cb0411s59.

[28] Seidenari S, Arginelli F, Dunsby C, French PMW, König K, et al., Multiphoton Laser Tomography and Fluorescence Lifetime Imaging of Melanoma: Morphologic Features and Quantitative Data for Sensitive and Specific Non-Invasive Diagnostics, PLoS ONE 8 (2013) e70682. doi:10.1371/journal.pone.0070682.

[29] Balu M, Zachary C B, Harris RM, Krasieva TB, König K, Tromberg BJ, Kelly KM, In Vivo Multiphoton Microscopy of Basal Cell Carcinoma, JAMA Dermatology 151 (2015) 1068–1074. doi:10.1001/jamadermatol.2015.0453.

[30] MacGowan A, Rogers C, Bowker K, In Vitro Models, In Vivo Models, and Pharmacokinetics: What Can We Learn from In Vitro Models?, Clin Infect Dis 33 (2001) S214-S220. doi:10.1086/321850.

[31] Oza VB, Smith C, Raman P, Koepf EK, Lashuel HA, Petrassi HM, Chiang KP, Powers ET, Sachettinni J, Kelly JW, Synthesis, Structure, and Activity of Diclofenac Analogues as Transthyretin Amyloid Fibril Formation Inhibitors, Journal of Medicinal Chemistry 45 (2002) 321-332. doi:10.1021/jm010257n.

[32] Hwang L, Shaka AJ, Water Suppression That Works. Excitation Sculpting Using Arbitrary Wave-Forms and Pulsed-Field Gradients, Journal of Magnetic Resonance Series A 112 (1995) 275-279. doi:10.1006/jmra.1995.1047.

[33] Yang XX, Wang XY, Yu F, Ma LL, Pan XH, Luo GJ, Lin S, Mo XM, He CL, Wang HS, Hyaluronic acid/EDC/NHS-crosslinked green electrospun silk fibroin nanofibrous scaffolds for tissue engineering, RSC Adv. 6 (2016) 99720–99728. doi:10.1039/ C6RA13713J.

[34] Tan Q, Li S, Ren J, Chen C, Fabrication of Porous Scaffolds with a Controllable Microstructure and Mechanical Properties by Porogen Fusion Technique, International Journal of Molecular Sciences 12 (2011) 890-904. doi:10.3390/ijms12020890.

[35] Guan J, Sacks MS, Beckman EJ, Wagner WR, Biodegradable poly(ether ester urethane)urea elastomers based on poly(ether ester) triblock copolymers and putrescine: synthesis, characterization and cytocompatibility, Biomaterials 25 (2004) 85-96. doi:10.1016/S0142-9612(03)00476-9.

[36] Hong Y, Guan J, Fujimoto KL, Hashizume R, Pelinescu AL, Wagner WR, Tailoring the degradation kinetics of poly(ester carbonate urethane)urea thermoplastic elastomers for tissue engineering scaffolds, Biomaterials 31 (2010) 4249-4258. doi:10.1016/j.biomaterials. 2010.02.005.

[37] Peppas NA, Sahlin J, A simple equation for the description of solute release. III. Coupling of diffusion and relaxation, International Journal of Pharmaceutics 57 (1989) 169-172. doi:10.1016/0378-5173(89)90306-2.

[38] Dash S, Murthy PN, Nath L, Chowdhury P, Kinetic modelling on drug release from controlled drug delivery systems, Acta Pol Pharm 67 (2010) 217–223.

[39] Hinderer S, Seifert J, Votteler M, Shen N, Rheinlaender J, Schäffer TE, Schenke-Layland K, Engineering of a bio-functionalized hybrid off-the-shelf heart valve, Biomaterials 35 (2014) 2130-2139. doi:10.1016/j.biomaterials.2013.10.080.

[40] Brauchle E, Johannsen H, Nolan S, Thude S, Schenke-Layland K, Design and analysis of a squamous cell carcinoma in vitro model system, Biomaterials 34 (2013) 7401–7407. doi:10.1016/j.biomaterials.2013.06.016.

[41] Albulescu R, Codorean E, Albulescu L, Caraene G, Vulturescu V, Tanase C, In vitro biocompatibility testing of implantable biomaterials, Romanian Biotechnological Letters 13 (2008) 3863-3872.

[42] Scott TG, Spencer RD, Leonard NJ, Weber G, Synthetic spectroscopic models related to coenzymes and base pairs. V. Emission properties of NADH. Studies of fluorescence lifetimes and quantum efficiencies of NADH, AcPyADH, [reduced acetylpyridineadenine dinucleotide] and simplified synthetic models, Journal of the American Chemical Society 92 (1970) 687-695. doi:10.1021/ja00706a043.

[43] Pudlas M, Koch S, Bolwien C, Thude S, Jenne N, Hirth T, Walles H, Schenke-Layland K, Raman spectroscopy: a non invasive analysis tool for the discrimination of human skin cells, Tiss. Eng. Part C Methods 17 (2011) 1027– 1040.

[44] Jorge LL, Feres CC, Teles VE, Topical preparations for pain relief: efficacy and patient adherence, Journal of Pain Research 4 (2011) 11-24. doi:10.2147/JPR.S9492.

[45] Meek IL, Van de Laar M, Vonkeman HE, Non-Steroidal Anti-Inflammatory Drugs: An Overview of Cardiovascular Risks, Pharmaceuticals 3 (2010) 2146-2162. doi:10.3390/ph3072146.

[46] Van Laar M, Pergolizzi JV, Mellinghoff HU, et al., Pain Treatment in Arthritis-Related Pain: Beyond NSAID, The Open Rheumatology Journal 6 (2012) 320-330. doi:10.2174/1874312901206010320.

[47] Crofford LJ, Use of NSAIDs in treating patients with arthritis, Arthritis Research & Therapy 15 (2013) S2-S11. doi:10.1186/ar4174.

[48] Kuritzky L, Samraj GP, Nonsteroidal anti-inflammatory drugs in the treatment of low back pain, Journal of Pain Research, 5 (2012) 579-590. doi:10.2147/JPR.S6775.

[49] Davenport K, Waine E, The Role of Non-Steroidal Anti-Inflammatory Drugs in Renal Colic, Pharmaceuticals 3 (2010) 1304-1310. doi:10.3390/ph3051304.

[50] Valentini M, Cannizzaro R, et al., Nonsteroidal antiinflammatory drugs for cancer pain: comparison between misoprostol and ranitidine in prevention of upper gastrointestinal damage, Journal of Clinical Oncology 13 (1995) 2637-2642.

[51] Pantziarka P, Sukhatme V, Bouche G, Meheus L, Sukhatme VP, Repurposing Drugs in Oncology (ReDO)-diclofenac as an anti-cancer agent, Ecancermedicalscience 10 (2016) 610. doi:10.3332/ecancer.2016.610.

[52] Al-Nimer MSM, Hameed HG, Mahmood MM, Antiproliferative effects of aspirin and diclofenac against the growth of cancer and fibroblast cells: In vitro comparative study, Saudi Pharmaceutical Journal 23 (2015) 483-486. doi:10.1016/j.jsps.2015.01.002.

[53] Mayorek N, Naftali-Shani N, Grunewald M, Diclofenac Inhibits Tumor Growth in a Murine Model of Pancreatic Cancer by Modulation of VEGF Levels and Arginase Activity, PLoS ONE 5 (2010) e12715. doi:10.1371/journal.pone.0012715.

[54] Bombardo M, Malagola E, Chen R, Rudnicka A, Graf R, Sonda S, Ibuprofen and diclofenac treatments reduce proliferation of pancreatic acinar cells upon inflammatory

injury and mitogenic stimulation, British Journal of Pharmacology 1 (2017) 1-13. doi:10.1111/bph.13867.

[55] Gan TJ, Diclofenac: an update on its mechanism of action and safety profile, Curr Med Res Opin 26 (2010) 1715-1731. doi:10.1185/03007995.2010.486301.

[56] Inoue A, Muranaka S, Fujita H, Kanno T, Tamai H, Utsumi K, Molecular mechanism of diclofenac-induced apoptosis of promyelocytic leukemia: dependency on reactive oxygen species, akt, bid, cytochrome and caspase pathway, Free Radical Biology and Medicine 37 (2004) 1290-1299. doi:10.1016/j.freeradbiomed.2004.07.003.

[57] Cleuvers M, Mixture toxicity of the anti-inflammatory drugs diclofenac, ibuprofen, naproxen, and acetylsalicylic acid, Ecotoxicology and Environmental Safety 59 (2004) 309-315. doi:10.1016/S0147-6513(03)00141-6.

[58] Masubuchi Y, Saito H, Horie T, Structural Requirements for the Hepatotoxicity of Nonsteroidal Anti-inflammatory Drugs in Isolated Rat Hepatocytes, Journal of Pharmacology and Experimental Therapeutics 287 (1998) 208-213.

[59] Uyemura SA, Santos AC, Mingatto FE, Jordani MC, Curti C, Diclofenac Sodium and Mefenamic Acid: Potent Inducers of the Membrane Permeability Transition in Renal Cortex Mitochondria, Archives of Biochemistry and Biophysics 342 (1997) 231-235. doi:10.1006/abbi.1997.9985.

[60] Tomic Z, et al., Diclofenac and ketoprofen liver toxicity in rat, Eur. J. Drug Metabol. Pharmacokinet. 33 (2008) 253–260. doi:10.1007/BF03190881.

[61] Whelton A, Nephrotoxicity of nonsteroidal anti-inflammatory drugs: physiologic foundations and clinical implications, The American Journal of Medicine 106 (1999) 13S -24S.

[62] Ng LE, Halliwell B, Wong KP, Nephrotoxic cell death by diclofenac and meloxicam, Biochemical and Biophysical Research Communications 369 (2008) 873-877. doi:10.1016/j.bbrc.2008.02.116.

[63] Hickey EJ, Raje RR, Reid VE, Gross SM, Ray SD, Diclofenac induced in vivo nephrotoxicity may involve oxidative stress-mediated massive genomic DNA fragmentation and apoptotic cell death, Free Radical Biology and Medicine 31 (2001) 139-152. doi:10.1016/S0891-5849(01)00560-3.

[64] Tolman KG, Hepatotoxicity of non-narcotic analgesics, Am. J. Med. 105 (1998) 13S-19S.

[65] D'Abril Ruíz-Leyja E, Villalobos-Molina R, López-Guerrero JJ, Gallardo-Ortíz IA, Estrada-Soto SE, Ibarra-Barajas M, Differential role of cyclooxygenase-1 and -2 on renal vasoconstriction to α1-adrenoceptor stimulation in normotensive and hypertensive rats, Life Sciences 93 (2013) 552-557. doi:10.1016/j.lfs.2013.08.014.

[66] Helfgott SM, Sandberg-Cook J, Zakim D, Nestler J, Diclofenac-Associated Hepatotoxicity. JAMA 264 (1990) 2660-2662. doi:10.1001/ jama.1990. 03450200068033.

[67] Iveson TJ, Ryley NG, Kelly PM, Trowell JM, McGee JO, Chapman RW, Diclofenac associated hepatitis, J Hepatol 10 (1990) 85-89.

[68] Sallie RW, Quinlan MF, McKenzie T, Shilkin KB, Reed WD, Diclofenac hepatitis, Australian and New Zealand Journal of Medicine 21 (1991) 251–255. doi:10.1111/j.1445-5994.1991.tb00455.x.

[69] Scully LJ, Clarke D, Barr RJ, Diclofenac induced hepatitis. 3 cases with features of autoimmune chronic active hepatitis, Digest Dis Sci 38 (1993) 744-751. doi:10.1007/ BF01316809

[70] Kretz-Rommel A, Boelsterli UA, Diclofenac Covalent Protein Binding Is Dependent on Acyl Glucuronide Formation and Is Inversely Related to P450-Mediated Acute Cell Injury in Cultured Rat Hepatocytes, Toxicology and Applied Pharmacology 120 (1993) 155-161. doi:10.1006/taap.1993.1097.

[71] Kretz-Rommel A, Boelsterli UA, Mechanism of covalent adduct formation of diclofenac to rat hepatic microsomal proteins. Retention of the glucuronic acid moiety in the adduct, Drug Metabolism and Disposition 22 (1994) 956-961.

[72] Jurima-Romet M, Crawford K, Huang HS, Comparative cytotoxicity of non-steroidal anti-inflammatory drugs in primary cultures of rat hepatocytes, Toxicology in Vitro 8 (1994) 55-66. doi:10.1016/0887-2333(94)90208-9.

[73] Bort R, Ponsoda X, Carrasco E, Gómez-Lechón MJ, Castell JV, Comparative metabolism of the nonsteroidal antiinflammatory drug, aceclofenac, in the rat, monkey, and human, Drug Metabolism and Disposition 24 (1996) 969-975.

[74] Ponsoda X, Bort R, Jover R, Gómez-Lechón MJ, Castell JV, Molecular mechanism of diclofenac hepatotoxicity: Association of cell injury with oxidative metabolism and decrease in ATP levels, Toxicology in Vitro 9 (1995) 439-444. doi:10.1016/0887-2333 (95)00035-7.

[75] Ponsoda X, Bort R, Jover R, Gómez-Lechón MJ, Castell JV, Diclofenac Toxicity to Hepatocytes: A Role for Drug Metabolism in Cell Toxicity, Journal of Pharmacology and Experimental Therapeutics 288 (1999) 65-72.

[76] Masubuchi J, Yamada S, Horie T, Possible Mechanism of Hepatocyte Injury Induced by Diphenylamine and Its Structurally Related Nonsteroidal Anti-Inflammatory Drugs, Journal of Pharmacology and Experimental Therapeutics 292 (2000) 982-987.

[77] Masubuchi Y, Nakayama S, Horie T, Role of mitochondrial permeability transition in diclofenac-induced hepatocyte injury in rats, Hepatology, 35 (2002) 544–551. doi:10.1053/ jhep.2002.31871.

[78] Ghosh R, Goswami SK, Feitoza LF, Hammock B, Gomes AV, Diclofenac induces proteasome and mitochondrial dysfunction in murine cardiomyocytes and hearts, International Journal of Cardiology 223 (2016) 923-935. doi:10.1016/j.ijcard. 2016.08.233.

[79] Baek SM, Ahn JS, Noh HS, Park J, Kang SS, Kim DR, Proteomic analysis in NSAIDs-treated primary cardiomyocytes, Journal of Proteomics 73 (2010) 721-732. doi:10.1016/j.jprot.2009.10.004.

[80] Petrescu I, Tarba C, Uncoupling effects of diclofenac and aspirin in the perfused liver and isolated hepatic mitochondria of rat, Biochimica et Biophysica Acta (BBA) - Bioenergetics 1318 (1997) 385-394. doi:10.1016/S0005-2728(96)00109-0.

[81] Moreno-Sánchez R, Bravo C, Vásquez C, Ayala G, Silveira SH, Martínez-Lavín M, Inhibition and uncoupling of oxidative phosphorylation by nonsteroidal anti-inflammatory drugs: Study in mitochondria, submitochondrial particles, cells, and whole heart, Biochemical Pharmacology 57 (1999) 743-752. doi:10.1016/S0006-2952(98)00330-X.

[82] Singh G, Maurya R, Kumar A, Sinha N, Role of apoptosis in mediating diclofenac-induced teratogenesis, Toxicology and Industrial Health 31 (2015) 614 – 623.

[83] Fredriksson L, Wink S, Herpers B, Benedetti G, Mackenzie H, De Bont H, Groothuis G, Luijten M, Danen E, de Graauw M, Meerman J, Van de Water B, Drug-Induced Endoplasmic Reticulum and Oxidative Stress Responses Independently Sensitize Toward TNFα-Mediated Hepatotoxicity, Toxicol Sci 140 (2014) 144-159. doi:10.1093/toxsci/kfu072.

[84] Gómez-Lechón MJ, Ponsoda X, O'Connor E, Donato T, Jover R, Castell JV, Diclofenac induces apoptosis in hepatocytes, Toxicology in Vitro 17 (2003) 675-680. doi:10.1016/S0887-2333(03)00105-X.

[85] Grattagliano I, Bonfrate L, Diogo CV, Wang HH, Wang DQ, Portincasa P, Biochemical mechanisms in drug-induced liver injury: Certainties and doubts, World Journal of Gastroenterology : WJG 15 (2009) 4865-4876. doi:10.3748/wjg.15.4865.

[86] Ulrich M, Pellacani G, Ferrandiz C, et al., Evidence for field cancerisation treatment of actinic keratoses with topical diclofenac in hyaluronic acid, Eur J Dermatol 24 (2014) 158-167. doi:10.1684/ejd.2014.2286

[87] Martin GM, Stockfleth E, Diclofenac sodium 3% gel for the management of actinic keratosis: 10+ years of cumulative evidence of efficacy and safety, J Drugs Dermatol 11 (2012) 600-608.

[88] Piccirillo G, Bochicchio B, Pepe A, Schenke-Layland K, Hinderer S, Electrospun poly-l-lactide scaffold for the controlled and targeted delivery of a synthetically obtained Diclofenac prodrug to treat actinic keratosis, Acta Biomaterialia 52 (2017) 187-196. doi:10.1016/j.actbio.2016.11.002.

[89] Cooper GM, The Cell: A Molecular Approach. 2nd edition (2000). Sunderland (MA, USA): Sinauer Associates.

[90] Krause MM, Brand MD, Krauss S, Meisel C, Vergin H, Burmester GR, Buttgereit F, Nonsteroidal antiinflammatory drugs and a selective cyclooxygenase 2 inhibitor uncouple mitochondria in intact cells, Arthritis & Rheumatism 48 (2003) 1438–1444. doi:10.1002/art.10969.

[91] Gottfried E, Lang SA, Renner K, et al., New Aspects of an Old Drug–Diclofenac Targets MYC and Glucose Metabolism in Tumor Cells, PLoS ONE 8 (2013) e66987. doi:10.1371/journal.pone.0066987.

[92] George TC, Basiji DA, Hall BE, Lynch DH., Ortyn WE, Perry DJ, Seo MJ, Zimmerman CA, Morrissey PJ, Distinguishing modes of cell death using the ImageStream® multispectral imaging flow cytometer, Cytometry 59A (2004) 237–245. doi:10.1002/cyto.a.20048

[93] Williams AC, Barry BW, Penetration enhancers, Advanced Drug Delivery Reviews 56 (2004) 603-618. doi:10.1016/j.addr.2003.10.025.

[94] Notman R, Den Otter WK, Noro MG, Briels WJ, Anwar J, The Permeability Enhancing Mechanism of DMSO in Ceramide Bilayers Simulated by Molecular Dynamics, Biophysical Journal 93 (2007) 2056-2068. doi:10.1529/biophysj.107.104703.

[95] Kim K, Luu YK, Chang C, Fang D, Hsiao BS, Chu B, Hadjiargyrou M, Incorporation and controlled release of a hydrophilic antibiotic using poly(lactide-co-glycolide)-based electrospun nanofibrous scaffolds, Journal of Controlled Release 98 (2004) 47-56. doi:10.1016/j.jconrel.2004.04.009.

[96] Korsemeyer RW, Peppas NA, Effect of the morphology of hydrophilic polymeric matrices on the diffusion and release of water soluble drugs, J Membr Sci 9 (1981) 211–227.

[97] Vannozzi L, Ricotti L, Filippeschi C, Sartini S, Coviello V, Piazza V, Pingue P, La Motta C, Dario P, Menciassi A, Nanostructured ultra-thin patches for ultrasound-modulated delivery of anti-restenotic drug, International Journal of Nanomedicine 11 (2016) 69-92. doi:10.2147/IJN.S92031.

[98] Gottlieb HE, Kotlyar V, Nudelman A, NMR Chemical Shifts of Common Laboratory Solvents as Trace Impurities, The Journal of Organic Chemistry 62 (1997) 7512-7515. doi:10.1021/jo971176v.

[99] Fulmer GR, Miller AJ, Sherden NH, Gottlieb HE, Nudelman A, Stoltz BM, Bercaw JE, Goldberg KI, NMR Chemical Shifts of Trace Impurities: Common Laboratory Solvents, Organics, and Gases in Deuterated Solvents Relevant to the Organometallic Chemist, Organometallics 29 (2010) 2176-2179. doi:10.1021/om100106e.

[100] Wong SC, Baji A, Leng S, Effect of fiber diameter on tensile properties of electrospun poly (ε-caprolactone), Polymer 49 (2008) 4713-4722. doi:10.1016/j.polymer. 2008.08.022.

[101] Chew SY, Hufnagel TC, Lim CT, Leong KW, Mechanical properties of single electrospun drug-encapsulated nanofibers, Nanotechnology 17 (2006) 3880-3891. doi:10.1088/0957-4484/17/15/045.

[102] Mosmann T, Rapid colorimetric assay for cellular growth and survival: Application to proliferation and cytotoxicity assays, Journal of Immunological Methods 65 (1983) 55-63. doi:10.1016/0022-1759(83)90303-4.

[103] Jamalzadeh L, Ghafoori H, Sariri R, Rabuti H, Nasirzade J, Hasani H, Reza M, Aghamaali MR, Cytotoxic Effects of Some Common Organic Solvents on MCF-7, RAW-264.7 and Human Umbilical Vein Endothelial Cells, Avicenna Journal of Medical Biochemistry 4 (2016) e33453. doi:10.17795/ajmb-33453

[104] Matsui JI, Ogilvie JM, Warchol ME, Inhibition of Caspases Prevents Ototoxic and Ongoing Hair Cell Death, Journal of Neuroscience 22 (2002) 1218-1227.

[105] Qi W, Ding D, Salvi RJ, Cytotoxic effects of dimethyl sulphoxide (DMSO) on cochlear organotypic cultures, Hearing Research 236 (2008) 52-60. doi:10.1016/ j.heares.2007.12.002.

[106] Kanduc D, Mittelman A, Serpico R, Sinigaglia E, Sinha AA, Natale C, Santacroce R, Di Corcia MG, Lucchese A, Dini L, Pani P, Santacroce S, Simone S, Bucci R, Farber E, Cell death: Apoptosis versus necrosis (Review), International Journal of Oncology 21 (2002) 165-170. doi:10.3892/ijo.21.1.165.

[107] Zhang AZ, Ficklscherer A, Gülecyüz MF, Paulus AC, Niethammer TR, Jansson V, Müller PE, Cell Toxicity in Fibroblasts, Tenocytes, and Human Mesenchymal Stem Cells-A Comparison of Necrosis and Apoptosis-Inducing Ability in Ropivacaine, Bupivacaine, and Triamcinolone, Arthroscopy: The Journal of Arthroscopic & Related Surgery 33 (2017) 840-848. doi:10.1016/j.arthro.2016.10.026.

[108] Bundscherer A, Malsy M, Lange R, Hofmann P, Metterlein T, Graf BM, Gruber M, Anticancer Research August 33 (2013) 3201-3204.

[109] Lin HJ, Herman P, Lakowicz JR, Fluorescence lifetime-resolved pH imaging of living cells, Cytometry 52A (2003) 77–89. doi:10.1002/cyto.a.10028

[110] Kumar S, Dunsby C, et al., Multifocal multiphoton excitation and time correlated single photon counting detection for 3-D fluorescence lifetime imaging, Opt. Express 15 (2007) 12548-12561. doi:10.1364/OE.15.012548.

[111] Marx U, How Drug Development of the 21st Century Could Benefit from Human Micro-Organoid In vitro Technologies, in Drug Testing in vitro: Breakthroughs and Trends in Cell Culture Technology (2006), Wiley-VCH, Weinheim, Germany. doi:10.1002/9783527609611.

[112] Connors T, Anticancer Drug Development: The Way Forward, The Oncologist 1 (1996) 180-181.

[113] Festing S, Wilkinson R, The ethics of animal research: talking point on the use of animals in scientific research, EMBO Rep 8 (2007) 526–530.

[114] Badyal DK, Desai C, Animal use in pharmacology education and research: The changing scenario, Indian Journal of Pharmacology, 46 (2014) 257-265. doi:10.4103/0253-7613.132153.

[115] Lush Prize. A global view of animal experiments (2014).

[116] Ferdowsian HR, Beck N, Ethical and Scientific Considerations Regarding Animal Testing and Research. PLoS ONE 6 (2011) e24059. doi:10.1371/journal.pone.0024059

[117] Aminu UK, Hasan Hussein AAS, Zobir HM, Sharida F, Palanisamy A, Development of a controlled-release anti-parkinsonian nanodelivery system using levodopa as the active agent, Int J Nanomedicine 8 (2013) 1103–1110.

[118] Dorniani D, Hussein MZB, Aminu UK, Sharida F, Halim SA, Zalinah A, Preparation of Fe3O4 magnetic nanoparticles coated with gallic acid fordrug delivery. Int J Nanomedicine 7 (2012) 5745–5756.

[119] Casper CL, Yamaguchi N, Kiick KL, Rabolt JF, Functionalizing Electrospun Fibers with Biologically Relevant Macromolecules, Biomacromolecules 6 (2005) 1998-2007. doi:10.1021/bm050007e.

[120] Goldstein J, Newbury D, et al., Scanning electron microscopy and x-ray microanalysis, 3rd edition. Academic Publishers, New York (2003). doi:10.1007/978-1-4615-0215-9.

[121] Soldatow VY, LeCluyse EL, Griffith LG, Rusyn I, In vitro models for liver toxicity testing, Toxicology research 2 (2013) 23-39. doi:10.1039/C2TX20051A.

[122] Edmondson R, Broglie JJ, Adcock AF, Yang L, Three-Dimensional Cell Culture Systems and Their Applications in Drug Discovery and Cell-Based Biosensors, Assay and Drug Development Technologies 12 (2014) 207-218. doi:10.1089/adt.2014.573.

[123] Fink SL, Cookson BT, Apoptosis, Pyroptosis, and Necrosis: Mechanistic Description of Dead and Dying Eukaryotic Cells, Infection and Immunity 73 (2005) 1907-1916. doi:10.1128/IAI.73.4.1907-1916.2005.

[124] Blacker TS, Duchen MR, Investigating mitochondrial redox state using NADH and NADPH autofluorescence, Free Radical Biology and Medicine 100 (2016) 53-65. , doi:10.1016/j.freeradbiomed.2016.08.010.

[125] Chetty P, Choi F, Mitchell T, Primary Care Review of Actinic Keratosis and Its Therapeutic Options: A Global Perspective, Dermatology and Therapy 5 (2015) 19-35. doi:10.1007/s13555-015-0070-9.

[126] Oppel T, Korting HC, Actinic Keratosis: The Key Event in the Evolution from Photoaged Skin to Squamous Cell Carcinoma, Skin Pharmacol Physiol 17 (2004) 67-76. doi:10.1159/000076016.

[127] Widgerow AD, Fabi SG, Palestine RF, Rivkin A, Ortiz A, Bucay VW, Chiu A, Naga L, Emer J, Chasan PE, Extracellular Matrix Modulation: Optimizing Skin Care and Rejuvenation Procedures, J Drugs Dermatol 15 (2016) s63-s71.

[128] Sherratt MJ, Tissue elasticity and the ageing elastic fibre, Age 31 (2009) 305-325. doi:10.1007/s11357-009-9103-6.

[129] Lu P, Takai K, Weaver VM, Werb Z, Extracellular Matrix Degradation and Remodeling in Development and Disease, Cold Spring Harbor perspectives in biology 3 (2011) 1-24. doi:10.1101/cshperspect.a005058.

[130] Lambert SR, Mladkova N, Gulati A, et al., Key differences identified between actinic keratosis and cutaneous squamous cell carcinoma by transcriptome profiling, British Journal of Cancer 110 (2014) 520-529. doi:10.1038/bjc.2013.760.

[131] Hussain SK, Sundquist J, Hemminki K, Incidence Trends of Squamous Cell and Rare Skin Cancers in the Swedish National Cancer Registry Point to Calendar Year and Age-Dependent Increases, Journal of Investigative Dermatology 130 (2010) 1323-1328. doi:10.1038/jid.2009.426.

[132] Tutrone WD, Saini R, Caglar S, Weinberg JM, Crespo J, Topical therapy for actinic keratoses, I: 5-Fluorouracil and imiquimod, Cutis 71 (2003) 365-370.

[133] Tutrone WD, Saini R, Caglar S, Weinberg JM, Crespo J, Topical therapy for actinic keratoses, II: Diclofenac, colchicine, and retinoids, Cutis 71 (2003) 373-379.

[134] Nelson CG, Diclofenac gel in the treatment of actinic keratosis, Therapeutics and Clinical Risk Management 7 (2011) 207-211. doi:10.2147/TCRM.S12498.

[135] Borne RF, Nonsteroidal anti-inflammatory agents. In: Foye's principle of medicinal chemistry edited by Williams AD, Lemke LT, 7th ed. Lippincot William and Wilkins (2013) 1009-1010.

[136] Maltusch A, Röwert-Huber J, Matthies C, Lange-Asschenfeldt S, Stockfleth E, Modes of action of diclofenac 3%/hyaluronic acid 2.5% in the treatment of actinic keratosis, JDDG: Journal der Deutschen Dermatologischen Gesellschaft 9 (2011) 1011–1017. doi:10.1111/j.1610-0387.2011.07700.x.

[137] Fecker LF, Stockfleth E, Nindl I, Ulrich C, Forschner T, Eberle J, The role of apoptosis in therapy and prophylaxis of epithelial tumors by nonsteroidal anti-inflammatory drugs (NSAIDs), British Journal of Dermatology 156 (2007) 25–33.

doi:10.1111/j.1365-2133.2007.07856.x.

[138] Naik A, Kalia YN, Guy RH, Transdermal drug delivery: overcoming the skin's barrier function, Pharmaceutical Science & Technology Today 3 (2000) 318-326.

[139] Peters DC, Foster RH, Diclofenac/Hyaluronic Acid, Drugs & Aging 14 (1999) 313-319. doi:10.2165/00002512-199914040-00006.

[140] Groeber F, Holeiter M, Hampel M, Hinderer S, Schenke-Layland K, Skin tissue engineering - In vivo and in vitro applications, Advanced Drug Delivery Reviews 63 (2011) 352-366. doi:10.1016/j.addr.2011.01.005.

[141] Hinderer S, Brauchle E, Schenke-Layland K, Generation and Assessment of Functional Biomaterial Scaffolds for Applications in Cardiovascular Tissue Engineering and Regenerative Medicine, Advanced Healthcare Materials 4 (2015) 2326–2341. doi:10.1002/adhm.201400762.

[142] Kumbar SG, Syam P, Nukavarapu SP, James R, Nair LS, Laurencin CT, Electrospunpoly(lactic acid-co-glycolic acid) scaffolds for skin tissue engineering, Biomaterials 29 (2008) 4100-4107. doi:10.1016/j.biomaterials.2008.06.028.

[143] Weir NA, Buchanan FJ, Orr JF, Dickson GR, Degradation of poly-L-lactide. Part 1: in vitro and in vivo physiological temperature degradation, Proc Inst MechEng H 218 (2004) 307-319. doi:10.1243/0954411041932782.

[144] Weir NA, Buchanan FJ, Orr JF, Dickson GR, Degradation of poly-L-lactide. Part 2: in vitro and in vivo physiological temperature degradation, Proc Inst Mech Eng H. 218 (2004) 321-330. doi:10.1243/0954411041932809.

[145] Li W, Zhou J, Xu Y, Study of the in vitro cytotoxicity testing of medical devices, Biomedical Reports 3 (2015) 617-620. doi:10.3892/br.2015.481.

[146] Boelsterli UA, Diclofenac-induced liver injury: a paradigm of idiosyncratic drug toxicity, Toxicology and Applied Pharmacology 192 (2003) 307-322. doi:10.1016/S0041-008X(03)00368-5.

[147] Seidenari S, Schianchi S, Azzoni P, Benassi L, et al., High-resolution multiphoton tomography and fluorescence lifetime imaging of UVB-induced cellular damage on cultured fibroblasts producing fibres, Skin Research and Technology 19 (2013) 251–257. doi:10.1111/srt.12034.

[148] Liang D, Hsiao BS, Chu B, Functional Electrospun Nanofibrous Scaffolds for Biomedical Applications, Advanced drug delivery reviews 59 (2007) 1392-1412. doi:10.1016/j.addr.2007.04.021.

[149] Garg T, Singh O, Arora S, Murthy R, Scaffold: a novel carrier for cell and drug delivery, Crit. Rev. Ther. Drug Carrier Syst. 29 (2012) 1-63. doi:10.1615/Crit.Rev.Ther.DrugCarrier Syst.v29.i1.10.

[150] Drumright RE, Gruber PR, Henton DE, Polylactic Acid Technology, Adv. Mater. 12 (2000) 1841–1846. doi:10.1002/1521-4095(200012)12:23<1841.

[151] Honarbakhsh S, Pourdeyhimi B, Scaffolds for drug delivery, part I: electrospun porous poly(lactic acid) and poly(lactic acid)/poly(ethylene oxide) hybrid scaffolds, J Mater Sci 46 (2010) 2874–2881. doi:10.1007/s10853-010-5161-5.

[152] Bushuven S, Heise D, Bolbrinker J, Diclofenac update - Part 1: Pharmacology and comparison with other drugs, Anasthesiol. Intensivmed. Notfallmed. Schmerzther. 49 (2014) 588-598. doi:10.1055/s-0034-1395170.

[153] Bushuven S, Heise D, Bolbrinker J, Diclofenac update - Part 2: Pharmacology and comparison with other drugs, Anasthesiol. Intensivmed. Notfallmed. Schmerzther. 49 (2014) 670-680. doi:10.1055/s-0040-100121.

[154] Zacher J, Altman R, Bellamy N, Brühlmann P, Da Silva J, Huskisson E, Taylor RS, Topical diclofenac and its role in pain and inflammation: an evidence-based review, Current Medical Research and Opinion 24 (2008) 925-950. doi:10.1185/030079908X273066.

[155] Merk HF, Topical diclofenac in the treatment of actinic keratosis, International Journal of Dermatology 46 (2007) 12–18. doi:10.1111/j.1365-4632.2007.03060.x

[156] Altman R, Bosch B, Brune K, Patrignani P, Young C, Advances in NSAID Development: Evolution of Diclofenac Products Using Pharmaceutical Technology, Drugs 75 (2015) 859–877. doi: 10.1007/s40265-015-0392-z.

[157] Brunner M, Dehghanyar P, Seigfried B, Martin W, Menke G, Müller M, Favorable dermal penetration of diclofenac after administration to the skin using a novel spray gel formulation, British Journal of Clinical Pharmacology 60 (2005) 573–577. doi:10.1111/j.1365-2125.2005.02484.x.

[158] Sidney LE, Heathman TR, Britchford ER, Abed A, Rahman CV, Buttery LD, Investigation of Localized Delivery of Diclofenac Sodium from Poly (D,L-Lactic Acid-co-Glycolic Acid)/ Poly (Ethylene Glycol) Scaffolds Using an In Vitro Osteoblast Inflammation Model, Tissue Eng Part A 21 (2015) 362-373. doi:10.1089/ ten.tea.2014.0100.

[159] Tammaro L, Russo G, Vittoria V, Encapsulation of Diclofenac Molecules into Poly (-Caprolactone) Electrospun Fibers for Delivery Protection, Journal of Nanomaterials (2009) Article ID 238206 8 pages. doi:10.1155/2009/238206.

[160] Gaitano RO, Calvo NL, Narda GE, Kaufman TS, Maggio RM, Brusau EV, Preparation and Physical Characterization of a Diclofenac-Ranitidine Co-precipitate for Improving the Dissolution of Diclofenac, Journal of Pharmaceutical Sciences 105 (2016) 1258-1268. doi:10.1016/j.xphs.2016.01.001.

[161] Huttunen KM, Raunio H, Rautio J, Prodrugs–from serendipity to rational design, Pharmacol. Rev. 63 (2011) 750–771. doi:10.1124/pr.110.003459.

[162] Yang Y, Aloysius H, Inoyama D, Chen Y, Hu L, Enzyme-mediated hydrolytic activation of prodrugs, Acta Pharmaceutica Sinica B 1 (2011) 143-159. doi:10.1016/j.apsb.2011.08.001.

[163] Behrendt R, White P, Offer J, Advances in Fmoc solid-phase peptide synthesis, J. Pept. Sci. 22 (2016) 4–27. doi:10.1002/psc.2836.

[164] Kumar S, Tyagi DK, Gupta A, Synthesis and evaluation of amide prodrugs of diclofenac, J. Pharm. Sci. Res. 2 (2010) 369–375.

[165] Hoekstra WJ, The 2-chlorotrityl resin: a worthy addition to the medicinal chemist's toolbox, Curr. Med. Chem. 8 (2001) 715–719. doi:10.2174/0929867013373192.

[166] Bollhagen R, Schmiedberger M, Barlos K, Grell E, A new reagent for the cleavage of fully protected peptides synthesized on 2-chlorotrityl chloride resin, Chem. Soc. Chem. Commun. 22 (1994) 2559-2560. doi:10.1039/C39940002559R.

[167] Barlos K, Chatzi O, Gatos D, Stavropoulos GK, 2-Chlorotrityl chloride resin - Studies on anchoring of Fmoc-amino acids and peptide cleavage, Int. J. Peptide Protein Res. 37 (1991) 513-520. doi:10.1111/j.1399-3011.1991.tb00769.x.

[168] Gashti MP, Alimohammadi F, Hulliger J, Burgener M, Oulevey-Aboulfad H, Bowlin GL, Current Microscopy Contributions to Advances in Science and Technology 1 (2012) 625-638.

[169] Chew SY, Hufnagel TC, Lim CT, Leong KW, Mechanical properties of single electrospun drug-encapsulated nanofibers, Nanotechnology 17 (2006) 3880-3891. doi:10.1088/0957-4484/17/15/045.

[170] Soliman S, Sant S, Nichol JW, Khabiry M, Traversa E, Khademhosseini A, Controlling the porosity of fibrous scaffolds by modulating the fiber diameter and packing density, J. Biomed. Mater. Res. 96A (2011) 566–574. doi:10.1002/jbm.a.33010.

[171] Milleret V, Benjamin S, Neuenschwander P, Hall H, Tuning electrospinning parameters for production of 3D-fiber-fleeces with increased porosity for soft tissue engineering applications, Eur Cell Mater 22 (2011) 286-303.

[172] Kesong L, Yaob X, Jiang L, Recent developments in bio-inspired special wettability, Chem. Soc. Rev. 39 (2010) 3240-3255. doi:10.1039/B917112F.

[173] Marmur A, Super-hydrophobicity fundamentals: implications to biofouling prevention, Biofouling: The Journal of Bioadhesion and Biofilm Research 22 (2006) 107-115. doi:10.1080/08927010600562328.

[174] Baeyens W, Van Der Weken G, Schelkens M, Diclofenac and naproxen analysis by microbore liquid chromatography (LC) with native fluorescence detection, Journal of fluorescence 5 (1995) 131–134. doi:10.1007/BF00727529.

[175] König K, Schenke-Layland K, Riemann I, Stock UA, Multiphoton autofluorescence imaging of intratissue elastic fibers, Biomaterials 26 (2005) 495-500. doi:10.1016/j.biomaterials.2004.02.059.

[176] Schenke-Layland K, Non-invasive multiphoton imaging of extracellular matrix structures, Journal of biophotonics 1 (2008) 451-462. doi:10.1002/jbio.200810045.

[177] Vielreicher M, Schürmann S, Detsch R, Schmidt MA, Buttgereit A, Boccaccini A, Friedrich O, Taking a deep look: modern microscopy technologies to optimize the design and functionality of biocompatible scaffolds for tissue engineering in regenerative medicine, Journal of the Royal Society Interface 10 (2013) 1-21. doi:10.1098/ rsif.2013.0263.

[178] Sun Y, Tan HY, Lin SJ, Lee HS, Lin TY, Jee SH, Young TH, Lo W, Chen WL, Dong CY, Imaging tissue engineering scaffolds using multiphoton microscopy, Microsc. Res. Tech. 71 (2008) 140–145. doi:10.1002/jemt.20537.

[179] Makadia HK, Siegel SJ, Poly Lactic-co-Glycolic Acid (PLGA) as Biodegradable Controlled Drug Delivery Carrier, Polymers 3 (2011) 1377-1397. doi:10.3390/ polym3031377.

[180] Pillay V, Dott C, Choonara YE, Tyagi C, Tomar L, Kumar P, Du Toit LC, Ndesendo VMK, A Review of the Effect of Processing Variables on the Fabrication of Electrospun Nanofibers for Drug Delivery Applications, Journal of Nanomaterials (2013) 1-22. doi:10.1155/2013/789289.

[181] Haider A, Haider S, Kang I, A comprehensive review summarizing the effect of electrospinning parameters and potential applications of nanofibers in biomedical and biotechnology, Arabian Journal of Chemistry 12 (2015) 1878-5352. doi:10.1016/ j.arabjc.2015.11.015.

[182] Coughlan DC, Corrigan OI, Release Kinetics of Benzoic Acid and its Sodium Salt From a Series of Poly(N-Isopropylacrylamide) Matrices with Various Percentage, Journal of Pharmaceutical Sciences 97 (2008) 318-330. doi:10.1002/jps.21095.

[183] Liu L, Bai S, Yang H, Li S, Quan J, Zhu L, Nie H, Controlled release from thermo-sensitive PNVCL-co-MAA electrospun nanofibers: The effects of hydrophilicity/ hydrophobicity of a drug, Mater Sci Eng C Mater Biol Appl 67 (2016) 581-589. doi:10.1016/j.msec.2016.05.083.

[184] Maleki M, Amani-Tehran M, Latifi M, Mathur S, Drug release profile in core–shell nanofibrous structures: A study on Peppas equation and artificial neural network modeling, Computer Methods and Programs in Biomedicine 113 (2014) 92-100. doi:10.1016/j.cmpb.2013.09.003.

[185] Repanas A, Glasmacher B, Dipyridamole embedded in Polycaprolactone fibers prepared by coaxial electrospinning as a novel drug delivery system, Journal of Drug Delivery Science and Technology 29 (2015) 132-142. doi:10.1016/j.jddst.2015.07.001.

[186] Cory AH, Owen TC, Barltrop JA, Cory JG, Use of an aqueous soluble tetrazolium/ formazan assay for cell growth assays in culture, Cancer Commun. 3 (1991) 207-212.

[187] Syed M, Skonberg C, Hansen SH, Mitochondrial toxicity of diclofenac and its metabolites via inhibition of oxidative phosphorylation (ATP synthesis) in rat liver mitochondria: Possible role in drug induced liver injury (DILI), Toxicology in Vitro 31 (2016) 93-102. doi:10.1016/j.tiv.2015.11.020.

[188] Uhlenhake EE, Optimal treatment of actinic keratosis, Clinical Interventions in Aging 8 (2013) 29-35. doi:10.2147/CIA.S31930.

[189] Berlin JM, Rigel DS, Diclofenac sodium 3% gel in the treatment of actinic keratosis post cryosurgery, J Drugs Dermatol 7 (2008) 669-673.

[190] Jorizzo J, Weiss J, Furst K, VandePol C, Levy SF, Effect of a 1-Week Treatment With 0.5% Topical Fluorouracil on Occurrence of Actinic Keratosis After Cryosurgery: A Randomized, Vehicle-Controlled Clinical Trial, Arch Dermatol 140 (2004) 813-816. doi:10.1001/archderm.140.7.813.

[191] Venugopal J, Ramakrishna S, Applications of polymer nanofibers in biomedicine and biotechnology, Appl Biochem Biotechnol 125 (2005) 147-158. doi:10.1385/ ABAB:125:3:147.

[192] Zahedi P, Rezaeian I, Ranaei-Siadat SO, Jafari SH, Supaphol P, A review on wound dressings with an emphasis on electrospun nanofibrous polymeric bandages, Polym. Adv. Technol. 21 (2010) 77–95. doi:10.1002/pat.1625.

[193] Toncheva A, Spasova M, Paneva D, Manolova N, Rashkov I, Polylactide (PLA)-Based Electrospun Fibrous Materials Containing Ionic Drugs as Wound Dressing Materials: A Review, International Journal of Polymeric Materials and Polymeric Biomaterials 63 (2014) 657-667. doi:10.1080/00914037.2013.854240.

[194] Lobo S, Li H, Farhan N, Yan G, Evaluation of Diclofenac Prodrugs for Enhancing Transdermal Delivery, Drug development and industrial pharmacy 40 (2014) 425-432. doi:10.3109/03639045.2013.767828.

[195] Karaman R, Jumaa S, Awwadallah H, Salah S, Khawaja Y, Karaman D, Intramolecular Processes and Their Applications in Prodrugs Approaches- Experimental and Computational Studies, Current Organic Chemistry 20 (2016) 289-315. doi: 10.2174/1385272819666150724232355.

[196] Hewitt NJ, Edwards RJ, Fritsche E, Goebel C, Aeby P, Scheel J, Reisinger K, Pfuhler S, Use of Human In Vitro Skin Models for Accurate and Ethical Risk Assessment:

Metabolic Considerations, Toxicological Sciences, 133 (2013) 209–217. doi: 10.1093/toxsci/kft080

[197] Gunn J, Zhang M, Polyblend nanofibers for biomedical applications: perspectives and challenges, Trends in Biotechnology 28 (2010) 189-197. doi:10.1016/j.tibtech. 2009.12.006.

[198] Bhattarai N, Li Z, Gunn J, Leung M, Cooper A, Edmondson D, Veiseh O, Chen MH, Zhang Y, Ellenbogen RG, Zhang M, Natural-Synthetic Polyblend Nanofibers for Biomedical Applications, Adv. Mater. 21 (2009) 2792–2797. doi:10.1002/adma. 200802513.

[199] Espíndola-González A, Martínez-Hernández AL, Fernández-Escobar F, et al., Natural-Synthetic Hybrid Polymers Developed via Electrospinning: The Effect of PET in Chitosan/Starch System, International Journal of Molecular Sciences 12 (2011) 1908-1920. doi:10.3390/ijms12031908.

[200] Martinova L, Lubasova D, Reasons for using polymer blends in the electrospinning process, AIP Conference Proceedings 1502 (2012) 115-128. doi:10.1063/1.4769138.

[201] Tipduangta P, Belton P, Fábián L, Ying Wang L, Tang H, Eddleston M, QiMol S, Electrospun Polymer Blend Nanofibers for Tunable Drug Delivery: The Role of Transformative Phase Separation on Controlling the Release Rate Pharmaceutics 13 (2016) 25–39. doi:10.1021/acs.molpharmaceut.5b00359.

[202] Heydarkhan-Hagvall S, Schenke-Layland K, Dhanasopon AP, et al., Three-dimensional electrospun ECM-based hybrid scaffolds for cardiovascular tissue engineering, Biomaterials 29 (2008) 2907-2914. doi:10.1016/ j.biomaterials.2008.03.034.

[203] Wang X, Ding B, Li B, Biomimetic electrospun nanofibrous structures for tissue engineering, Materials Today 16 (2013) 229-241. doi:10.1016/j.mattod.2013.06.005.

[204] Schenke-Layland K, Special Issue “Extracellular Matrix Proteins and Mimics”, Acta Biomaterialia 52 (2017) IV. doi:10.1016/j.actbio.2017.03.029.

[205] Jiang W, et al., Nanoparticle-mediated cellular response is size-dependent, Nat. Nanotechnol. 3 (2008) 145–150. doi:10.1038/nnano.2008.30.

[206] Gerardo-Nava J, et al., Human neural cell interactions with orientated electrospun nanofibers in vitro, Nanomed. 4 (2009) 11–30. doi:10.2217/17435889.4.1.11.

[207] Chen H, Peng Y, Wu S. Tan LP, Electrospun 3D Fibrous Scaffolds for Chronic Wound Repair, Materials 9 (2016) 272-283. doi:10.3390/ma9040272.

[208] Liu W, Thomopoulos S, Xia Y, Electrospun Nanofibers for Regenerative Medicine Advanced healthcare materials 1 (2012) 10-25. doi:10.1002/adhm.201100021.

[209] Lyu S, Huang C, Yang H, Zhang X, Electrospun Fibers as a Scaffolding Platform for Bone Tissue Repair, Journal of orthopaedic research: official publication of the Orthopaedic Research Society 31 (2013) 1382-1389. doi:10.1002/jor.22367.

[210] Bonvallet PP, Schultz MJ, Mitchell EH, et al., Microporous Dermal-Mimetic Electrospun Scaffolds Pre-Seeded with Fibroblasts Promote Tissue Regeneration in Full-Thickness Skin Wounds, PLoS ONE 10 (2015) e0122359. doi:10.1371/journal.pone. 0122359.

[211] Khajavi R, Abbasipour M, Electrospinning as a versatile method for fabricating coreshell, hollow and porous nanofibers, Scientia Iranica 19 (2012) 2029-2034. doi:10.1016/j.scient.2012.10.037.

[212] Kishan AP, Cosgriff-Hernandez EM, Recent advancements in electrospinning design for tissue engineering applications: A review, J Biomed Mater Res Part A 00A (2017) 1-14. doi:10.1002/jbm.a.36124.

[213] Lee GH, Song, JC, Yoon KB, Controlled wall thickness and porosity of polymeric hollow nanofibers by coaxial electrospinning, Macromol. Res. 18 (2010) 571-576. doi:10.1007/s13233-010-0607-9.

[214] Loh QL, Choong C, Three-Dimensional Scaffolds for Tissue Engineering Applications: Role of Porosity and Pore Size, Tissue Engineering Part B: Reviews 19 (2013) 485-502. doi:10.1089/ten.teb.2012.0437.

[215] Sundararaghavan HG, Metter RB, Burdick JA, Electrospun Fibrous Scaffolds with Multi-scale and Photopatterned Porosity, Macromolecular bioscience 10 (2010) 265-270. doi:10.1002/mabi.200900363.

[216] Rnjak-Kovacina J, Weiss AS, Increasing the pore size of electrospun scaffolds. Tissue Engineering Part B: Reviews 17 (2011) 365-372. doi:10.1089/ten.teb.2011.0235.

[217] Blakeney BA, Tambralli A, Anderson JM, et al., Cell Infiltration and Growth in a Low Density, Uncompressed Three-Dimensional Electrospun Nanofibrous Scaffold, Biomaterials 32 (2011) 1583-1590. doi:10.1016/j.biomaterials.2010.10.056.

[218] Kim K, Yu M, Zong X, Chiu J, Fang D, Seo Y, Hsiao BS, Chu B, Hadjiargyrou M, Control of degradation rate and hydrophilicity in electrospun non-woven poly(d,l-lactide) nanofiber scaffolds for biomedical applications, Biomaterials 24 (2003) 4977-4985. doi:10.1016/S0142-9612(03)00407-1.

[219] Ramakrishna S, Fujihara K, Teo W, Yong T, Ma Z, Ramaseshan R, Electrospun nanofibers: solving global issues, Materials Today 9 (2006) 40-50. doi:10.1016/S1369-7021(06)71389-X.

[220] Pham QP, Sharma U, Mikos AG, Electrospinning of Polymeric Nanofibers for Tissue Engineering Applications: A Review, Tissue Engineering 12 (2006) 1197-1211. doi:10.1089/ten.2006.12.1197.

[221] Greiner A, Wendorff JH, Electrospinning: A Fascinating Method for the Preparation of Ultrathin Fibers, Angewandte Chemie International Edition 46 (2007) 5670–5703. doi:10.1002/anie.200604646.

[222] Xiao L, Wang B, Yang G, Gauthier M, Poly(Lactic Acid)-Based Biomaterials: Synthesis, Modification and Applications. In: Biomedical Science, Engineering and Technology edited by Ghista DN (2012) 247-282.

[223] Cheng Y, Deng S, Chen P, Ruan R, Polylactic acid (PLA) synthesis and modification: a review, Front. Chem. China 4 (2009) 259-264.

[224] Gupta B, Revagade N, Hilborn J, Poly(lactic acid) fiber: An overview, Prog. Polym. Sci. 32 (2007) 455-482.

[225] Boland ED, Wnek GE, Simpson DG, Pawlowski KJ, Bowlin GL, Tailoring tissue engineering scaffolds using electrostatic processing techniques: a study of poly (glycolic acid) electrospinning, Journal Of Macromolecular Science Part A 38 (2001) 1231-1243.

[226] Gentile P, Chiono V, Carmagnola I, Hatton PV, An Overview of Poly(lactic-co-glycolic) Acid (PLGA)-Based Biomaterials for Bone Tissue Engineering, International Journal of Molecular Sciences 15 (2014) 3640-3659. doi:10.3390/ijms15033640.

[227] Dong Y, Liao S, Ngiam M, Chan CK, Ramakrishna S, Degradation Behaviors of Electrospun Resorbable Polyester Nanofibers, Tissue Engineering Part B: Reviews 15 (2009) 333-351. doi:10.1089/ten.teb.2008.0619.

[228] Liu H, Wang S, Qi N, Controllable structure, properties, and degradation of the electrospun PLGA/PLA-blended nanofibrous scaffolds. J. Appl. Polym. Sci. 125 (2012): E468–E476. doi:10.1002/app.36757.

[229] Li WJ, et al., Electrospun nanofibrous structure: a novel scaffold for tissue engineering, J. Biomed. Mater. Res. 60 (2002), 613–621.

[230] Khorshidi S, Solouk A, Mirzadeh H, Mazinani S, Lagaron JM, Sharifi S, Ramakrishna S, A review of key challenges of electrospun scaffolds for tissue-engineering applications, J Tissue Eng Regen Med 10 (2016) 715–738. doi:10.1002/term.1978.

[231] Matthews JA, et al., Electrospinning of collagen nanofibers, Biomacromolecules 3 (2002) 232–238.

[232] Li M, et al., Electrospun protein fibers as matrices for tissue engineering, Biomaterials 26 (2005) 5999–6008.

[233] Schiffman JD, Schauer C, A Review: Electrospinning of Biopolymer Nanofibers and their Applications, Polymer Reviews 48 (2008). doi:10.1080/15583720802022182.

[234] Dang, JM, Leong KW, Natural polymers for gene delivery and tissue engineering, Adv. Drug Deliv. Rev. 58 (2006) 487–499.

[235] Zeugolis DI, Khew ST, et al., Electro-spinning of pure collagen nano-fibres – Just an expensive way to make gelatin?, Biomaterials 29 (2008) 2293-2305. doi:10.1016/ j.biomaterials.2008.02.009.

[236] Evrova O, et al., Hybrid Randomly Electrospun Poly(lactic-co-glycolic acid):Poly (ethylene oxide) (PLGA:PEO) Fibrous Scaffolds Enhancing Myoblast Differentiation and Alignment, ACS Appl. Mater. Interfaces 8 (2016) 31574–31586. doi:10.1021/ acsami.6b11291.

[237] Huang L, Nagapudi K, Apkarian R, Chaikof E, Engineered collagen–PEO nanofibers and fabrics, J. Biomater. Sci. Polymer Edn 12 (2001) 979–993.

[238] Liu Y, et al., Engineering of bio-hybrid materials by electrospinning polymer-microbe fibers, PNAS 106 (2009) 14201–14206. doi:10.1073/pnas.0903238106.

[239] Reneker DH, Yarin AL, Electrospinning jets and polymer nanofibers, Polymer 49 (2008) 2387-2425. doi:10.1016/j.polymer.2008.02.002.

[240] Nandakumar A, Barradas A, De Boer J, Moroni L, Van Blitterswijk C, Habibovic P, Combining technologies to create bioactive hybrid scaffolds for bone tissue engineering, Biomatter 3 (2013) e23705. doi:10.4161/biom.23705.

[241] Sionkowska A, Current research on the blends of natural and synthetic polymers as new biomaterials: Review, Progress in Polymer Science 36 (2011) 1254-1276. doi:10.1016/j.progpolymsci.2011.05.003.

[242] Kwon K, Matsuda T, Co-Electrospun Nanofiber Fabrics of Poly(l-lactide-co-ε-caprolactone) with Type I Collagen or Heparin, Biomacromolecules 6 (2005) 2096-2105. doi:10.1021/bm050086u.

[243] Zhang Y, Su B, Venugopal J, Ramakrishna S, Lim C, Biomimetic and bioactive nanofibrous scaffolds from electrospun composite nanofibers, International Journal of Nanomedicine 2 (2007) 623-638.

[244] Eastoe JE, The amino acid composition of mammalian collagen and gelatin, Biochemical Journal 61 (1955) 589-600.

[245] Jones RT, Gelatin: Manufacture and Physio-Chemical Properties. In: Pharmaceutical Capsules edited by Podczeck F, Jones BE, Pharmaceutical Press, London, UK (2004) 23–60.

[246] Lai JY, Biocompatibility of chemically cross-linked gelatin hydrogels for ophthalmic use, J. Mater. Sci. Mater. Med. 21 (2010) 1899–1911.

[247] De la Mata A, Nieto-Miguel T, López-Paniagua M, Galindo S, Aguilar, MR, García-Fernández L, Gonzalo S, Vázquez B, Román JS, Corrales RM, et al., Chitosan-gelatin biopolymers as carrier substrata for limbal epithelial stem cells, J. Mater. Sci. Mater. Med. 24 (2013) 2819–2829.

[248] Tonsomboon K, Strange DGT, Oyen ML, Gelatin Nanofiber-Reinforced Alginate Gel Scaffolds for Corneal Tissue Engineering, Proceedings of the Engineering in Medicine and Biology Society 1 (2013) 6671–6674. doi:10.1109/EMBC.2013.6611086.

[249] Bohidar HB, Jena SS, Study of sol-state properties of aqueous gelatin solutions, J. Chem. Phys. 100 (1994) 6888–6895.

[250] Butcher AL, Koh CT, Oyen ML, Systematic mechanical evaluation of electrospun gelatin meshes, Journal of the Mechanical Behavior of Biomedical Materials 69 (2017) 412-419. doi:10.1016/j.jmbbm.2017.02.007.

[251] Rose JB, Pacelli S, Haj AJE, Dua HS, Hopkinson A, White LJ, Rose F, Gelatin-Based Materials in Ocular Tissue Engineering, Materials 7 (2014) 3106-3135. doi:10.3390/ma7043106.

[252] Parenteau-Bareil R, Gauvin R, Berthod F, Collagen-Based Biomaterials for Tissue Engineering Applications, Materials 3 (2010) 1863-1887. doi:10.3390/ma3031863.

[253] Tomihata K, Ikada Y, Cross-Linking of Gelatin with Carbodiimides, Tissue Engineering 2 (2007) 307-313. doi:10.1089/ten.1996.2.307.

[254] Sisson K, et al., Evaluation of Cross-Linking Methods for Electrospun Gelatin on Cell Growth and Viability, Biomacromolecules 10 (2009) 1675–1680. doi:10.1021/ bm900036s.

[255] Digenis GA, et al., Cross-Linking of Gelatin Capsules and Its Relevance to Their in Vitro-in Vivo Performance, Journal of Pharmaceutical Sciences 83 (1994) 915 – 921. doi:10.1002/jps.2600830702.

[256] Cammarata CR, Hughes ME, Ofner CM, Carbodiimide Induced Cross-Linking, Ligand Addition, and Degradation in Gelatin, Molecular Pharmaceutics 12 (2015) 783-793. doi:10.1021/mp5006118.

[257] Zhou Z, Yang Z, et al., Effect of Chemical Cross-linking on Properties of Gelatin/Hyaluronic Acid Composite Hydrogels, Polymer-Plastics Technology And Engineering 52 (2013). doi:10.1080/03602559.2012.718400.

[258] Jarquín-Yáñez K, et al., Structural Effect of Different EDC Crosslinker Concentration in Gelatin Hyaluronic Acid Scaffolds, J Bioengineer & Biomedical Sci 6 (2016) e1000182. doi:10.4172/2155-9538.1000182.

[259] Lou X, Chirila T, Swelling behaviour and mechanical properties of chemically cross-linked gelatin gels for biomedical use, J. Biomater. Appl. 14 (1999) 184–191.

[260] Natu MV, Sardinha JP, Correia IJ, Gil MH, Controlled release gelatin hydrogels and lyophilisates with potential application as ocular inserts, Biomed. Mater. 2 (2007) 241–249.

[261] Lai JY, Hsieh AC, A gelatin-g-poly(N-isopropylacrylamide) biodegradable in situ gelling delivery system for the intracameral administration of pilocarpine, Biomaterials 33 (2012) 2372–2387.

[262] Jain D, Carvalho E, Banthia AK, Banerjee R, Development of polyvinyl alcohol-gelatin membranes for antibiotic delivery in the eye, Drug Dev. Ind. Pharm. 37 (2011) 167–177.

[263] Hsu WM, Chen KH, Lai JY, Hsiue GH, Transplantation of human corneal endothelial cells using functional biomaterials: Poly(N-isopropylacrylamide) and gelatin, J. Exp. Clin. Med. 5 (2013) 56–64.

[264] Gómez-Guillén MC, Giménez B, López-Caballero ME, Montero MP, Functional and bioactive properties of collagen and gelatin from alternative sources: A review, Food Hydrocoll. 25 (2011) 1813–1827.

[265] Lai JY, Lu PL, Chen KH, Tabata Y, Hsiue GH, Effect of charge and molecular weight on the functionality of gelatin carriers for corneal endothelial cell therapy, Biomacromolecules 7 (2006) 1836–1844.

[266] Lai J, Lin P, Hsiue G, Cheng H, Huang S, Low bloom strength gelatin as a carrier for potential use in retinal sheet encapsulation and transplantation, Biomacromolecules 10 (2009) 310–319.

[267] Lai JY, The role of bloom index of gelatin on the interaction with retinal pigment epithelial cells, Int. J. Mol. Sci. 10 (2009) 3442–3456.

[268] Usta M, Piech DL, MacCrone RK, Hillig WB, Behavior and properties of neat and filled gelatins, Biomaterials 24 (2003) 165–172.

[269] Bigi A, Panzavolta S, Rubini K, Relationship between triple-helix content and mechanical properties of gelatin films, Biomaterials 25 (2004) 5675–5780.

[270] Katagiri Y, Brew SA, Ingham KC, All six modules of the gelatin-binding domain of fibronectin are required for full affinity, J. Biol. Chem. 278 (2003) 11897–11902.

[271] Lai JY, Li YT, Cho CH, Yu TC, Nanoscale modification of porous gelatin scaffolds with chondroitin sulfate for corneal stromal tissue engineering, Int. J. Nanomed. 7 (2012) 1101–1114.

[272] Tondera C, Hauser S, Krüger-Genge A, et al., Gelatin-based Hydrogel Degradation and Tissue Interaction in vivo: Insights from Multimodal Preclinical Imaging in Immunocompetent Nude Mice, Theranostics 6(2016) 2114-2128. doi:10.7150/thno.16614.

[273] Park K, Ju YM, Son JS, Ahn K, Han DK, Surface modification of biodegradable electrospun nanofiber scaffolds and their interaction with fibroblasts, J Biomater Sci Polym Ed 18 (2007) 369-382. doi:10.1163/156856207780424997.

[274] Aoki M, Miyamoto S, Okamura K, Yamashita T, Ikada Y, Matsuda S, Tensile properties and biological response of poly(L-lactic acid) felt graft: An experimental trial for rotator-cuff reconstruction, J. Biomed. Mater. Res. 71B (2004) 252–259. doi:10.1002/jbm.b.30084.

[275] Groot W, Van Krieken J, Sliekersl O, De Vos S, Production and Purification of Lactic Acid and Lactide. In: Poly(Lactic Acid): Synthesis, Structures, Properties, Processing, and Applications edited by Auras R, Lim L, Selke S, Tsuji H, Wiley-VCH, Weinheim, Germany (2010) 1-18. doi:10.1002/9780470649848.

[276] Raquez JM, Mincheva R, Coulembier O, Dubois P, Polymer Science: A Comprehensive Reference 1 (2012) 761–778.

[277] Södergård A, Stolt M, Industrial Production of High Molecular Weight Poly(Lactic Acid). In: Poly(Lactic Acid): Synthesis, Structures, Properties, Processing, and

Applications edited by Auras R, Lim L, Selke S, Tsuji H, Wiley-VCH, Weinheim, Germany (2010) 27-41. doi:10.1002/9780470649848.

[278] Shenoy SL, Bates WD, Frisch HL, Wnek GE, Role of chain entanglements on fiber formation during electrospinning of polymer solutions: Good solvent, non-specific polymer-polymer interaction limit, Polymer 46 (2005) 3372-3384. doi:10.1016/j.polymer. 2005.03.011.

[279] Bernkopf M, Sterilisation of bioresorbable polymer implants, Med Device Technol 18 (2007) 26-29.

[280] Athanasiou KA, Niederauer GG, Agrawal CM, Sterilization, toxicity, biocompatibility and clinical applications of polylactic acid/ polyglycolic acid copolymers, Biomaterials (1996) 93-102. doi:10.1016/0142-9612(96)85754-1.

[281] Engelberg I, Kohn J, Physico-mechanical properties of degradable polymers used in medical applications: A comparative study, Biomaterials 12 (1991) 292-304. doi:10.1016/0142-9612(91)90037-B.

[282] Ajioka M, Enomoto K, Suzuki K, et al., The basic properties of poly(lactic acid) produced by the direct condensation polymerization of lactic acid, J Environ Polym Degr 3 (1995) 225-234. doi:10.1007/BF02068677

[283] Urayama H, Kanamori T, Kimura Y, Properties and Biodegradability of Polymer Blends of Poly(L-lactide)s with Different Optical Purity of the Lactate Units, Macromol. Mater. Eng. 287 (2002) 116–121. doi:10.1002/1439-2054(20020201)287:2<116::AID-MAME116>3.0.CO;2-Z.

[284] Garlotta D, A Literature Review of Poly(Lactic Acid), Journal of Polymers and the Environment 9 (2001) 63-84. doi:10.1023/A:1020200822435.

[285] Södergård A, Stolt M, Properties of lactic acid based polymers and their correlation with composition, Progress in Polymer Science 27 (2002) 1123-1163. doi:10.1016/s0079-6700(02)00012-6.

[286] Lee SH, Song WS, Enzymatic Hydrolysis of Polylactic Acid Fiber, Appl Biochem Biotechnol 164 (2011) 89-102. doi: 10.1007/s12010-010-9117-7.

[287] Agarwal CM, Koelling KW, Chalmers JJ, Characterization of the Degradation of Polylactic Acid Polymer in a Solid Substrate Environment, Biotechnol Progress 14 (1998) 517–526. doi:10.1021/bp980015p.

[288] Beslikas T, Gigis I, Goulios V, Christoforides J, Papageorgiou GZ, Bikiaris DN, Crystallization Study and Comparative in Vitro–in Vivo Hydrolysis of PLA Reinforcement Ligament, International Journal of Molecular Sciences 12 (2011) 6597-6618. doi:10.3390/ijms12106597.

[289] Gorrasi G, Pantani R, Effect of PLA grades and morphologies on hydrolytic degradation at composting temperature: Assessment of structural modification and kinetic parameters, Polymer Degradation and Stability 98 (2013) 1006-1014. doi:10.1016/j.polymdegradstab.2013.02.005.

[290] Bergsma JE, Rozema FR, Bos RM, et al., Biocompatibility and degradation mechanisms of predegraded and non-predegraded poly(lactide) implants: an animal study, J Mater Sci: Mater Med 6 (1995) 715–724. doi:10.1007/BF00134307.

[291] Maurus PB, Kaeding CC, Bioabsorbable implant material review, Operative Techniques in Sports Medicine 12 (2004) 158-160. doi:10.1053/j.otsm.2004.07.015.

[292] Das D, et al., Bioresorption and Degradation of Biomaterials. In: Tissue Engineering III: Cell - Surface Interactions for Tissue Culture. Advances in Biochemical Engineering Biotechnology, vol 126 (2011) edited by Kasper C, Witte F, Pörtner R. Springer, Berlin, Heidelberg. doi:10.1007/10_2011_119.

[293] Necas J, et al., Hyaluronic acid (hyaluronan): a review. Veterinarni Medicina 53 (2008) 397-411.

[294] Kim TG, Chung HJ, Park TG, Macroporous and nanofibrous hyaluronic acid/collagen hybrid scaffold fabricated by concurrent electrospinning and deposition/leaching of salt particles, Acta Biomaterialia 4 (2008) 1611-1619.

[295] Chen WYJ, Abatangelo G, Functions of hyaluronan in wound repair, Wound Repair and Regeneration 7 (1999) 79-89.

[296] Collins MN, Birkinshaw C, Comparison of the effectiveness of four different crosslinking agents with hyaluronic acid hydrogel films for tissue-culture applications, Journal of Applied Polymer Science 104 (2007) 3183-3191.

[297] Matou-Nasri S GJ, Kumar S, Slevin M, Oligosaccharides of hyaluronan induce angiogenesis through distinct CD44 and RHAMM-mediated signaling pathways involving Cdc2 and gamma-adducin, Int J Oncol 35 (2009) 761-773.

[298] Xie Y, Upton Z, Richards S, Rizzi SC, Leavesley DI, Hyaluronic acid: Evaluation as a potential delivery vehicle for vitronectin: growth factor complexes in wound healing applications, Journal of Controlled Release 153 (2011) 225-232.

[299] Frantz C, Stewart KM, Weaver VM, The extracellular matrix at a glance, Journal of Cell Science 123 (201) 4195-4200. doi:10.1242/jcs.023820.

[300] Papakonstantinou E, Roth M, Karakiulakis G, Hyaluronic acid: A key molecule in skin aging, Dermato-endocrinology 4 (2012) 253-258. doi:10.4161/derm.21923.

[301] Zhu G, et al, Raman spectra of amino acids and their aqueous solutions, Spectrochimica Acta Part A: Molecular and Biomolecular Spectroscopy 78 (2011) 1187-1195.

[302] Shurvell HF, et al., Raman spectra of L(+)-glutamic acid and related compounds, Journal of Raman Spectroscopy 20 (1989) 163–168.

[303] Navarette JT, et al., IR and Raman spectra of L-aspartic acid and isotopic derivatives, Biopolymers 34 (1994) 1065–1077.

[304] Kister G, et al., Effects of morphology, conformation and configuration on the IR and Raman spectra of various poly(lactic acid)s, Polymer 39 (1998) 267-273.

[305] Qin D, Kean R, Crystallinity Determination of Polylactide by FT-Raman Spectrometry, Appl. Spectrosc. 52 (1998) 488-495.

[306] Vogt C, et al., Degradation of poly(L-lactic acid) coating on permanent coronary metal stent investigated ex vivo by micro Raman spectroscopy, J. Raman Spectrosc. 48 (2017) 711- 719. doi:10.1002/jrs.5111.

[307] Tallawi M, Rosellini E, Barbani N, et al., Strategies for the chemical and biological functionalization of scaffolds for cardiac tissue engineering: a review, Journal of the Royal Society Interface 12 (2015) e20150254. doi:10.1098/rsif.2015.0254.

[308] Kim CH, Khil MS, Kim HY, Lee HU, Jahng KY, An improved hydrophilicity via electrospinning for enhanced cell attachment and proliferation, J. Biomed. Mater. Res. 78B (2006) 283–290. doi:10.1002/jbm.b.30484

[309] Esmonde-White KA, Le Clair SV, Roessler BJ, Morris MD, Effect of Conformation and Drop Properties on Surface-Enhanced Raman Spectroscopy of Dried Biopolymer Drops, Applied spectroscopy 62 (2008) 503-511. doi:10.1366/000370208784344370.

[310] Yova D, Hovhannisyan V, Theodossiou T, Photochemical effects and hypericin photosensitized processes in collagen, J. Biomed. Opt. 6 (2001) 52-57. doi:10.1117/1.1331559.

[311] Sun MY, Hiroshi U, Sachiko I, Yasuhiko T, Fabrication of Non-woven Mats of Gelatin/Poly(L-lactic acid) Composites by Electrospinning and Their Application for Scaffold of Cell Proliferation, Chemistry Letters 35 (2006) 564-565. doi:10.1246/cl.2006.564.

[312] Jaiswal AK, Kadam SS, Soni VP, Bellare JR, Improved functionalization of electrospun PLLA/gelatin scaffold by alternate soaking method for bone tissue

engineering, Applied Surface Science 268 (2013) 477-488. doi:10.1016/j.apsusc.2012.12.152.

[313] Kim HW, Yu HS, Lee HH, Nanofibrous matrices of poly(lactic acid) and gelatin polymeric blends for the improvement of cellular responses, J. Biomed. Mater. Res. 87A (2008) 25–32. doi:10.1002/jbm.a.31677.

[314] An K, Liu H, Guo S, Kumar D, Wang Q, Preparation of fish gelatin and fish gelatin/poly(l-lactide) nanofibers by electrospinning, International Journal of Biological Macromolecules 47 (2010) 380-388. doi:10.1016/j.ijbiomac.2010.06.002.

[315] Yan S, Xiaoqiang L, Shuiping L, Hongsheng W, Chuanglong H, Fabrication and properties of PLLA-gelatin nanofibers by electrospinning, J. Appl. Polym. Sci. 117 (2010) 542–547. doi:10.1002/app.30973.

[316] Li Z, Wang C, Effects of Working Parameters on Electrospinning in: One-Dimensional nanostructures. SpringerBriefs in Materials (2013) 15-28. doi:10.1007/978-3-642-36427-3_2.

[317] Fridrikh SV, Yu JH, Brenner MP, Rutledge GC, Controlling the Fiber Diameter during Electrospinning, Phys. Rev. Lett. 90 (2003), 144502. doi:10.1103/PhysRevLett.90. 144502.

[318] Lai JY, Ma DHK, Lai MH, Li YT, Chang RJ, et al., Characterization of Cross-Linked Porous Gelatin Carriers and Their Interaction with Corneal Endothelium: Biopolymer Concentration Effect, PLoS ONE 8 (2013) e54058. doi:10.1371/journal.pone.0054058.

[319] Nguyen TH, Lee BT, The effect of cross-linking on the microstructure, mechanical properties and biocompatibility of electrospun polycaprolactone–gelatin/PLGA–gelatin/PLGA–chitosan hybrid composite, Science and Technology of Advanced Materials, 13 (2012) 035002. doi:10.1088/1468-6996/13/3/035002.

[320] Nguyen T, Lee B, Fabrication and characterization of cross-linked gelatin electrospun nano-fibers. Journal of Biomedical Science and Engineering 3 (2010) 1117-1124.

doi:10.4236/jbise.2010.312145.

[321] Pan JF, Liu NH, Sun H, Xu F, Preparation and Characterization of Electrospun PLCL/Poloxamer Nanofibers and Dextran/Gelatin Hydrogels for Skin Tissue Engineering, PLoS ONE 9 (2014) e112885. doi:10.1371/journal.pone.0112885.

[322] Meng ZX, Wang YS, Ma C, Zheng W, Li L, Zheng YF, Electrospinning of PLGA/gelatin randomly-oriented and aligned nanofibers as potential scaffold in tissue engineering, Materials Science and Engineering:C 30 (2010) 1204-1210. doi:10.1016/j.msec.2010.06.018.

[323] Bencherif SA, Braschler TM, Renaud P, Advances in the design of macroporous polymer scaffolds for potential applications in dentistry, Journal of Periodontal & Implant Science 43 (2013) 251-261. doi:10.5051/jpis.2013.43.6.251.

[324] Kharaziha M, Nikkhah M, Shin S, Annabi N, Masoumi N, Gaharwar AK, Camci-Unal G, Khademhosseini A, PGS:Gelatin nanofibrous scaffolds with tunable mechanical and structural properties for engineering cardiac tissues, Biomaterials 34 (2013) 6355-6366. doi:10.1016/j.biomaterials.2013.04.045.

[325] Detta N, Errico C, Dinucci D, et al., Novel electrospun polyurethane/gelatin composite meshes for vascular grafts, J Mater Sci: Mater Med 21 (2010) 1761-1769. doi:10.1007/s10856-010-4006-8.

[326] Zhang Y, Ouyang H, Lim CT, Ramakrishna S, Huang ZM, Electrospinning of gelatin fibers and gelatin/PCL composite fibrous scaffolds, J. Biomed. Mater. Res. 72B (2005) 156–165. doi:10.1002/jbm.b.30128.

[327] Jing X, Salick MR, Cordie T, Mi H, Peng X, Turng L, Electrospinning Homogeneous Nanofibrous Poly(propylene carbonate)/Gelatin Composite Scaffolds for Tissue Engineering, Ind. Eng. Chem. Res. 53 (2014) 9391–9400. doi:10.1021/ie500762z.

[328] Razavi S, Karbasi S, Morshed M, Zarkesh Esfahani H, Golozar M, Vaezifar S, Cell Attachment and Proliferation of Human Adipose-Derived Stem Cells on PLGA/Chitosan Electrospun Nano-Biocomposite, Cell Journal (Yakhteh) 17 (2015) 429-437. doi:10.22074/cellj.2015.4.

[329] Yue M, Zhou B, Jiao K, Qian X, Xu Z, Teng K, Zhao L, Wang J, Jiao Y, Switchable hydrophobic/hydrophilic surface of electrospun poly (l-lactide) membranes obtained by CF4 microwave plasma treatment, Applied Surface Science 327 (2015) 93-99. doi:10.1016/j.apsusc.2014.11.149.

[330] Sharma S, Gupta D, Mohanty S, Jassal M, Agrawal AK, Tandon R, Surface-Modified Electrospun Poly(ε-Caprolactone) Scaffold With Improved Optical Transparency and Bioactivity for Damaged Ocular Surface Reconstruction, Invest. Ophthalmol. Vis. Sci. 55 (2014) 899-907. doi:10.1167/iovs.13-12727.

[331] Schaub NJ, Le Beux C, Miao J, Linhardt RJ, Alauzun JG, et al., The Effect of Surface Modification of Aligned Poly-L-Lactic Acid Electrospun Fibers on Fiber Degradation and Neurite Extension, PLoS ONE 10 (2015) e0136780. doi:10.1371/journal.pone.0136780.

[332] Martins A, Pinho ED, Faria S, Pashkuleva I, Marques AP, Reis RL, Neves NM, Surface Modification of Electrospun Polycaprolactone Nanofiber Meshes by Plasma Treatment to Enhance Biological Performance, Small 5 (2009) 1195–1206. doi:10.1002/smll.200801648.

[333] Burdick JA, Prestwich GD, Hyaluronic Acid Hydrogels for Biomedical Applications, Advanced materials 23 (2011) H41-H56. doi:10.1002/adma.201003963.

[334] Kim IL, Mauck RL, Burdick JA, Hydrogel design for cartilage tissue engineering: A case study with hyaluronic acid, Biomaterials 32 (2011) 8771-8782. doi:10.1016/j.biomaterials.2011.08.073.

[335] Prestwich GD, Hyaluronic Acid-Based Clinical Biomaterials Derived for Cell and Molecule Delivery in Regenerative Medicine, Journal of controlled release : official

journal of the Controlled Release Society 155 (2011) 193-199. doi:10.1016/j.jconrel. 2011.04.007.

[336] Um IC, et al., Electro-Spinning and Electro-Blowing of Hyaluronic Acid, Biomacromolecules 5 (2004) 1428–1436. doi:10.1021/bm034539b.

[337] Collins MN, Birkinshaw C, Hyaluronic acid based scaffolds for tissue engineering-A review, Carbohydrate Polymers 92 (2013) 1262-1279. doi:10.1016/j.carbpol.2012.10.028.

[338] Brenner EK, Schiffman JD, Thompson EA, Toth LJ, Schauer CL, Electrospinning of hyaluronic acid nanofibers from aqueous ammonium solutions, Carbohydrate Polymers 87 (2012) 926-929. doi:10.1016/j.carbpol. 2011.07.033.

[339] Li J, He A, Han CC, Fang D, Hsiao BS, Chu B, Electrospinning of Hyaluronic Acid (HA) and HA/Gelatin Blends. Macromol. Rapid Commun. 27 (2006) 114–120. doi:10.1002/marc.200500726.

[340] Ji Y, Ghosh K, et al., Electrospun three-dimensional hyaluronic acid nanofibrous scaffolds, Biomaterials, 27 (2006) 3782-3792. doi:10.1016 /j.biomaterials.2006.02.037.

[341] Maleki A, Kjøniksen AL, Nyström B, Effect of pH on the Behavior of Hyaluronic Acid in Dilute and Semidilute Aqueous Solutions, Macromol. Symp. 274 (2008) 131–140. doi:10.1002/masy.200851418.

[342] Kotzianová A, Řebíček J, Pokorný M, et al., Raman spectroscopy analysis of biodegradable electrospun nanofibers prepared from polymer blends, Monatshefte für Chemie - Chemical Monthly 147 (2016) 919-923. doi:10.1007/s00706-015-1639-9.

[343] Itenov TS, Kirkby NS, Bestle MH, Nilsson AC, Erlandsen EJ, Peters L, Jensen JU, Hyaluronic Acid Assays: Turbidimetric or Enzyme-Based Immune Assay? A Method Comparison Study, J. Clin. Lab. Anal. 30 (2016) 524–528. doi:10.1002/jcla.21897.

[344] Kenne L, Gohil S, Nilsson EM, Karlsson A, Ericsson D, Kenne AH, Nord LI, Modification and cross-linking parameters in hyaluronic acid hydrogels-Definitions and

analytical methods, Carbohydrate Polymers 91 (2013) 410-418. doi:10.1016/ j.carbpol.2012.08.066.

[345] Delpech B, Bertrand P, Maingonnat C, Immunoenzymoassay of the hyaluronic acid-hyaluronectin interaction: Application to the detection of hyaluronic acid in serum of normal subjects and cancer patients, Analytical Biochemistry 149 (1985) 555-565. doi:10.1016/0003-2697(85)90613-X.

[346] Raucci MG, Alvarez-Perez MA, Demitri C, Sannino A, Ambrosio L, Proliferation and osteoblastic differentiation of hMSCs on cellulose-based hydrogels, J Appl Biomater Function Mater 10 (2012) 302-307.

[347] Bacakova L, Filova E, Parizek M, Ruml T, Svorcik V, Modulation of cell adhesion, proliferation and differentiation on materials designed for body implants, Biotechnology Advances 29 (2011) 739-767. doi:10.1016/j.biotechadv.2011.06.004.

RINGRAZIAMENTI

In primo luogo vorrei ringraziare Donato, Luca ed anche Tommaso, per quello che hanno rappresentato per me e che hanno saputo darmi, perché sono convinto che, anche se le vicissitudini della vita possano allontanarci e dividerci, quello che ci ha unito e ci unisce ancora sia più forte. Ed anche se noi stessi cresciamo e cambiamo, in una parte del mio cuore resteremo per sempre Dok, Tok, Luque e Shje. Un grazie infinito anche a mio padre e mia madre perché mi hanno sempre apprezzato, sostenuto e voluto bene per quello che sono. Poi vorrei ringraziare tutti i ragazzi e le ragazze che si sono alternati nel laboratorio di Potenza nel periodo in cui l'ho frequentato e che penso come me si siano impegnati per poterne fare un luogo bello, libero e indipendente, seppur in un contesto difficile e poco stimolante. Per questo ringrazio Mauro, Carmen, Alessandra, Angelica, Valentina, Dora e Alessandro da una parte, e Mariantonietta, Federica, Inge e Alessio dall'altra. Ringrazio anche la dott.ssa Crudele per il suo aiuto. Un grazie speciale va poi a Sandro per avere sempre ascoltato le mie idee e proposte, anche se spesso stupide, e per aver sempre trovato del tempo da dedicarmi. Ringrazio la Prof.ssa Pepe per gli spettri NMR, la Prof.ssa Bochicchio per avermi permesso di svolgere una grossa parte della tesi in Germania ed il Prof. Bracalello per le conversazioni scientifiche (e non). Un grazie infinee alla musica ed alla mia moto per essere state lì' nei miei momenti di solitudine.

DANKSAGUNGEN

Zuerst möchte ich Katja und Svenja meinen Dank für die Chance sagen, die sie mir gegeben haben. Ohne die Zeit in Tübingen wäre nichts aus dieser Doktorarbeit geworden. In dieser Zeit habe ich Leidenschaft für die Forschung wiedergefunden. Außerdem möchte ich mich aus ganzem Herzen bei all den Menschen bedanken, die in der Gruppe (gewesen) sind , und zwar Daniel, Anne, Eva, Nora, Diana, Simone L. (und Frieda), Simone P., Rebecca, Pirmin, Ruben, Hannah, Nian, Julia M., Julia B., Jonas, Shannon, Melanie, Aline, Martin, Alejandro, Katrin, Matthias, Kratika, Grazia, Jana, Monica, Michael usw. Herzlichen Dank für die Hilfe, die Unterstützung, die Geduld, das Verständnis, und für alles, was ihr mir gebracht habt, als Wissenschaftler und als Menschen. Ein Dankeschön auch an Herrn Schulz, für seine Verfügbarkeit und die Freudlichkeit zu uns und unseren Scaffolds. Außerdem möchte ich meinen Dank all den Menschen sagen, die ich in dieser Zeit kennengelernt habe, vor allem meinen Mitbewohnerinnen, Maike, Marie, Jeanette und Esther. Ich habe mich immer wohl gefühlt, und jede einzelne Minute geschätzt, die wir zusammen verbracht haben. Es hat mir an nichts gefehlt, und wenn ja, dann war alles in dem Augenblick schon weg, in dem ich wieder in der WG war, und selbst nur eine von euch gesehen, oder einfach gehört habe. Meinen Dank möchte ich auch Alex, Sebastian, Ani, Maren und Simon sagen. Ich habe mit euch Allen unvergessliche Tage verbracht. Zuletzt ein spezieller Dank gilt für Peter. Er ist für mich immer viel mehr als ein Deutschlehrer gewesen, und es ist immer noch so.